DESIGN, FABRICATION, AND LOCOMOTION ANALYSIS OF AN UNTETHERED, MINIATURE, LEGGED, COMPRESSIBLE, SOFT ROBOT: CSQUAD

A THESIS SUBMITTED TO

THE GRADUATE SCHOOL OF ENGINEERING AND SCIENCE

OF BILKENT UNIVERSITY

IN PARTIAL FULFILLMENT OF THE REQUIREMENTS FOR

THE DEGREE OF

MASTER OF SCIENCE

IN

MECHANICAL ENGINEERING

By

Mert Ali İhsan Kalın

September 2021

DESIGN, FABRICATION, AND LOCOMOTION ANALYSIS OF AN UNTETHERED, MINIATURE, LEGGED, COMPRESSIBLE, SOFT ROBOT: CSQUAD

By Mert Ali İhsan Kalın

September 2021

We certify that we have read this thesis and that in our opinion it is fully adequate, in scope and in quality, as a thesis for the degree of Master of Science.

Onur Özcan(Advisor)

Bilge Baytekin

Evren Samur

Approved for the Graduate School of Engineering and Science:

Ezhan Karaşan
Director of the Graduate School

ABSTRACT

DESIGN, FABRICATION, AND LOCOMOTION ANALYSIS OF AN UNTETHERED, MINIATURE, LEGGED, COMPRESSIBLE, SOFT ROBOT: CSQUAD

Mert Ali İhsan Kalın
M.S. in Mechanical Engineering
Advisor: Onur Özcan
September 2021

Conventional robotics has been effective for industrial applications such as fast, precise and accurate production or for sophisticatedly controlled systems for the last couple of centuries. However, as the robots become more ubiquitous in everyday lives of people, the drawbacks of conventional and rigid robots have become more and more apparent. One of the biggest problems that soft robots solve is the safe interactions with humans. Whether it be a minimally invasive surgery or a search and rescue operation under rubble, the soft robots offer better performance especially in terms of compliance compared to their rigid counterparts.

With especially the search and rescue environments in mind, this study presents an untethered, miniature, legged and compressible soft quadruped (cSQuad). This robot is equipped with C-shaped legs for better locomotion performance on unstructured surfaces. It is made out of soft materials, mainly from polydimethylsiloxane (PDMS), it utilizes a flexible printed circuit board (PCB) and only some small sensors, actuators and electronic components are made out of rigid materials. The main goal of this robot is to have the ability to pass through openings that are smaller than its cross-section. In order to achieve this goal, the robot is designed to be compressible. Both the body of the robot and its C-shaped legs can compress themselves using shape memory alloy (SMA) springs. The design and fabrication steps of cSQuad is explained in detail and the tests have been done to verify that the robot can reduce its cross-section area by at least 25%.

cSQuad is the successor of SQuad which is also a soft quadruped with C-shaped legs. Before starting the design of cSQuad, the locomotion performance of SQuad was studied to make sure that it would be worth continuing to design

new generation of soft quadrupeds. This study was a comparative study between the soft quadruped (SQuad) and its rigid and hybrid twins. The study consisted of speed, pitch and roll angle, body centroid position and obstacle climbing performance analysis. The results of this analyses showed that even though the soft robot was slower it gave better performance in terms of obstacle climbing and smooth locomotion. This gave us the confidence to continue improving the robot which resulted in designing of cSQuad.

SMA springs of cSQuad are placed on specifically calculated locations on the body and the legs of the robot to achieve optimum compression performance. To transmit power to the SMAs on continuously rotating legs, a custom slip-ring device was built utilizing pogo pins. The compression tests for the legs and the body were conducted separately. Then, a robot with both leg and body compression was built and tested.

As a result, a robot with the capability of reducing its cross-section area by at least 25% is built and tested. This robot can be used as a base design for the new generation of robots that could be used in search and rescue operations. It has the potential to be equipped with specific sensors for specific tasks. The fabrication and design steps can also be considered as a framework for fabricating soft robots in general.

Keywords: soft robotics, miniature robotics, bio-inspired systems, locomotion analysis, legged robots, mobile robots, quadruped robots, compressible robots, shape memory alloys.

ÖZET

KABLOSUZ, MİNYATÜR, BACAKLI, SIKIŞABİLEN VE ESNEK ROBOT CSQUAD'IN TASARIMI, ÜRETİMİ VE YÜRÜYÜŞ ANALİZİ

Mert Ali İhsan Kalın
Makine Mühendisliği, Yüksek Lisans
Tez Danışmanı: Onur Özcan
Eylül 2021

Geleneksel robotik hızlı ve hassas üretim uygulamaları ve sofistike kontrole sahip endüstriyel sistemler için son birkaç yüzyıldır efektif olmuştur. Robotların insanlar tarafından kullanımının yaygınlaşması ile birlikte geleneksel robotiğin dezavantajları daha çok gün yüzüne çıkmaya başlamıştır. Yumuşak ve esnek robotların çözdüğü en büyük problemlerden biri de robotların insanlarla olan güvenli etkileşimleridir. Bu robotlar ameliyatlarda veya enkaz altında arama kurtarma çalışmaları gibi faaliyetler sırasında katı ve rijit robotlara kıyasla özellikle esneklik ve uyumluluk konusunda daha yüksek performans sunmaktadır.

Bu çalışmada sunulan kablosuz, minyatür, bacaklı ve sıkışabilme kabiliyetine sahip dörtayaklı robot (cSQuad), özellikle arama kurtarma çalışmalarına destek olmak fikri ile tasarlanmıştır. Bu robot, bozuk yüzeylerde daha iyi yürüme performansına sahip olması için C şeklindeki bacaklarla donatılmıştır. cSQuad, PDMS (polidimetilsiloksan) gibi çoğunlukla esnek olan malzemelerden üretilmiştir. Robot gövdesi, bacakları ve elektronik kartı esnek iken sadece sensörler, motorlar ve bazı elektronik parçalar rijit materyallerden üretilmiştir. Bu robotun temel amacı kendi orijinal kesit alanından daha dar geçitlerden geçebilmektir. Bu amaca ulaşabilmek için robotun sıkışabilir olması gerekmektedir. Robotun gövde ve C şeklindeki bacaklarına şekil hafızalı alaşımlar (ŞHA) sayesinde sıkışabilme yeteneği kazandırılmıştır. cSQuad'ın bütün tasarım ve üretim aşamaları detaylı bir şekilde açıklanmış ve deneyleri yapılmıştır. Deneyler sonucunda robotun kesit alanını en az %25 küçültebildiği doğrulanmıştır.

cSQuad, kendisi gibi esnek, C bacaklı ve dörtayaklı bir robot olan SQuad robotu üzerine inşa edilmiştir. cSQuad'ın tasarımına başlamadan önce SQuad

üzerinde yapılan yürüme deneylerinden elde edilen sonuçlardan istifade edilmiştir. Bu deneyler sırasında esnek bir robot olan SQuad ile aynı tasarıma sahip fakat tamamen rijit veya kısmen rijit materyallerden üretilmiş farklı robot versiyonları karşılaştırılmıştır. Bu karşılaştırmada robotun hızı, yunuslama açısı, yatış açısı, gövdenin geometrik merkezinin pozisyonu ve robotun engel aşma performansı gibi parametreler kullanılmıştır. Bu deneyler yumuşak robot olan SQuad'ın diğer robotlara kıyasla daha yavaş olsa da engel tırmanma kabiliyeti ve sarsıntısız yürüme performansı konularında daha üstün olduğunu göstermiştir. Bu sonuçlar sayesinde SQuad'ın gelişme potansiyeline sahip olduğu anlaşılmış ve cSQuad tasarlanmıştır.

cSQuad'ın ŞHA materyalinden üretilen yayları, robotun gövdesi ve bacakları üzerinde spesifik olarak belirlenen pozisyonlara bağlanmıştır. Bu sayede optimum sıkışma performansına ulaşmak hedeflenmiştir. Özellikle bacaklar üzerinde bulunan ŞHA yaylarına elektrik akımı aktarabilmek için pogo pin isimli yaylı pinler kullanılmıştır. Bu pinler bacaklar üzerine bağlanmıştır ve gövde üzerine yerleştirilen kontak bilezikleri ile bacağın dönüşü esnasında sürekli temas halinde olmaları ve bacak üzerine sürekli elektrik aktarımı sağlanmıştır. İlk önce bacak sıkışması ve gövde sıkışması ayrı olarak robota entegre edilmiş ve testleri yapılmıştır. Daha sonra ise bütün sistemler birleştirilerek hem gövde hem de bacak sıkışmasına sahip olan cSQuad'ın üretimi ve testleri başarıyla tamamlanmıştır.

Sonuç olarak kesit alanını en az %25 küçültebilen bir esnek robot üretilmiş ve test edilmiştir. Bu robotun tasarımı ve üretimde kullanılan yöntemler gelecekte üretilecek yeni nesil arama kurtarma robotları için bir temel olarak kullanılabilir. Ayrıca cSQuad, spesifik görevleri gerçekleştirmek için spesifik sensörlerle donatılabilme potansiyeline da sahiptir. Robotun üretim ve tasarım aşamalarında paylaşılan bilgiler ve yöntemler, esnek robot üretimi için genel bir kılavuz olarak da kullanılabilir.

Anahtar sözcükler: yumuşak robotlar, minyatür robotlar, biyo-ilhamlı sistemler, yürüyüş analizi, bacaklı robotlar, mobil robotlar, dört ayaklı robotlar, sıkışabilen robotlar, şekil hafızalı alaşımlar.

Acknowledgement

I would like to start with thanking my adviser, Prof. Onur Özcan who accepted me to his laboratory 6 years ago and helped me start an academic career. Without his guidance, I wouldn't have started a master's degree and this work wouldn't have been possible. He supported me during every hardship that I faced with my research and together we were able to achieve great results that I will forever be proud of.

The work presented in this thesis wouldn't have been possible without the help of the members of the Miniature Robotics Lab. I was both lucky and delighted to work with Cem Aygül, Ahmet Furkan Güç, Altay Türkmen, Nima Mahkam, Amirali Abazari, Doğa Özbek, Mustafa Uğur, Alihan Bakır, Cem Karakadıoğlu, Mohammad Askari and Kutay Şentürk. I feel blessed to know each and every one of you.

Moreover, I would like to thank the head of our machine shop, Şakir Duman. He taught me everything I know about machining and classical fabrication. The parts that we fabricated together make this thesis possible.

Last but not least, I want to thank my family who have always supported me with every decision I make. I dedicate this work to them and especially to my nephew Bora Güngör. I wish him the best that life has to offer.

Finally, I would like to acknowledge the Scientific and Technological Research Council of Turkey, TUBİTAK, for financially supporting this research under Grant No. 216M195.

Contents

1 Introduction **1**

1.1 Motivation and Objectives 1

1.2 Literature Review on Soft Robotics 2

1.3 Thesis Structure 5

2 Design, Fabrication and Control **7**

2.1 Examining CQuad, the Predecessor of SQuad and cSQuad 8

2.2 Design and Fabrication of SQuad 10

2.2.1 Material Selection 10

2.2.2 Fabrication Guidelines for Soft Polymers 11

2.2.3 Body Design and Fabrication 13

2.2.4 Leg Design and Fabrication 17

2.2.5 Tail Design and Fabrication 22

2.2.6 Electronics Design and Fabrication 23

2.2.7 Assembly of SQuad 27

2.3 Design of Compressible SQuad (cSQuad) 30

2.3.1 Choosing Compression Method 30

2.3.2 Design and Fabrication of Shape Memory Alloy Springs . . 31

2.3.3 Leg Design and Fabrication 33

2.3.4 Body Design and Fabrication 57

2.3.5 Electronics Design 67

2.3.6 Assembly of cSQuad 70

2.4 Control of SQuad and cSQuad 72

3 Experiments and Results 74

3.1 Experiments and Results for SQuad 75

3.1.1 Speed Analysis 75

3.1.2 Pitch and Roll Angle Analysis 77

3.1.3 Body Centroid Position Analysis 81

3.1.4 Obstacle Climbing Analysis 83

3.1.5 Testing Maximum Climbing Angle on an Inclined Surface . 84

3.1.6 Testing the Onboard Microphone 86

3.2 Compression Performance of cSQuad 88

3.2.1 C Shaped Leg Compression Tests 88

3.2.2 Body Compression Tests 93

3.2.3 Final Compression Tests of the Untethered Robot 95

4 Conclusion and Future Directions **98**

4.1 Summary and Conclusion 98

4.2 Contributions 101

4.3 Future Directions 101

Bibliography **107**

List of Figures

2.1 Fully assembled C-Legged Quadruped: CQuad 8

2.2 (a) Micro DC motor and IR sensor. (b) Black and white stripped encoder. (c) Close view of the encoder with folded C-shaped leg. . 9

2.3 Obstacle climbing experiment of CQuad 9

2.4 Assembled version of SQuad [1] 10

2.5 Two parts required to make PDMS 12

2.6 The vacuum setup for degassing the polymers 12

2.7 The oven used for curing the polymers 13

2.8 The initial design for the body of SQuad 14

2.9 The 3D printed mold with 7 mm rod (right side) for the initial design for the body of SQuad 15

2.10 The final design for the body of SQuad 15

2.11 The 3D printed mold with the 3D printed motor caps for the final design for the body of SQuad 16

2.12 The 3D printed motor caps used in the final body design of SQuad 16

2.13 The fabricated PDMS body of SQuad 17

2.14 Stress analysis of a c-shaped leg. 18

2.15 Mold design for the c-shaped leg 19

2.16 Initial motor connector part for the c-shaped leg 20

2.17 Initial motor connector embedded in PDMS leg 20

2.18 Final design for motor connector assembly 21

2.19 The c-shaped leg along with the sensor and motor connector . . . 21

2.20 The tail design assembled onto the SQuad's body 22

2.21 The tail design assembled onto the SQuad's body 22

2.22 (a) Arduino schematics for SQuad PCB. (b) Power schematics for SQuad PCB. 24

2.23 The schematic for L293DD motor drivers of SQuad PCB 25

2.24 The board design for SQuad PCB 26

2.25 The PCB manufactured in China for SQuad on the initial version of the soft body 27

2.26 The 3D CAD image of the assembled SQuad 28

2.27 Walking pictures of 4 different robot configurations. (a) SQuad, (b) soft body - hard leg, (c) hard body - hard leg, (d) hard body - soft leg. 29

2.28 Nitinol Shape Memory Alloy wire with 0.5mm diameter 31

2.29 Setup for spring making 32

2.30 Released(top) and compressed(bottom) SMA springs 33

2.31 Initial leg designs inspired from accordions 34

2.32 Improved accordion leg design 35

2.33 The mold design for the accordion leg 35

2.34 The 3D printed mold for the accordion leg (left), and the accordion leg made from Ecoflex (right). 36

2.35 The accordion leg with an SMA spring inside. 36

2.36 The initial(left) and the compressed(right) accordion leg with an SMA spring inside. 37

2.37 The four bar mold design for accordion leg 37

2.38 The fabricated four bar leg using PDMS and Ecoflex 38

2.39 The piston cylinder four bar mold design for accordion leg 39

2.40 The fabricated parts for the piston cylinder four bar mold 40

2.41 The fabricated piston cylinder four bar leg (right side is compressed) 40

2.42 The frontal(left) and trimetric(right) view of the C-shaped leg design for cSQuad 41

2.43 The mold design of the C-shaped leg for cSQuad 42

2.44 3D printed connection parts for SMA springs 42

2.45 Kinematic analysis of the compression of the C shaped leg 43

2.46 The first prototype of the C shaped compressible leg, relaxed(left) and compressed(right) 44

2.47 The initial electrical design for a slip-ring 45

2.48 The slip-ring fabricated with a CNC router 45

2.49 CNC masked (top) and laser masked (bottom) slip-rings 46

2.50 The FR2 copper plate for slip-rings after chemical etching 47

2.51 The FR2 copper plate for slip-rings after the nail polish is removed 47

2.52 The first fabricated slip-ring prototype 48

2.53 The pogo pins that are used for the final slip-ring design 49

2.54 The final electrical design for the slip-ring 50

2.55 The final slip-ring design fabricated with FR4 50

2.56 The back of the final slip-ring design with cables soldered 51

2.57 The final slip-ring with the pogo pins attached to the C shaped leg 52

2.58 The initial design for a tube-ring attached to the DC motor . . . 52

2.59 Partly (a) and fully (b) assembled tube-ring prototype 53

2.60 (a) CNC milled die for obtaining a D shaft. (b) Final version of the tube-ring 54

2.61 (a) Top view of the final C shaped half circle leg design. (b) The design of the mold for the final version of the leg. 54

2.62 (a) The CAD design of the final C shaped leg mold. (b) The 3D printed mold for the final C shaped leg. 55

2.63 The pogo pins connected to the 3D printed motor connector . . . 56

2.64 The molds for final C leg design filled with RTV2 silicone 56

2.65 The final C shaped legs made with RTV2 silicone 57

2.66 The mold design (left) and the fabricated compressible body (right). 58

2.67 The separation problem between the Ecoflex and PDMS for the compressible body. 59

2.68 The mold design for the improved compressible body. 60

2.69 The fabricated mold for the improved compressible body. 60

2.70 The fabricated compressible body with additional components such as motors, encoders and PTFE tubes. 61

2.71 The mold design for the compressible body with X shaped center. 62

2.72 The fabricated body with X shaped center. 62

2.73 The front view of the fully assembled robot with X shaped center. 63

2.74 The buckling problem for the X shaped compressible body. 63

2.75 The motor interference problem during body compression. 64

2.76 The first (left) and the second (right) iteration for the mold of the final body design. 64

2.77 The FEM analysis of the X shaped compressible body (side view). 65

2.78 The FEM analysis of the X shaped compressible body (top view). 66

2.79 The second iteration (left) and the last (right) iteration of the final compressible body design. 67

2.80 The motor package with the slip-ring, the DC motor and the encoder assembled.. 67

2.81 The PCB made for DRV8835 motor drivers. 68

2.82 Huike HK23F-DC5V-SHG 5V relay. 69

2.83 Three relays with cables ready to be soldered into the flexible PCB for cSQuad. 70

2.84 The CAD assembly of the final design of the compressible SQuad (cSQuad). 71

2.85 The parts required to assemble a pair of C-shaped legs for cSQuad. 72

2.86 The front view of the cSQuad without leg compression. 72

2.87 The fully compressible cSQuad. 73

3.1 Walking pictures of 4 different robot configurations. (a) SQuad, (b) soft body - hard leg, (c) hard body - hard leg, (d) hard body - soft leg. 76

3.2 Pitch Angle Data of Soft and Hard Bodies 78

3.3 Roll Angle Data of Soft and Hard Bodies 80

3.4 Centroid Height Data of Soft and Hard Bodies 82

3.5 SQuad climbing the obstacle 1.44 times its body height. 84

3.6 SQuad climbing a slope of 52°. 85

3.7 (a)SQuad is moving with the LED turned of. (b) SQuad detects sound, it stops and lights the LED. 87

3.8 (a) Test setup for the slip-ring. (b) An SMA spring before (left) and after (right) a current is applied. 88

3.9 Uncompressed (left) and compressed (right) C shaped PDMS leg with the slip-ring 89

3.10 The rotational test setup for the initial slip-ring desing 90

3.11 (a) The compression of PDMS C leg after 3 seconds of rotation. (b) The compression of PDMS C leg during 8 seconds of rotation. 91

3.12 The failure of the PDMS C shaped leg during compression 92

3.13 The final slip-ring with the pogo pins attached to the C shaped leg 92

3.14 The test for final design of the slip-ring with the RTV2 silicone C shaped leg 93

3.15 The robot body equipped with 4 slip-ring systems for the final leg compression test 93

3.16 (a) Final compression test for 4 C legs (uncompressed). (b) Final compression test for 4 C legs (compressed). 94

3.17 The uncompressed (top) and compressed (bottom) body with X shaped center. 95

3.18 (a) Final compression test for the body (uncompressed). (b) Final compression test for the body (compressed). 96

3.19 (a) The uncompressed cSQuad unable to go through the narrowing path. (b) Compressed cSQuad locomoting through the narrowing path. (c) Compressed cSQuad exiting the test setup. 97

4.1 The first prototype body equipped with 4 soft sensors. 102

List of Tables

3.1 Translational Speeds in terms of Body Lengths per Second for Different Configurations 76

3.2 Maximum Obstacles Scaled in terms of Body Height 83

Chapter 1

Introduction

1.1 Motivation and Objectives

The main motivation of this work is to design and fabricate an untethered miniature quadruped robot that can reduce its cross-sectional area by utilizing soft materials. By doing this, it is aimed that the robot will have the ability to locomote through openings that are smaller than its original cross sectional area. This idea is inspired by the nature especially from mice. It is observed in nature that if a mouse can fit its head through an opening, the rest of its body can also fit through the opening.

To design a compressible soft quadruped robot, we have utilized our past experience coming from our lab's first soft quadruped, SQuad. The SQuad robot proved that the soft legged and soft bodied version of SQuad have advantages over its rigid and hybrid twins in terms of obstacle climbing performance [1]. We wanted to use SQuad as a starting point for the compressible soft quadruped(cSQuad) and extend its capabilities.

Like most of the robots created in Bilkent Miniature Robotics Lab, cSQuad is planned to be used in search and rescue operations. The fact that the soft robots

have the ability to conform to unstructured surfaces makes them ideal to be used in search and rescue operations such as on the rubble of a collapsed building after an earthquake. Even though soft robots naturally change their shape by conforming to their surroundings, there is rarely an intention of reducing the cross-sectional area of the robot for performing specific tasks. To our knowledge cSQuad is the first untethered miniature soft quadruped robot that can compress both its body and C shaped legs with the purpose of reducing its cross-sectional area. In the future it can be equipped with specific sensors for specific tasks.

In this work, the design process and more importantly the challenges that we faced and the creative solutions that we came up with to obtain the cSQuad is explained in detail. The know-how that this thesis provides not only includes compression mechanisms but it also includes a general framework to obtain soft and/or quadruped robots in general. In the future, this work can be used to design and improve soft quadruped search and rescue robots.

1.2 Literature Review on Soft Robotics

Conventional robotics focuses on obtaining high precision and high speed in tasks that are usually related to industrial applications. Soft robotics on the other hand, is a relatively new field which is inspired by nature, especially by animals to achieve both industrial tasks and also tasks related to human interactions. Soft robots offer safe interactions with humans and makes it possible to achieve complex tasks even with simple designs.

The definition of the softness of a robot has been a controversial topic and there are many different views on what constitutes a "soft" robot. In a review work by Laschi et al. [2] many different definitions have been presented and one of the most excepted definition is based on the interaction of a soft robot with its environment rather than the materials used on the robot. According to this definition, a robot's compliance to its surrounding environment hints whether a robot would be considered soft or rigid. Therefore a soft robot is not necessarily

required to be made out of fully soft materials to be considered a soft robot. To our best knowledge, there is only one robot that satisfies the criteria of being fully soft which is the Octobot [3].

The first examples of soft robots date back to late 1970s in the form of soft grippers [4]. Later on, in the early 1990s there have been few more studies about soft robots in the field of flexible micro actuators which used fiber reinforced rubber [5, 6]. As of then, the research in soft robotics have been dormant until the early 2000s. One of the first successful soft robots that is worth mentioning is the pneumatically actuated OctArm [7]. The OctArm is one of the first of many examples of soft robots being used in tasks related to grasping and gripping. This is expected since a transition from conventional robotics into soft robotics may bring along the old tendencies of utilizing robots for industrial applications.

Soft grippers have a great potential to be used extensively in tasks such as picking and placing fragile or irregularly shaped items on industrial conveyors during production or distribution phases. Soft grippers can make use of granular jamming [8, 9], they can be 3D printed [10, 11], magnetically switchable [12] or they can even be untethered [13]. As mentioned before, most soft grippers can be considered as a product of the transition phase from conventional robotics to soft robotics. However, soft robotics is an emerging field and it has evolved in many different directions using state of the art technologies of today. There are even soft robots that use combustive gasses as an actuation method [14]. However, one of the most popular actuation methods used in soft robotics is the utilization of shape memory alloys or SMAs [15, 16, 17]. Even though SMAs are made out of metals such as nickel and titanium they are widely used in soft robotic applications. One of the reasons for this is that even though they are rigid in nature, SMAs resemble the biological muscles of mammals where the actuation is not limited with predetermined rigid links. One other aspect of SMAs which makes them suitable for use as artificial muscles is their high power density. They can apply relatively high forces in a short amount of time in small volumes and they can be programmed into practically any shape. After they are deformed, they can go back to their programmed shapes using thermal or electrothermal stimulus. One of the well known robots that utilize SMAs as actuators is the

octopus robot [18, 19]. The soft electrically actuated quadruped, SEAQ [15] is another example of an SMA based robot and it is a similar robot to cSQuad in terms of being a quadruped and employing SMAs. However, the difference is that it uses SMAs for locomotion rather than the objective of reducing the cross-sectional area of the robot. In addition to the robots explained above, there are also examples of soft robots that use pneumatic actuators[20, 21, 22, 23, 24]. However, one of the disadvantages of using a pneumatic actuator is that they require a stable and continuous pressure source hence it is difficult to obtain an untethered soft robot using pneumatic actuators.

From materials perspective, silicone based elastomers such as PDMS is widely used in soft robotics including in the robots presented in this work [1, 21]. Recently, there have also been studies that propose the use of gelatin based biogels that both provide sufficient stiffness and also the ability to degrade over time for sustainability [25].

All soft robots have the ability to change their shape to some degree by definition. However there are only a few examples of untethered mobile robots that change their shape with the intention of improving their locomotion or obstacle scaling capabilities [26, 27]. These robots that were developed by Lee et al. are both wheeled robots that have rigid bodies and they either use origami style wheel and a motor driven actuation [27] or a flexible wheel made out of copper-Kapton films that uses SMAs as actuators [26]. The soft robot presented in this thesis, cSQuad also uses SMAs to compress its legs. The main difference and the novelty is that cSQuad compresses both its legs and body together and it is a legged robot instead of a wheeled robot and it has a soft body rather than a rigid body. This makes cSQuad a rare, if not a unique soft robot in the literature of soft robotics.

1.3 Thesis Structure

This thesis consists of the following chapters:

Chapter 2: Design Fabrication and Control: This chapter is the backbone of the thesis and it consists of the key steps towards obtaining the soft compressible quadruped, cSQuad. The chapter starts with explaining the design and fabrication processes of the cSQuad by inspecting its predecessors SQuad and CQuad. The soft material selection process and fabrication guidelines for making the robots are discussed. The initial design steps and every design step until the final designs for both SQuad and cSQuad is explained thoroughly by sharing CAD images, 3D printed molds and the fabricated PDMS parts. Later on, a compression method using shape memory alloys (SMA) were introduced. The process of making SMA springs out of SMA wires is demonstrated. Moreover, the modifications that the robot had to go through for implementing the SMA springs is discussed in detail especially for the C shaped leg design.Since the C shaped legs rotate continuously, an unconventional method for an electrical connection had to be designed. The parts for rotating electrical connections are called slip rings due to their ring shape and slipping electrical connections. The slip ring designs were improved by using miniature bearings and the new design, so called tube-rings, are also explained towards the end of the chapter. Moreover, all of the electronic circuit designs are explained by sharing the schematic designs and actual board designs. At the end of the chapter, the control method for controlling our quadruped motors are explained briefly.

Chapter 3: Experiments and Results: This chapter consists of the results that were obtained using SQuad and cSQuad. First, a comparison between the soft quadruped SQuad, and its hard twin and hybrid configurations were compared in terms of speed, pitch and roll angle, centroid position and obstacle climbing performance. The results presented for SQuad were published in [1]. Later on, the performance for an on-board microphone was tested to measure the potential use of SQuad during search and rescue operations. Additionally, the maximum slope that SQuad can climb was measured. For the cSQuad,various

experiments to measure the compression amount was carried out. First, the results for the leg and body compression of cSQuad were tested separately, then the fully compressible version was tested and its results were discussed.

Chapter 4: Conclusion and Future Directions: This chapter consists of a discussion of the results obtained in Chapter 3. It summaries the work presented in the thesis and it emphasizes the importance of it. The contributions of this work to the science literature was also discussed. Finally, discussion was made about the possible improvements and future directions for this work. One of the possible improvements for cSQuad and other soft robots that we've made is to get rid of the hard components as much as possible. To make this happen, the use of a new type of locomotion control that uses soft sensors instead of rigid encoders were recommended. Finally, embedding the electronic traces inside the soft body of the robot by using silver ink printing technology was discussed.

Chapter 2

Design, Fabrication and Control

This chapter presents the design, fabrication, and control stages of the compressible soft quadruped. The compressible soft quadruped robot presented in this work is the final version of a series of quadruped robots that have been designed and fabricated in Bilkent Miniature Robotics Lab. In order to understand the robot fully, one has to inspect its predecessors as well. Therefore at the beginning of the chapter, the first C-Legged quadruped (CQuad) and the first soft quadruped (SQuad) that we fabricated are presented. Later, the design and fabrication of the compressible soft quadruped (cSQuad) is explained in detail. Moreover, the control method for SQuad and cSQuad is presented. Some of the content of this chapter was published in [28] and [1].

2.1 Examining CQuad, the Predecessor of SQuad and cSQuad

C-Quad is a miniature quadruped that is made out of PET sheets. The flat PET sheets are cut in a laser and then it is folded to obtain the legs and the body of the robot. The fully assembled CQuad is presented in Fig. 2.1. This work was published in the IEEE ROBIO Conference in 2017 [28].

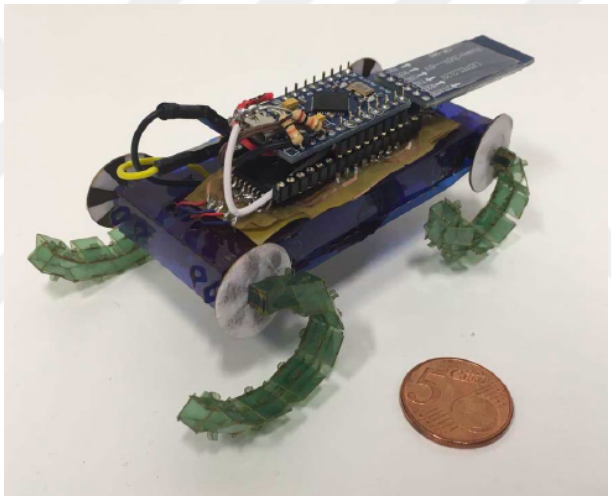

Figure 2.1: Fully assembled C-Legged Quadruped: CQuad

CQuad is an important milestone for the cSQuad because just like cSQuad, it has four C-shaped legs that are driven individually using micro DC motors. One of our initial aims with this robot was to obtain complex maneuvers such as in-place turning. This required controlling every motor individually where a position value is assigned for every leg. We used a primitive design which contains of an infrared light sensor and a disc of black and white stripes as our initial sensors. The motor-sensor assembly design, the encoder disc design and their assembly is presented in Fig. 2.2.

CQuad provided a great amount of know-how for our future soft quadrupeds because it contained every required feature to build an untethered, miniature, light-weight robot. It taught us how to design electronic circuits, how to control four individual motors and how to interpret sensor feedback.CQuad also showed

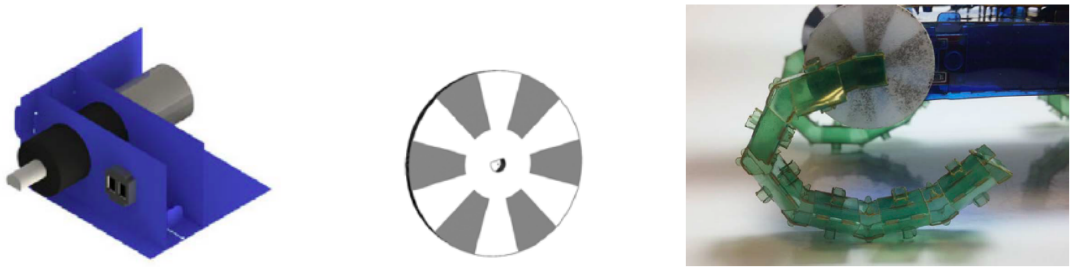

(a) (b) (c)

Figure 2.2: (a) Micro DC motor and IR sensor. (b) Black and white stripped encoder. (c) Close view of the encoder with folded C-shaped leg.

great performance regarding speed and maneuverability. It could reach speeds of 2.7 body lengths per second and it could scale objects as high as 0.64 times its body height(2.5 cm.). The screen shots for the climbing experiments can be seen in Fig. 2.3. However, the fact that this robot was made out of fully rigid components made its ability to conform less compared to soft robots. We believed that making the body and the legs of the robot from soft materials would increase the obstacle scaling performance and the robot could adapt better to unstructured surfaces which may be crucial for some search and rescue operations. Hence, we continued to make the soft version of CQuad which we named SQuad.

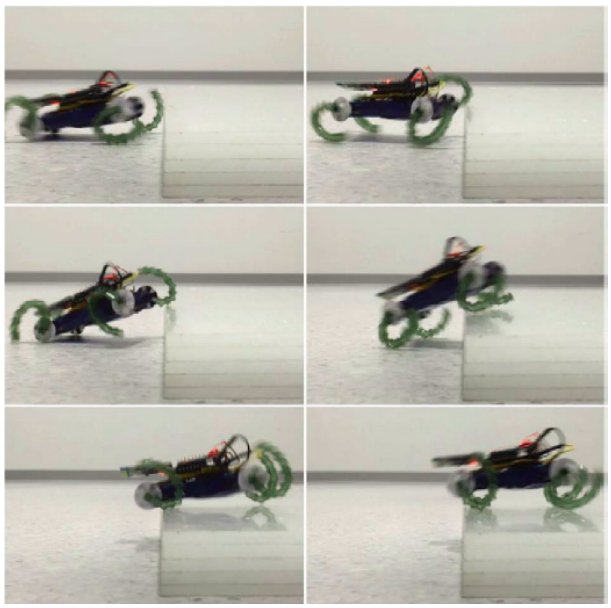

Figure 2.3: Obstacle climbing experiment of CQuad

2.2 Design and Fabrication of SQuad

SQuad is the first soft quadruped that we have designed and fabricated in our laboratory. It has four soft C-shaped legs that are controlled individually and its body is soft as well. It is the successor of CQuad and even though they share many aspects, they are also very different. The first difference is the material that was used in SQuad, which the selection process is discussed in this section. The fact that we use a different material changes every step of our fabrication methods and design processes as well and they are explained in detail in this section. Finally our electronics design and PCB fabrication was explained at the end of the section. This work was published in the IEEE Robotics and Automation Letters [1] and an assembled version of the robot can be seen in Fig. 2.4.

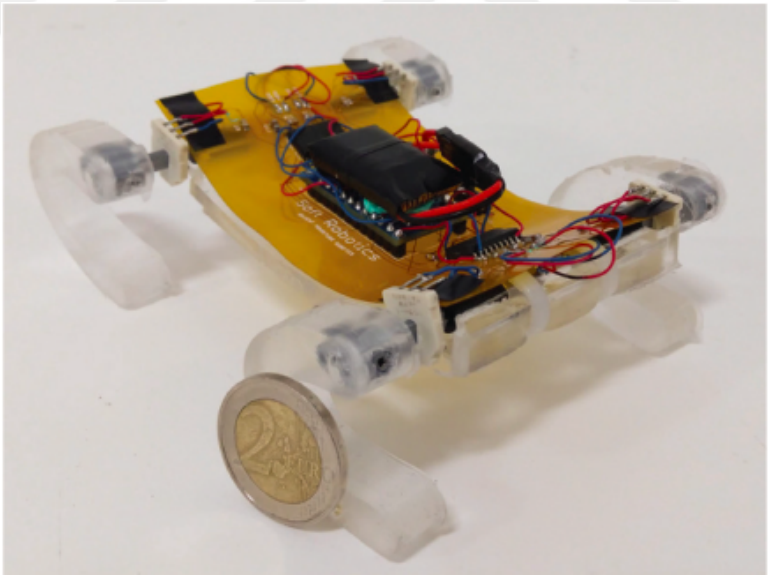

Figure 2.4: Assembled version of SQuad [1]

2.2.1 Material Selection

Like most soft quadrupeds, SQuad is intended to be a biologically inspired robot. Its aim is to reach and even surpass the locomotion and climbing performances of some mammals in the same weight category such as mice. This was a starting point for the material selection and a decision had to be made about how soft the

material was going to be. It had to be soft enough to utilize the advantages of being soft and not too soft that it cannot support itself structurally. We decided that PDMS (Polydimethylsiloxane) was a good candidate as it was a medium soft material in the Shore A scale. Our initial tests showed that this material could withstand the weight and additional forces on the robot and it could provide acceptable traction during locomotion. Hence, we continued with using PDMS.

2.2.2 Fabrication Guidelines for Soft Polymers

As mentioned earlier, switching from using hard materials to soft materials requires change in every fabrication steps. In this section, the general guidelines on how to fabricate soft polymers will be discussed in detail. Note that these are only general guidelines and specific information regarding material properties and additional steps will be given in the following sections.

The first step is to prepare a mold. The mold should have to be designed in a way that the fabricated part could be removed easily after it's cured. To achieve this, the concave features must be avoided as much as possible as it might cause the part to be removed impossible. Also, thin features tend to break or rip apart easily compared to thick features. After the mold is fabricated using a CNC (computerized numerical control) machine or a 3D printer, it should be sprayed with a mold release agent specific to the material being used.

Second step is to prepare the polymer. For PDMS, a two-part solution has to be prepared. The first part is the polymer itself and the second part is the curing agent. They should be added into a cup at a specific weight ratio and then they should be mixed thoroughly. The change in mixture ratio will result in different material properties and different curing times. The two parts required for making PDMS is presented in Fig. 2.5.

Third step is to degas the polymer. During the mixing part, some bubbles form inside the solution and if these bubbles are not removed, it results in trapped air inside the part which changes the strength of the part unpredictably. Therefore,

Figure 2.5: Two parts required to make PDMS

we put our solutions inside a custom-built vacuuming system where the bubbles are sucked out of the solution under low pressure. This process is repeated until there are no visible bubbles in the solution. The vacuuming system that consists of a pump and a vacuum chamber is presented in Fig. 2.6.

Figure 2.6: The vacuum setup for degassing the polymers

Fourth step is to pour the solution into the mold and to put the mold into the oven. The oven temperature usually does not change the material properties,

however it changes the curing time considerably. For most of our parts, we use 60 degrees Celsius which cures the PDMS in two hours. The oven that is used for curing our polymers is presented in Fig. 2.7.

Figure 2.7: The oven used for curing the polymers

The final step is to remove the part from the mold after the curing is complete. A set of tweezers with dull edges makes it easier to remove the part without ripping it apart.

2.2.3 Body Design and Fabrication

The first design iterations of SQuad's body were challenging since it was the first time that we've used molding and casting as a fabrication tool and it required thinking backwards and always thinking a few steps ahead. Since we don't have any injection molding equipment in our lab, our designs were limited by our fabrication methods. As explained in the last section, we fabricate our soft parts by pouring PDMS directly into the 3D printed molds. This means that we can have more complicated shapes at the bottom of the mold, but the top part should always be flat due to gravity. The initial design for the body of SQuad is presented in Fig. 2.8. In this design, the bottom of the body is completely flat whereas

some cavities and complex shapes are present in the top surfaces of the body. The top surface of the body corresponds to the bottom surface of the mold and vice versa. In this design, the openings for the motors are obtained by placing a 7 mm metal rod inside the mold and these rods are removed when the PDMS cures fully using the openings at the top of the body as it can be seen in Fig. 2.9.

The length, the width and the thickness of the body are 100 mm, 55 mm and 7.5 mm respectively. This body design was used in our Robotics and Automation Letters publication [1] as it can be seen in Fig. 2.4.

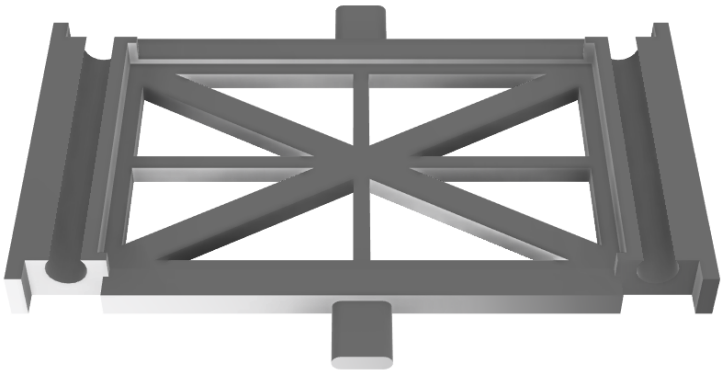

Figure 2.8: The initial design for the body of SQuad

A stiffness study was done in order to demonstrate the flexibility of the soft robot.The analysis tool of the Autodesk Fusion 360 CAD software was used to perform the analysis. The Young's Modulus of 10:1 ratio PDMS is found as 1.37 MPa using a tensile testing machine. The X axis is along the length of the body and the Y axis is along the width of the body. The stiffness around the Y axis was found to be 0.4316 N/m for the soft PDMS body and the stiffness around the X axis was found to be 4.62 N/m. Later on we improved this design so that it preserves its flexibility characteristics but it is easier to fabricate and assemble.

In the second iteration of the body design our first priority was to fix the rotary encoder sensors in the body so that they cannot move relative to the body. This is important because once the sensors rotate with the leg, the data is shifted as the amount of the encoder rotation which gives us false data and confuses the control code that we use. This results in imperfections in gait control of the legs and reduces the control performance considerably. The new and final design

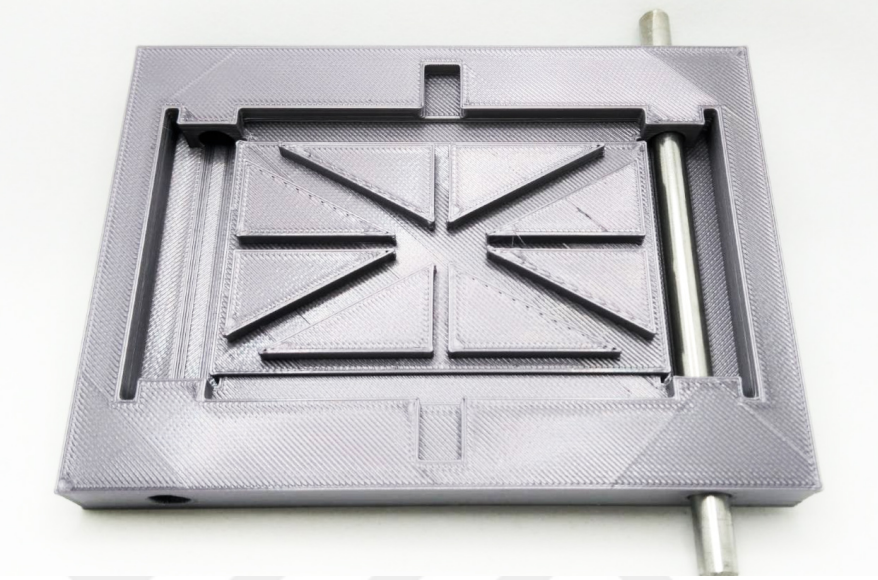

Figure 2.9: The 3D printed mold with 7 mm rod (right side) for the initial design for the body of SQuad

for SQuad's body can be seen in Fig. 2.10. In this design it can be seen that every sensor has a specific groove where they can be placed on the body. These grooves ensure a tight fit of the sensors hence the performance of the control code is maximized. It also solves some alignment issues which helps the components to wear less during operation.

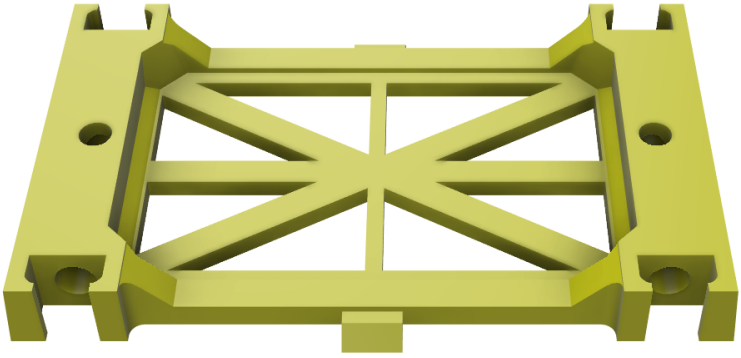

Figure 2.10: The final design for the body of SQuad

There are some other improvements as well, such as the redesigning of the motor holes. In this final iteration, instead of using a metal rod we designed a 3D printed motor cap that is screwed on to the body from 4 sides of the mold as can be seen in Fig. 2.11. To make it easier to understand, the bottom right

motor cap was removed from the design in Fig. 2.11. Additionally, by adding a small cylindrical prism at the bottom of the mold, we obtain an opening at the top of the body for the motor cables to exit the body.

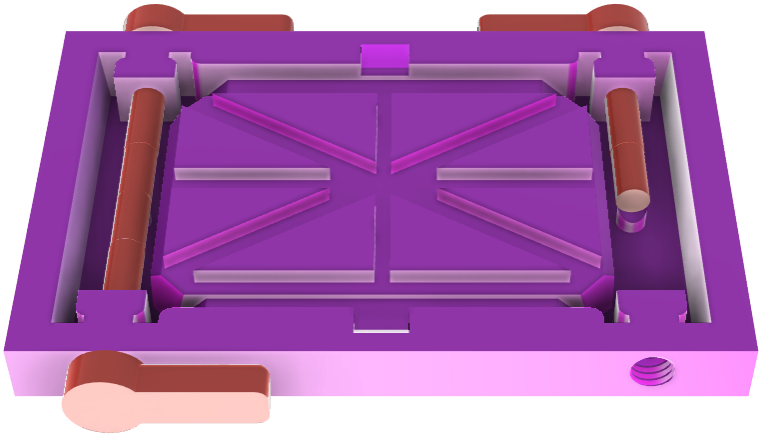

Figure 2.11: The 3D printed mold with the 3D printed motor caps for the final design for the body of SQuad

The motor caps of which one of them is presented in more detail in Fig. 2.12, create a hollow tube for the motors to sit tightly inside the body. Once the body is cured, these motor caps are removed by rotating them anticlockwise. The surface that was highlighted with blue in Fig. 2.12 has a smaller diameter than the base of the motor cap which allows the motors to sit more tightly inside the body without any use of glue, tapes or cable ties. Hence, we obtain a cleaner, less crowded body and it also makes the assembly easier.

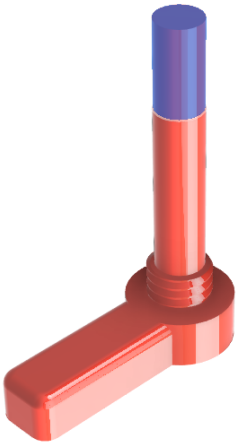

Figure 2.12: The 3D printed motor caps used in the final body design of SQuad

Finally, the mold presented in Fig. 2.11 incorporates almost no sharp edges or straight walls as opposed to the mold in Fig. 2.9. The sharp edges were smoothed by adding a chamfer or a fillet during the design stage and the straight walls that are especially deep as well were given a slope of at least 5 degrees in order to make it easier to remove the PDMS body from the mold. These modifications drastically reduce the scrap rate and they improve the quality of the fabricated body because without them the body tends to partially rip apart during the removal process.

The PDMS body fabricated with the final version of the mold is presented in Fig. 2.13.

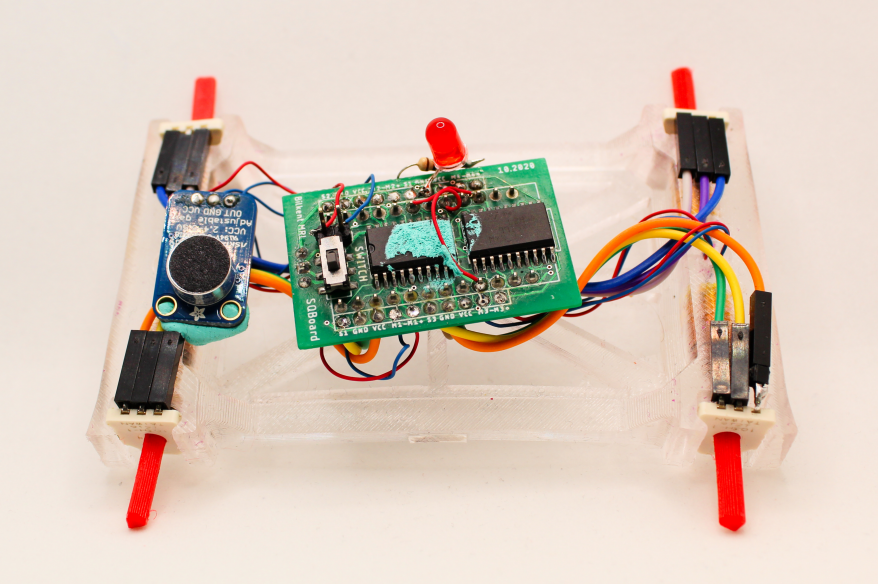

Figure 2.13: The fabricated PDMS body of SQuad

2.2.4 Leg Design and Fabrication

In order to utilize the softness of the robot to the maximum possible extent, a simple leg design is chosen. A simple leg design would allow the body to adapt to the surface conditions without requiring much control effort. Among potential candidates, c-shaped legs, first introduced in Rhex [29], were chosen because of their impressive obstacle scaling capabilities. It is also a design, whose stiffness

can easily be manipulated using different materials, and it can be manufactured easily. Its rounded shape provides the distribution of stresses upon impact. Last but not least, such a leg design has previously been shown to work on miniature legged robots [28], [30]. The reasons given above lead us to design and fabricate specially designed c-shaped legs to be used for SQuad locomotion. In order to make the c-shaped legs strong enough to carry the robot's weight; different thicknesses and radii were put to trial and a crude search on the c-shaped leg design space was carried out. The analysis tool of the Autodesk Fusion 360 CAD software was used in order to estimate the displacements and stresses. By improving and iterating the c-shaped leg design, the dimensions of the leg are determined in order to make four legs carry the robot (refer to Fig. 2.14).

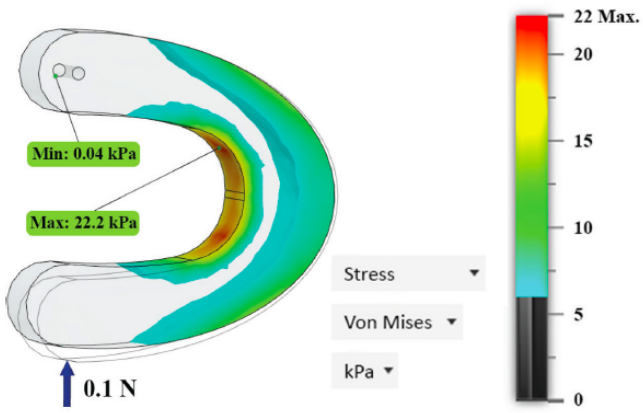

Figure 2.14: Stress analysis of a c-shaped leg.

The Young's Modulus of 5:1 ratio PDMS is found as 1.54 MPa using a tensile test machine The analyses distributed the weight of the body and external components such as the PCB and a battery to four legs in order to see if they would be able to carry the body. One single leg supports about 10.15 grams of mass and this corresponds to a displacement of 2.75 mm at the tip of the leg using the current design. Therefore the stiffness of the PDMS leg becomes 36.17 N/m. The maximum length of the leg in x and y directions are 36 mm and 40 mm, respectively and the thickness is 10 mm. The weight of a single PDMS leg is 7 grams. Initial mold design of the leg is presented in Fig. 2.15.

In order to attach the leg to the motor, there should be an interface between

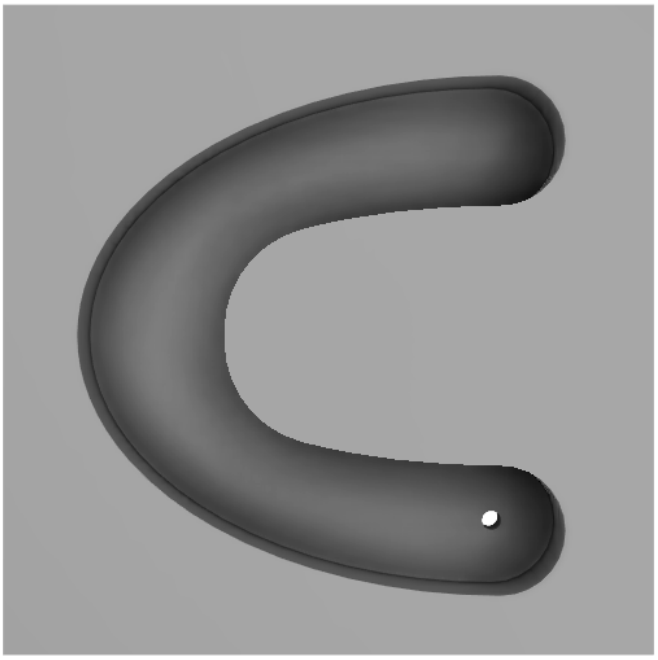

Figure 2.15: Mold design for the c-shaped leg

them. First generation legs that we produced had a 3D printed motor connector part that was embedded inside the leg during the curing process. This part, that is shown in Fig. 2.16, gives the leg the ability to be connected to the motor. This part is fixed inside the leg and it is not removable as seen in 2.17. After the leg is cured, first a rotationary encoder sensor is assembled onto the D-shaped shaft and then the D-shaped tip of this part is glued on the motor shaft. However, once the motor shaft is glued to the motor connector, the system becomes impossible to repair in case of a failure. It means that we cannot change any part if it's broken without scrapping the rest of the components. For example if a motor stops working it means that the leg is also going to be scrapped. In order to solve these issues a new design was proposed that is presented in Fig. 2.18.

The new motor connector design allows us to change the sensors in case of a failure. It also allows the legs to be changed just like a regular car tire. It also solves the problem of leg directions. In the old design, the legs had to be manufactured with a specific direction in mind. The left side of the robot and the right side of the robot has legs that are mirrored and they had specific molds for the left and right legs. If a right leg was broken it couldn't be replaced with

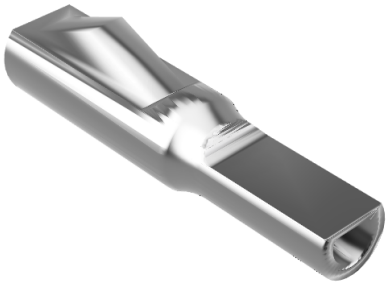

Figure 2.16: Initial motor connector part for the c-shaped leg

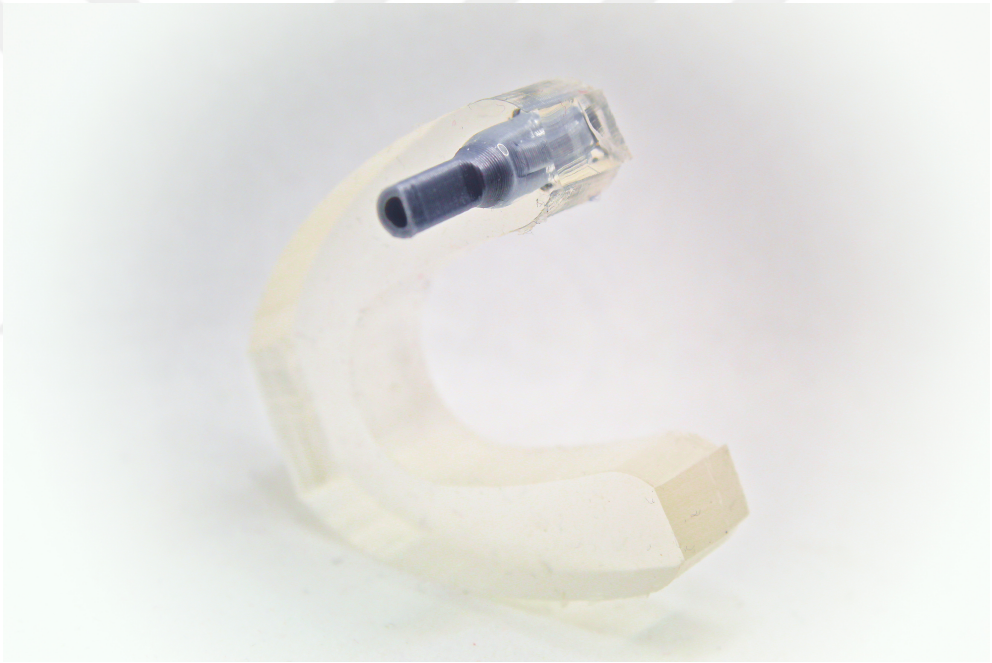

Figure 2.17: Initial motor connector embedded in PDMS leg

a left leg since they were not compatible. With the new design it is possible to remove the leg, then flip its direction and then attach it back to the motor shaft which gives us flexibility in reusing the parts. In order to visualize it better the assembled version of the leg, the sensor and the motor is presented in Fig. 2.19.

In order to obtain the system presented in Fig. 2.13, first the motor connector assembly (refer to Fig. 2.18) is embedded inside the mold shown in Fig. 2.15. The motor connector assembly has a 3D printed grey(female) and a red(male) part. The grey part has an M3 thread where a setscrew can be screwed on. After the red part is placed inside the grey part, the setscrew is tightened and it fixes

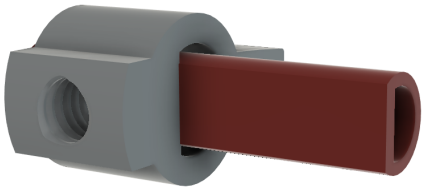

Figure 2.18: Final design for motor connector assembly

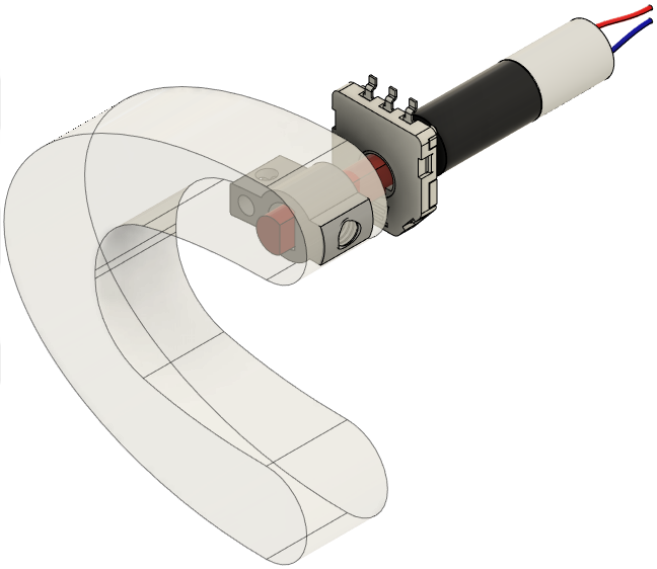

Figure 2.19: The c-shaped leg along with the sensor and motor connector

the red part into the gray part. After the mold is cured, the set screw is loosened and the red part is removed. Later on, the red part is glued on to the motor shaft. Hence, the motor can be attached to any leg design, regardless of being in the right or left configuration, that contains the female grey part. It gives us great flexibility when we iterate our designs to find the best possible leg design or when we replace a broken part.

2.2.5 Tail Design and Fabrication

One of the benefits of having soft materials in a robot is to take advantage of the conformity that these materials provide. Confirming to the surfaces during locomotion, increases performance during climbing or scaling obstacles. We wanted to measure the maximum climbing slope that the SQuad can achieve and in order to do this, we added a tail structure onto the robot. This tail can be added or removed depending on the required task that robot is supposed to achieve. The design is presented in Fig. 2.20.

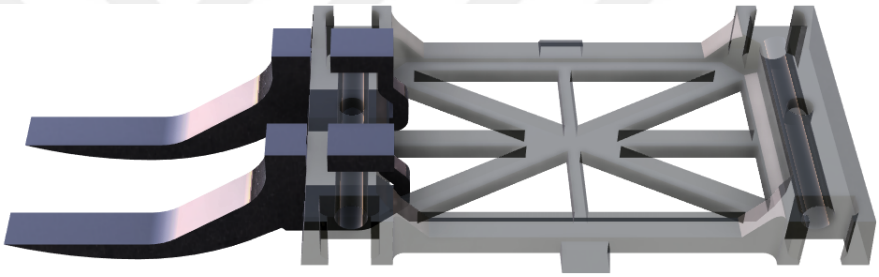

Figure 2.20: The tail design assembled onto the SQuad's body

As mentioned, this tail is not embedded in the body and it is fabricated separately. We used a soft thermo polyurethane (TPU) filament and printed this part with a 3D printer. It is designed in a way that it can be assembled by attaching only 2 cable ties through the holes that were highlighted with blue color in Fig. 2.21.

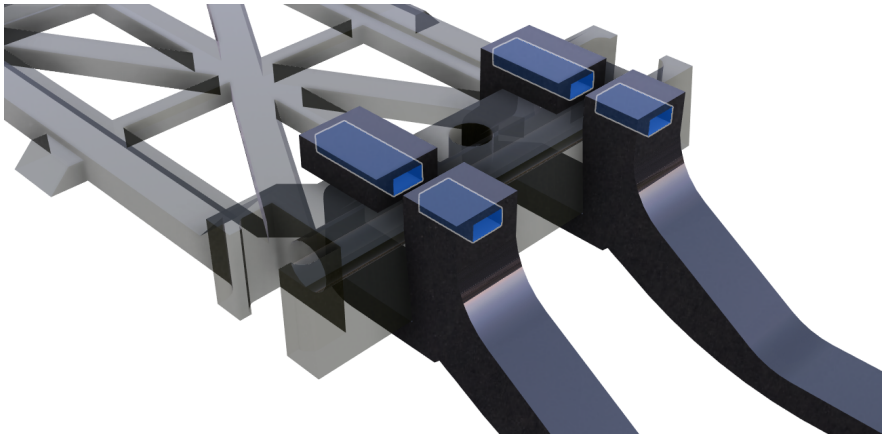

Figure 2.21: The tail design assembled onto the SQuad's body

2.2.6 Electronics Design and Fabrication

In this section, the design and fabrication steps of the electronic board of the SQuad will be presented. Firstly, the design of the board and the logic behind it will be discussed. And then the different fabrication attempts will be explained. In order to fabricate the PCB for SQuad, we have tried several different methods. All of the methods will be discussed separately in the following sections.

2.2.6.1 Design of the PCB of SQuad

Before starting a new electronic design we should determine the requirements that the PCB should satisfy. First of all, we are required to drive 4 micro DC motors using feedback from 4 encoder sensors. Along with these, a micro controller is necessary to embed our control code and to give commands to the motors. Hence, basically we need motor drivers and a micro controller as our fundamental components.

L293DD motor drivers are based on an H-Bridge design and one of them can drive 2 DC motors. Hence, we use two L293DD motor driver integrated circuits (IC's).

Arduino Pro Micro has been used in our previous robots and it proved itself to be capable of completing the required controlling tasks and also it is one of the smallest and lightest micro controllers in the market. Hence, it was our first choice to use with SQuad.

Additionally a voltage regulator had to be used. In order to keep the weight of the robot minimum, we use a single cell 3.7 V lithium ion battery. Arduino Pro Micro does not have an onboard regulator to step up this voltage to 5 V. Hence we use a 3.7 V to 5 V step-up voltage regulator.

There are some other non-essential components such as a switch to be able to turn on or off the robot and some capacitors to act as a high pass filter to smooth

the data coming from the sensors and the data going to the motor drivers. These capacitors improve the quality of the signals and hence improves the performance of the controller.

First of all, the necessary components are added into the schematic design window of Autodesk Eagle Software. The connections made for the Arduino Pro Micro and the connections required for powering the system are presented in Fig. 2.22.

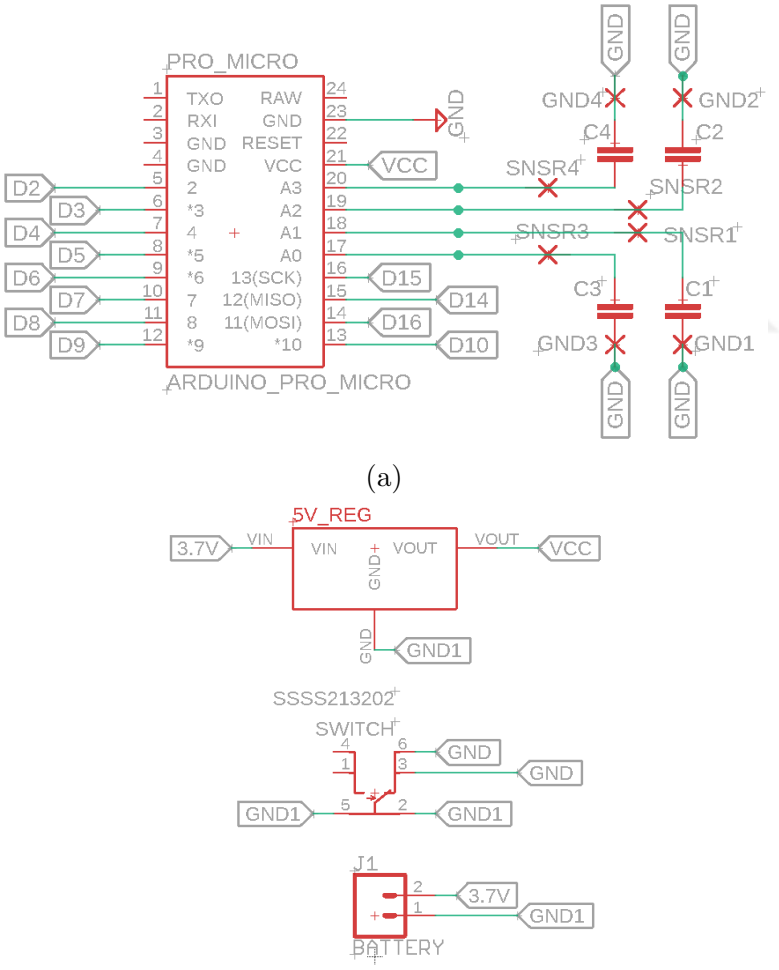

(a)

(b)

Figure 2.22: (a) Arduino schematics for SQuad PCB. (b) Power schematics for SQuad PCB.

In the schematic design, we first choose the pins that are going to be used and labels are assigned to them. For example "D2" label in Fig. 2.22a means that the

digital 2 pin of the Arduino is labeled and it can be connected to other pins in the design. The pins that are able to generate PWM (pulse width modulation) signals are assigned to be used for motor enable pins. In SQuad's case, D3 D5 D6 and D10 pins are connected to the enable pins of the L293DD motor controllers as seen in 2.23. The rest of the digital pins of the Arduino is assigned only for controlling the directions of the motors. The four analog reading pins of Arduino; A1, A2, A3, and A4 are connected to the sensor signals along with SMD capacitors with a value of 0.1 μF as seen in Fig. 2.22a. The connections for the voltage regulator, the switch and the battery pins are also presented in Fig. 2.22b.

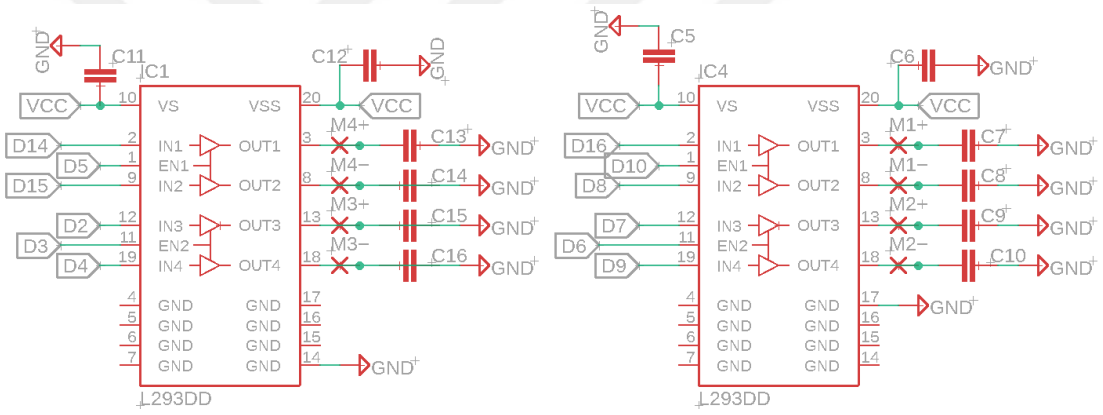

Figure 2.23: The schematic for L293DD motor drivers of SQuad PCB

The L293DD is a two channel motor driver and it requires 3 signals to run a single motor. As mentioned before, 1 of them is an enable signal which regulates the speed of the motor using PWM signals. As the duty cycle of the signal increases, the speed of the motor increases. The other 2 pins are both digital and they control the direction. If opposite values are given to these 2 pins, the motors turn in one direction. And if the values are reversed, the motor turns in the reverse direction. These 3 pins are connected for 4 individual motors as seen in Fig. 2.23. From the same figure it can be seen that the motor outputs are connected to surface mount device (SMD) capacitors to ensure a smoother signal. And the VS pin which powers the motors are directly connected to the voltage regulator so that the power hungry motors do not damage the integrated circuits.

Once the schematic design is complete, the physical board design is initialized

in the same software. The size of the board was adjusted to be the same as the top surface of the SQuad's body and the required components were placed in a way that soldering them would be convenient as seen in Fig. 2.24.

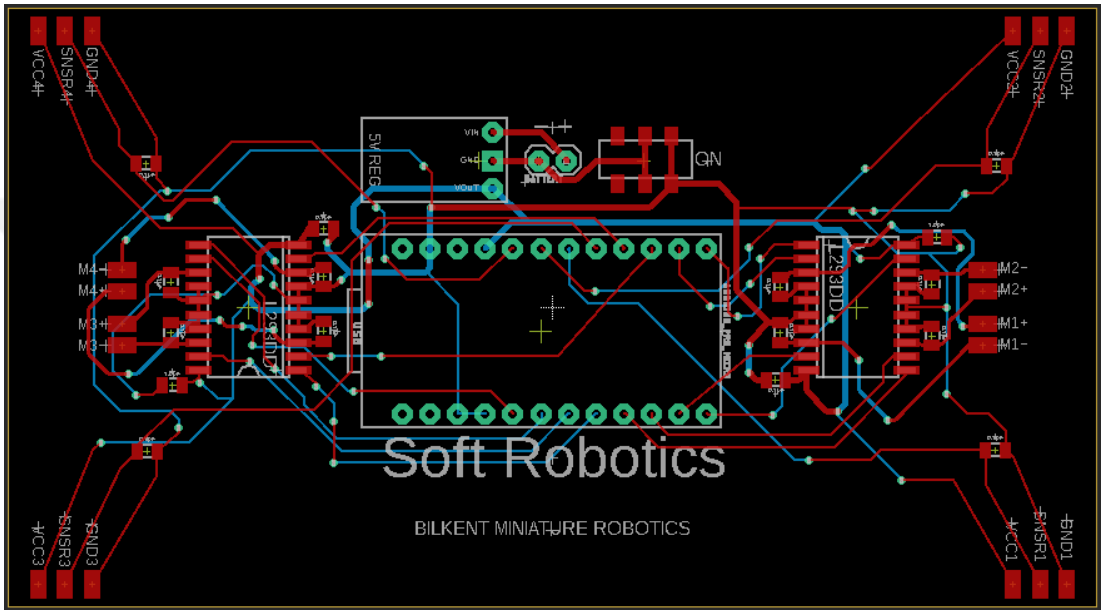

Figure 2.24: The board design for SQuad PCB

2.2.6.2 Fabricating the PCB of SQuad

The PCB of SQuad was planned to be made out of flexible materials. Otherwise, a rigid PCB that is made out of FR4 (Flame Retardant 4) or FR2 boards would increase the stiffness of the robot considerably, invalidating our efforts of making a soft robot.

To make a soft PCB, we tried several methods. First, we tried to make these PCB's in our lab. A flexible double sided copper sheet was cleaned and coated with black nail polish. Then, the traces were etched from the copper sheet using a carbon dioxide laser, removing the nail polish and exposing the copper. The exposed copper parts were chemically etched using hydrochloric acid and hydrogen peroxide. Finally, the surface that was protected with nail polish was removed using acetone. We obtained promising results with this method, but since our boards were double sided, we almost always had issues with aligning

the two sides of the board. In order to solve the alignment issues and have a precise and controlled environment during manufacturing, we decided to use a 2 axis CNC system which transfers ink onto the flexible copper sheet. Hence, we used an existing pen plotter design and we built a plotting machine which drew our traces onto the copper using special types of inks that protected the traces during chemical etching of copper. The main issue with this process was that the pen tips were too wide to create our desired traces and we almost always had short circuits between traces. It was decided that even though we were able to make some working PCB's manually, it was extremely labor intensive and it was more feasible to outsource this job. Therefore, the final PCB's were ordered from China. Double-sided copper-clad polyimide film, which is a flexible material was used for making our PCB's. One of them is presented in Fig. 2.25.

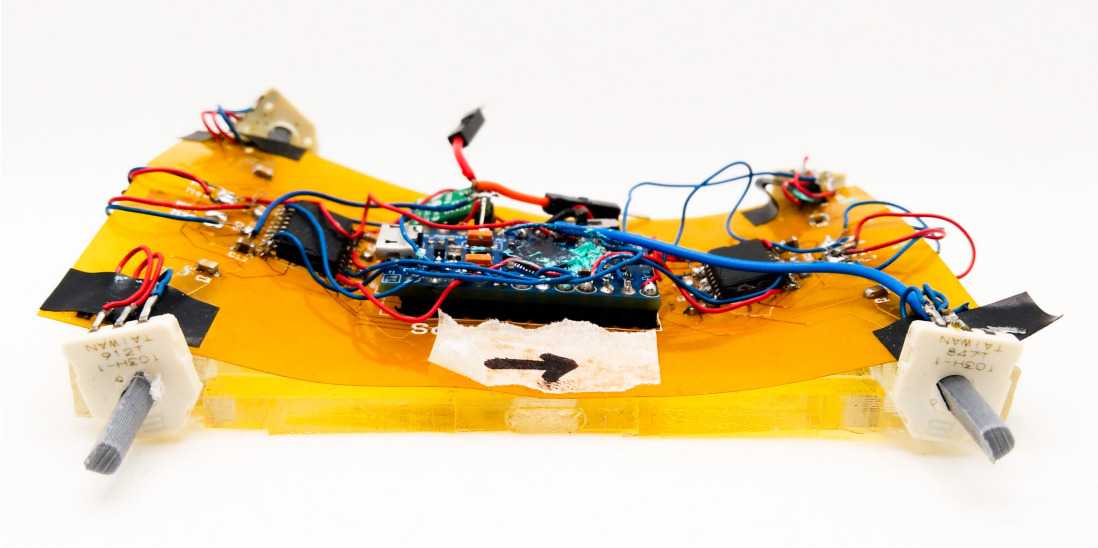

Figure 2.25: The PCB manufactured in China for SQuad on the initial version of the soft body

2.2.7 Assembly of SQuad

After every component was designed and fabricated, the assembly process of the SQuad began. First, the assembly was done on a CAD software to make sure there were no dimensional error on the parts. The 3D CAD image of the assembled SQuad is presented in Fig. 2.25.

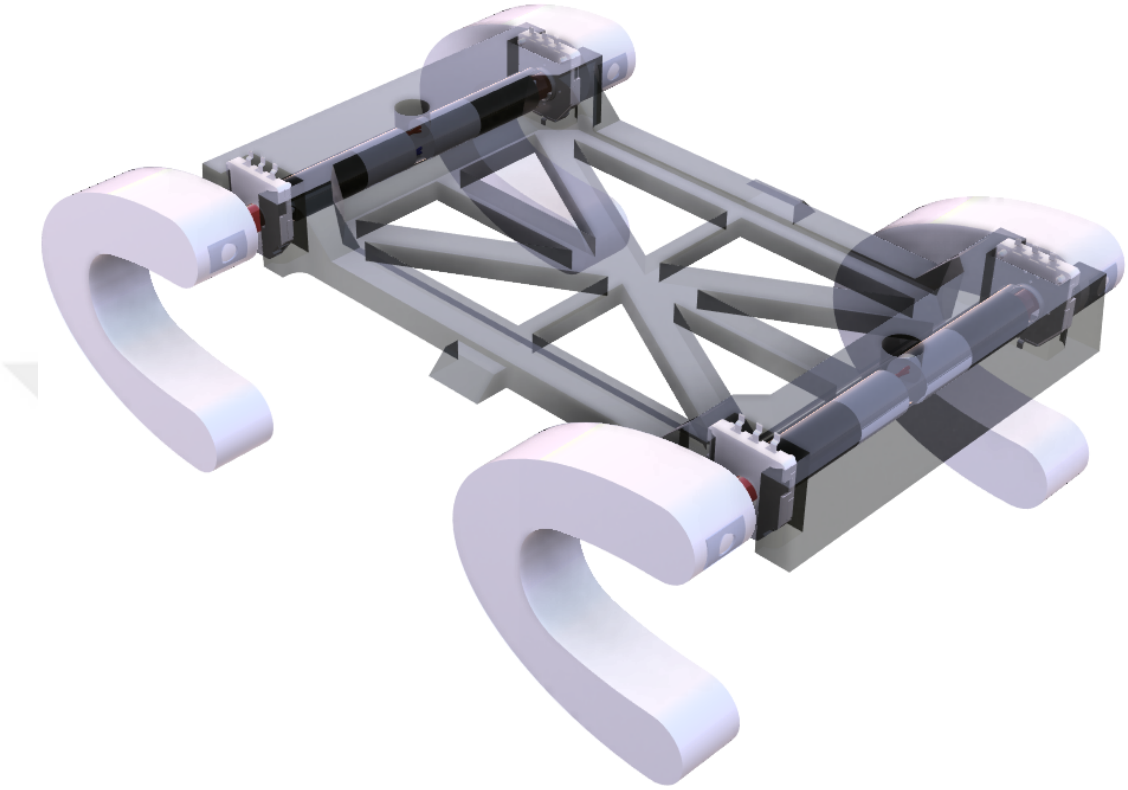

Figure 2.26: The 3D CAD image of the assembled SQuad

Then, the actual SQuad was assembled and some tests were conducted which will be explained in the following chapter. Moreover, at this stage we realized that there was an opportunity for us to fabricate the same quadruped using different materials so that we can compare them during the tests. In order to do this, we fabricated 4 different configurations of SQuad. The first configuration is the original SQuad with a completely soft body and legs which is presented in Fig. 2.27a.

The second configuration is fabricated using the same design but with a fully rigid set of legs made out of PLA using a 3D printer and a fully soft body and it is presented in Fig. 2.27b. The rigid PLA legs were coated with a thin layer of PDMS so that friction coefficients of the legs wouldn't differ during the experiments.

The third configuration is the fully rigid version of SQuad. Both the body and

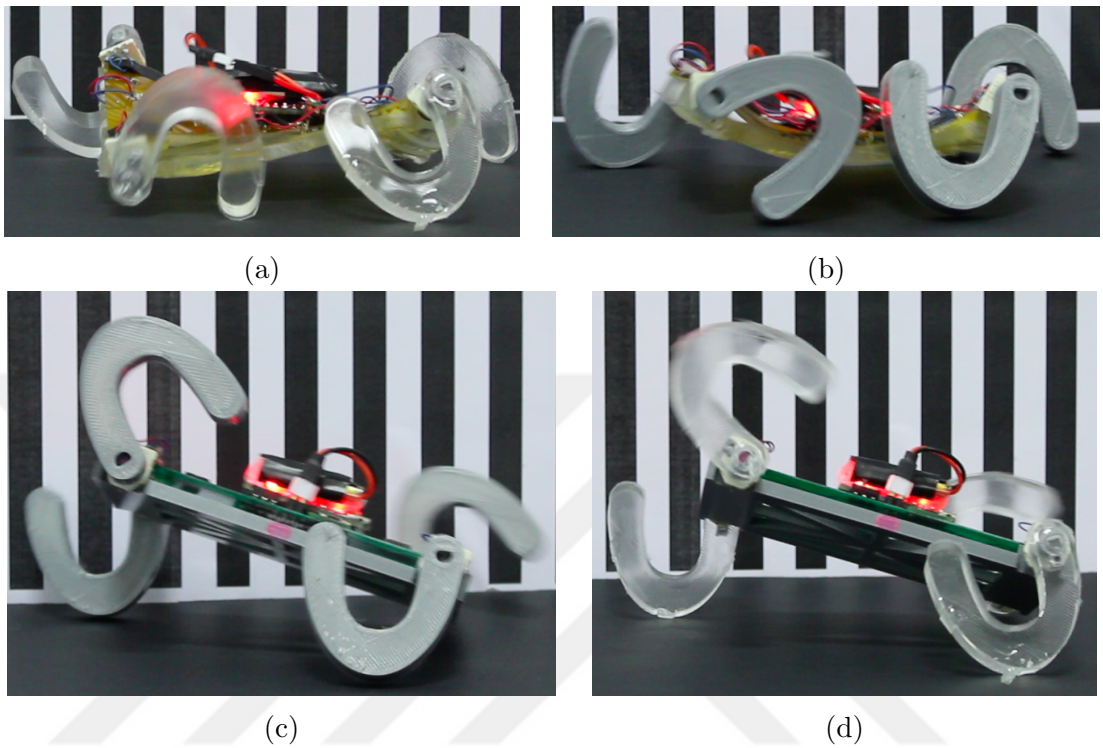

Figure 2.27: Walking pictures of 4 different robot configurations. (a) SQuad, (b) soft body - hard leg, (c) hard body - hard leg, (d) hard body - soft leg.

the legs were 3D printed with PLA and it is presented in Fig. 2.27c. As in the second configuration, the rigid legs were coated with PDMS.

The final configuration has a fully rigid body and PDMS legs and it is presented in Fig. 2.27d.

Every part in every configuration is compatible with each other thanks to the motor connector design that was explained in Fig. 2.18. Hence, any type of leg can be attached to any type of body which ensures flexibility during experiments. It also makes sure that the same set of soft legs or same set of hard legs are used during an experiment for each body so that the minor differences or imperfections of different batches do not effect the experiment results.

2.3 Design of Compressible SQuad (cSQuad)

As the name suggests, the compressible SQuad, cSQuad, is a design based on the original SQuad. The aim with this new design is to better utilize the softness of the robot by giving it the ability to shrink its size which rigid robots do not have the ability to achieve such a task because of their nature. The requirements for this robot is specified so that both the legs and the body should be able to reduce their size by compression. Initially it is aimed that the final design of the robot would be able to reduce its frontal area by 25%.

2.3.1 Choosing Compression Method

The first major decision to make for cSQuad was to find a technique for compression. One of the first techniques that comes to mind is a technique that involves a pneumatic system. However, since we want our robot to be untethered this method seemed to be not applicable for our system. Even though there may be ways to make a pneumatic untethered robot, for example by using small pressurized cans, they need additional actuators, such as an actively regulated valve and they are relatively dangerous to work with in a lab environment. Moreover, these additional parts will not be soft and they will make the robot stiffer. Same is true for pressurized hydraulic systems and both of these suggestions have other major problems such as loss of pressure due to possible leakage or the need to utilize heavy components such as on-board pumps. Therefore, an alternative method was searched and shape memory alloys were the best candidate for cSQuad due to the reasons that are explained below.

Shape memory alloys, SMA's in short, are metals that have the ability to remember a given shape, and when they are deformed, they can go back to the remembered shape by direct application of heat to the metal. There are several materials that SMA's can be made out of. For our system we ordered a specific SMA called nitinol which is an alloy of nickel and titanium. The nitinol wire with a diameter of 0.5mm was ordered and it is presented in Fig. 2.28.

Figure 2.28: Nitinol Shape Memory Alloy wire with 0.5mm diameter

The compression amount in a shape memory alloy is directly proportional to the amount of material. Hence, a long wire is necessary to obtain a decent amount of compression. In order to have this kind of compression in a limited volume, we decided to turn the SMA wires into springs. Even though there are readily available nitinol springs in the market, they usually have too large spring diameters to be utilized in a miniature robot and their wire diameters are also too large, making them unnecessarily thick and heavy. Also, we cannot configure their lengths as well, they are either too short or too long. By ordering the nitinol in the wire form, we were not limited by the prefabricated spring parameters and we could make our own springs. The spring making process is explained in the next section.

2.3.2 Design and Fabrication of Shape Memory Alloy Springs

The first parameter that was chosen was the 0.5 mm diameter of the wire which was the thinnest wire available in the market during the time of purchase. Then the diameter of the spring needed to be determined. We used an M3 (metric

three) threaded rod that had a diameter of 2.8 mm and we wound the spring around this rod. In order to do this, a setup needed to be built. This machine is designed from scratch and it is presented in Fig. 2.29.

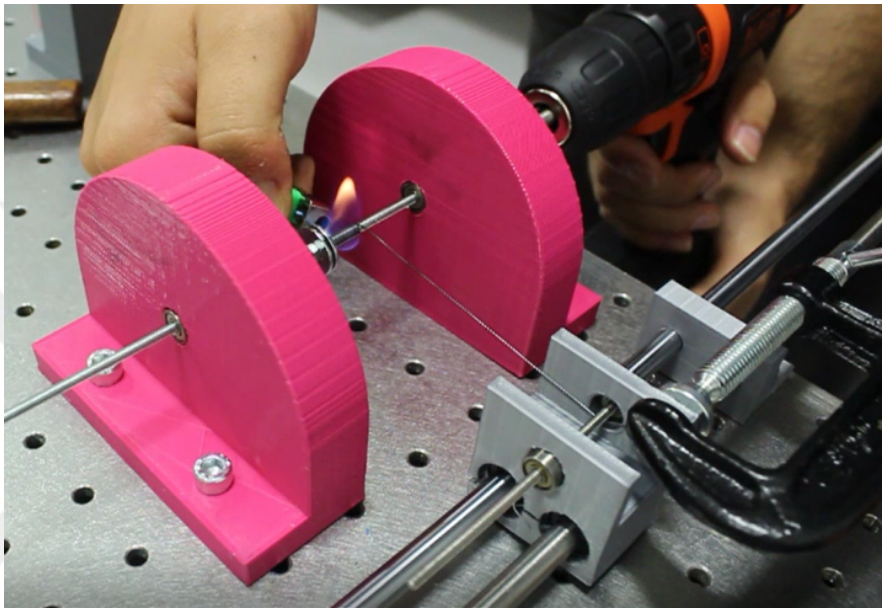

Figure 2.29: Setup for spring making

In the bottom right corner of Fig. 2.29, a clamp can be seen. This clamp makes sure the wire remains tight during the winding process. The 2.8 mm rod is placed between two stands (made out of pink nGen filament) and rotates freely on miniature bearings. One end of the rod is connected to a hand held electric drill which provides the necessary torque required to obtain a tight winding. At the start of the winding process, the free end of the wire is fixed onto the 2.8 mm rod using washers and nuts. As the drill rotates, the spring is created and its length increases proportional to the rotation amount. The clamp, which can freely move in 1 axis is moved conveniently as the spring length changes so that there is a right angle between the wire axis and the rod axis. Once the required spring length is achieved, the winding process stops. However, the clamp and the drill are not released until a memory is given to the spring. To make the SMA remember its spring form, heat must be applied while its movement is restricted. If the movement is not restricted, the metal would want to go back to its old memory which is a straight wire. With the help of the tension in the clamp, the SMA is not able to move during the curing process. We give a new memory to the

SMA by exposing the spring to a lighter flame which can reach temperatures upto 2000° Celsius depending on the type of the lighter fluid. This heating process is applied for at least three minutes and the tension on the wire is released. The excess wire from both ends of the spring is cut with pliers and the 2.8 mm rod is removed from the stands. Finally, the wire is unscrewed from the threaded rod by rotating it counterclockwise just like a standard nut. The resulting spring has an outer diameter of 3.8 mm and it was measured that a spring with a length of 7 mm can extend upto 150 mm. Hence, it shows that it can compress a system down to 5% of its original length which is extremely useful for our purpose. A spring made with this method is presented in Fig. 2.30.

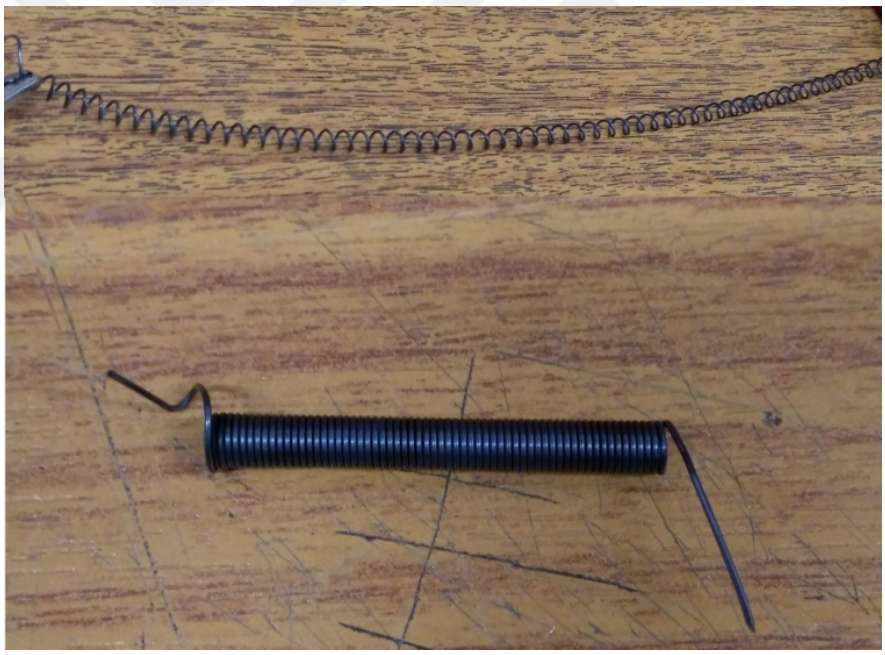

Figure 2.30: Released(top) and compressed(bottom) SMA springs

2.3.3 Leg Design and Fabrication

The initial designs of SQuad did not have C-shaped legs. Initially a four bar linkage design was used in SQuad but these initial designs were scrapped because the four bar legs couldn't support the weight of the robot especially during locomotion. However, for the cSQuad since we plan to embed a metal spring into

the design, we decided to go through with the four bar linkage design expecting that the added springs would give additional strength to the legs.

In this section, initially the four bar leg design is explained in detail. However, after the first results, it was decided to use the C-shaped legs and the design process for them is also explained in this section.

2.3.3.1 Four-Bar Leg Design and Fabrication

Before designing the whole four bar system, the single link that was going to be compressed had to be designed. The main requirement was for the leg to be still operational after it's compressed.

A conceptual design effort was carried out initially to decide on the shape of the compressible link. During these efforts, the main focus was to see whether a design was going to work or not without thinking about manufacturing them using PDMS via molding. The initial designs were inspired form the shape of an accordion and they were fabricated with flexible filaments using a 3D printer and they are presented in Fig. 2.31.

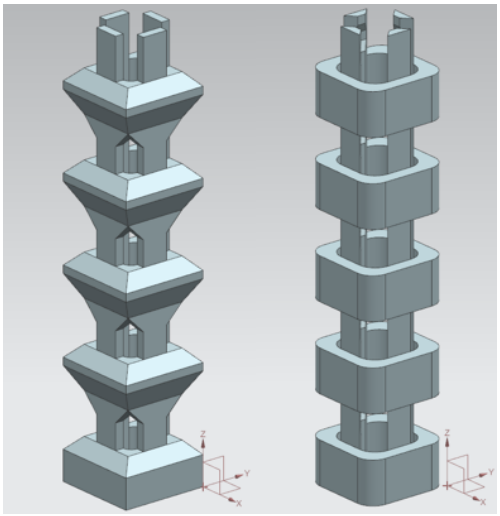

Figure 2.31: Initial leg designs inspired from accordions

The initial designs were fabricated from flexible TPU filaments and they

showed promising results, however it was realized that these designs were not compatible with molding. Molding could be possible but it would be impossible to remove them without breaking the mold and it was inconvenient to make new molds for every single part. Hence, some revisions were made to make these parts compatible with molding. Both the inner and the outer surfaces of the leg were designed using cylindrical features and the new design is presented in Fig. 2.32.

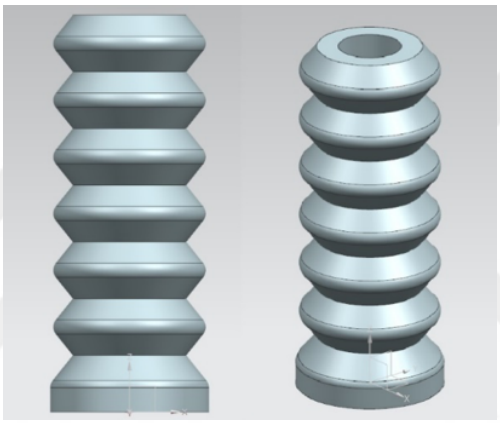

Figure 2.32: Improved accordion leg design

The mold design required to make the leg presented in Fig. 2.32 is presented in Fig. 2.33

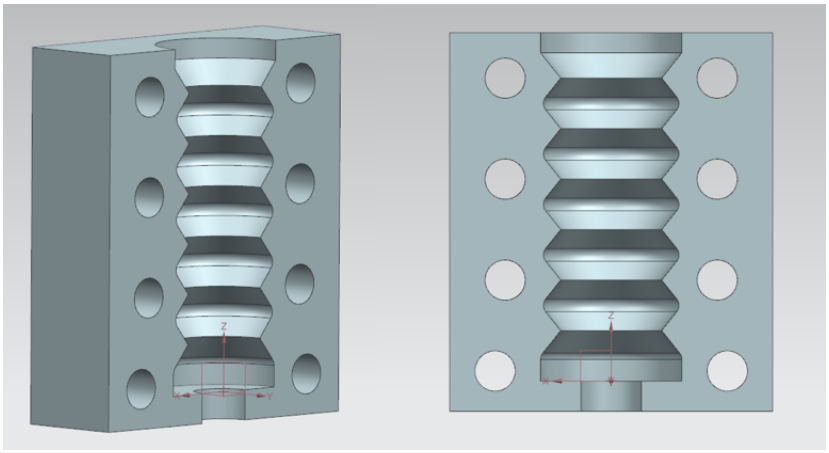

Figure 2.33: The mold design for the accordion leg

The mold for the accordion leg was first used with PDMS, however, it was observed that PDMS was too stiff for this shape. Hence, Ecoflex, a much flexible

material was used instead of PDMS and the fabricated Ecoflex accordion leg along with the 3D printed mold are presented in Fig. 2.34.

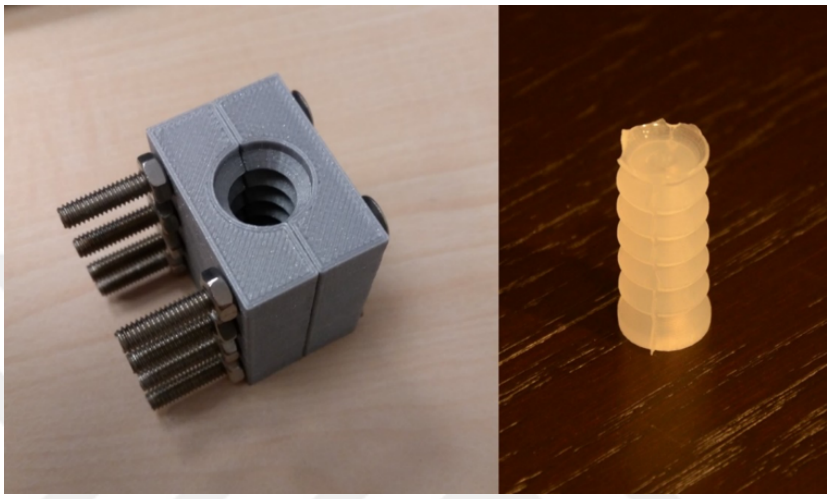

Figure 2.34: The 3D printed mold for the accordion leg (left), and the accordion leg made from Ecoflex (right).

For the next step, the SMA spring was implemented inside the accordion leg. A hollow tube was obtained inside the leg by screwing an M4 (metric four) bolt through the bottom of the mold in Fig. 2.33. After the leg was cured, the spring was assembled inside the leg as seen in Fig. 2.35.

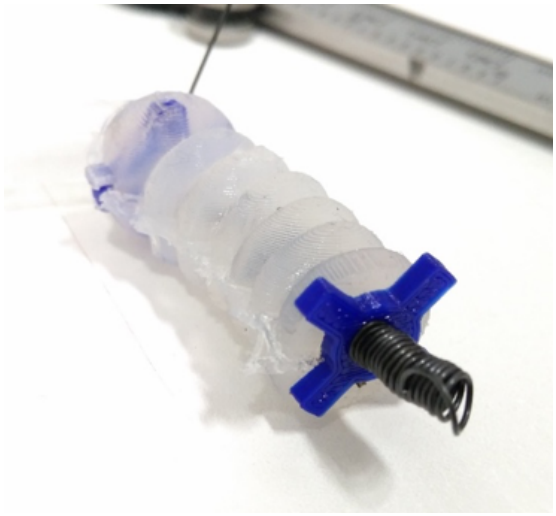

Figure 2.35: The accordion leg with an SMA spring inside.

The blue parts seen in Fig. 2.35 are used to attach the two ends of the springs. A long spring was used in case the portion of the spring inside the leg needed to

be extended. The excess part of the spring that is outside the leg did not have any effect during compression. The initial tests for this leg showed that a 40 mm leg could be compressed down to 30 mm. and the screenshot from the experiment is presented in Fig. 2.36.

Figure 2.36: The initial(left) and the compressed(right) accordion leg with an SMA spring inside.

Since the leg was too flexible, buckling was also observed alongside axial compression. This design which offers 25% compression, was selected to be integrated into the four bar leg system. The initial mold design for the four bar leg is presented in Fig. 2.37.

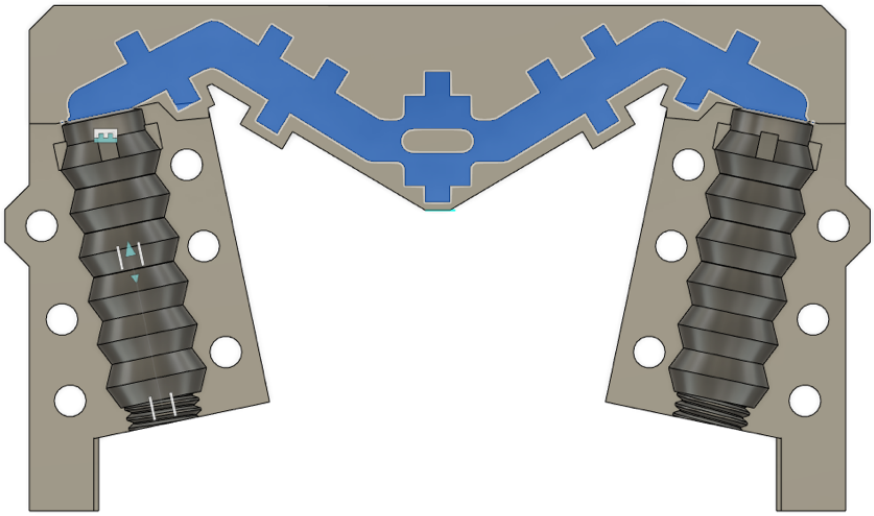

Figure 2.37: The four bar mold design for accordion leg

During first fabrication attempts, it was observed that making the whole part from Ecoflex resulted in some problems especially in the section which is highlighted with blue in Fig. 2.37. This part is where the leg is connected to the body

of the robot and it was seen that Ecoflex is too soft for this interface. Hence, that section was planned to be made out of PDMS. In order to do this, first the Ecoflex sections (the compressible leg sections) were cured first while the mold sit in an upright position. After the curing of Ecoflex was complete, the mold was laid flat on the table and the PDMS section was poured into the mold. The fabricated leg is presented in Fig. 2.38.

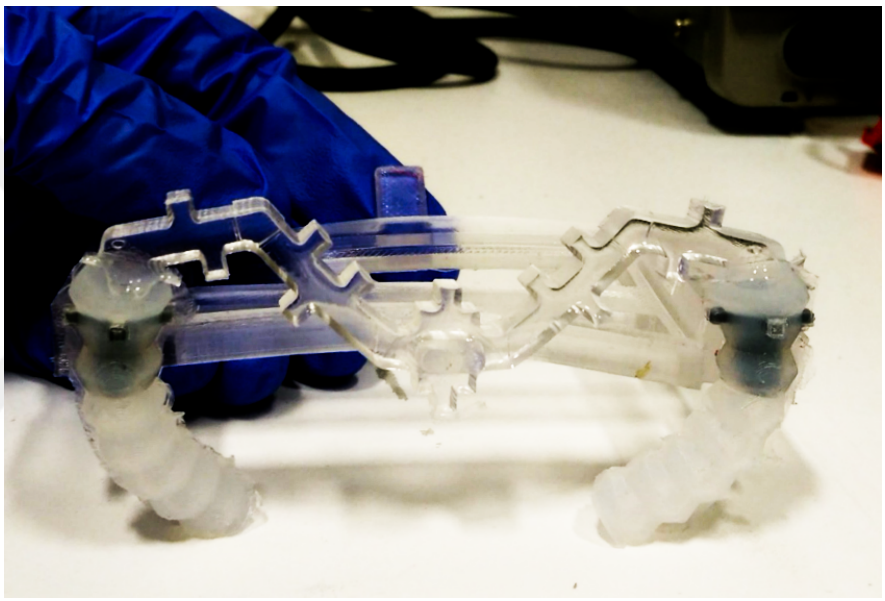

Figure 2.38: The fabricated four bar leg using PDMS and Ecoflex

After the leg was fabricated, it was confirmed that the compression was working as intended. However there were a couple of problems with the leg presented in Fig. 2.38. First, the interface between the PDMS and the Ecoflex was too weak and prone to separating from each other. Even though there were no problems during testing, it didn't reassure us that it would work for longer periods without failing. The second problem was the buckling of the legs. Even after adding springs inside the accordion legs, the four bar leg could not carry the load of the body of the robot properly. It was observed that the buckling of the legs occurred randomly and unpredictably. Even though this problem could have been reduced in way that it doesn't effect the locomotion of the robot, it still caused a lot of unknowns for the modeling team who had to take into account every design parameter. Hence, a new design improvement was made to limit the motion of the leg to only one axis.

The new version of the four bar leg had a piston cylinder mechanism which solved the buckling problem of the Ecoflex part of the leg. The piston cylinder four bar mold design is presented in Fig. 2.39.

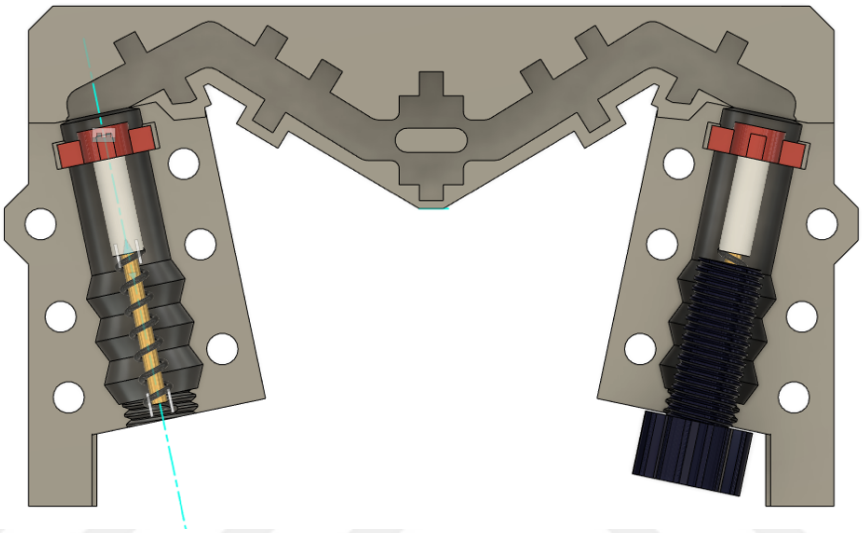

Figure 2.39: The piston cylinder four bar mold design for accordion leg

The white tubes that are used as the pistons in Fig. 2.39 are called PTFE (polytetrafluoroethylene) tubes and they are made out of Teflon. They are commonly used in 3D printers and they have an outer diameter of 4 mm and an inner diameter of 2 mm. These tubes were used because they had low friction coefficients hence they did not require any lubrication which made them ideal for our case. The yellow cylinder in Fig. 2.39 is actually a brass nail that has a hole at its tip for the attachment of the SMA spring. The other end of the spring is attached to the red 3D printed part in Fig.2.39. The dark blue part is a 3D printed bolt on the outer surface and a hollow tube in the inner surface and its job is to cover the SMA springs so that they are not filled with Ecoflex during molding. The 3D printed mold and other required parts for the piston cylinder four bar mold is presented in Fig. 2.40.

The piston cylinder four bar leg design solves the buckling problem completely and it offers a flexible, yet strong leg. However, since half of the leg is filled with a rigid piston, the available length that is possible to be compressed is reduced compared to the leg presented in Fig. 2.38.

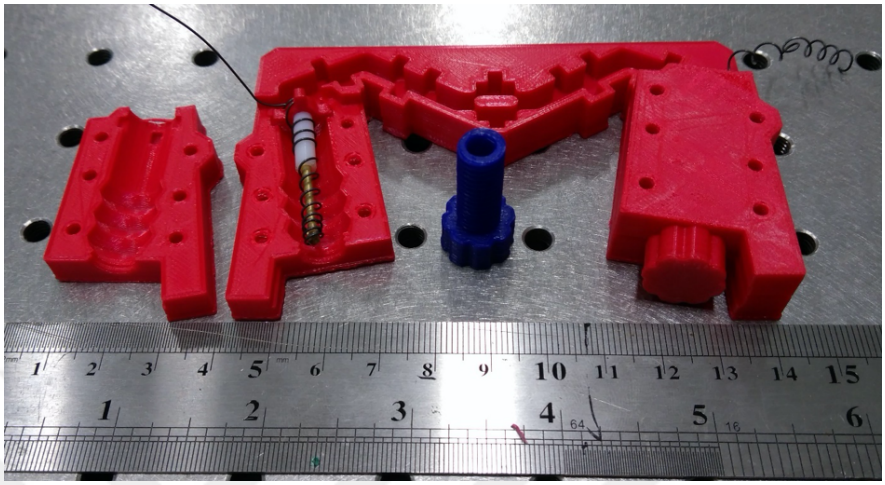

Figure 2.40: The fabricated parts for the piston cylinder four bar mold

The fabricated piston cylinder four bar leg is presented in Fig. 2.41. In this figure, the right leg of the four bar is compressed while the left leg is relaxed. It was observed that the leg was compressed to 26 mm from its initial length of 35 mm. The 9 mm compression amount provides a reduction of approximately 25% in the frontal cross sectional area of the robot.

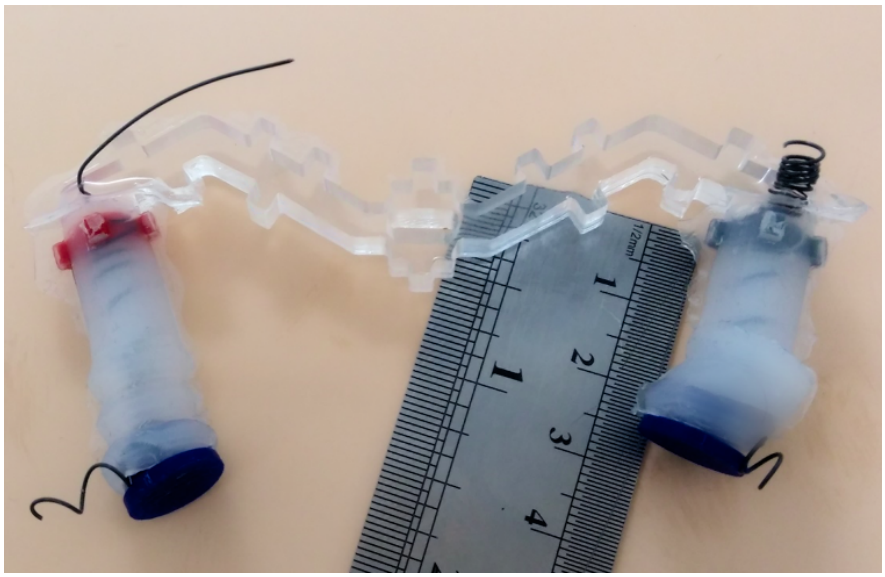

Figure 2.41: The fabricated piston cylinder four bar leg (right side is compressed)

Even though the compression amount and the overall performance of this leg could be improved, it was decided that having a kinematic chain in the form of a four bar mechanism undermined the possibilities and the advantages of the robot

being soft. It was decided that the C shaped legs would be more appropriate to use in a soft robot, hence the design was revised to be used with a C shaped leg in the next section.

2.3.3.2 C-Shaped Leg Initial Design and Fabrication

Unlike the four bar mechanism, the C legs continuously rotate independently from the body. Therefore, the electrical connections pose a great challenge since the cables coming out from the body cannot be connected to the leg directly. Hence, an interface between the electrical cables of the body and the leg needs to be designed. This interface is widely known as a slip-ring and it will be discussed in this section. However, initially the design of the legs will be presented.

Unlike the four bar leg, the C shaped leg does not need to resemble an accordion design in order to obtain a decent amount of compression. In fact, the compression for C leg is more straightforward. Placing an SMA spring between two points on the C leg is sufficient to compress the leg. In this new design, the shape of the C leg is different than the one used in SQuad that is presented in Fig. 2.15. The leg is made thinner in order for it to be compressed more easily. The shape was also simplified in order to make it easier for the modeling team to work on it. The CAD drawings of the new design is presented in Fig. 2.42.

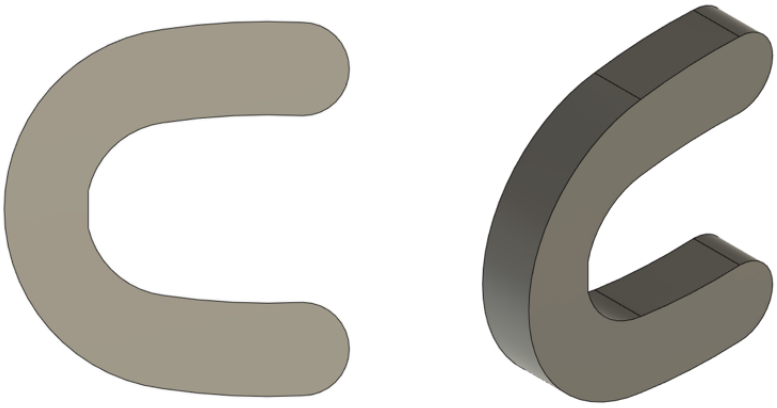

Figure 2.42: The frontal(left) and trimetric(right) view of the C-shaped leg design for cSQuad

In order to fabricate this leg a mold was designed as seen in Fig. 2.43.

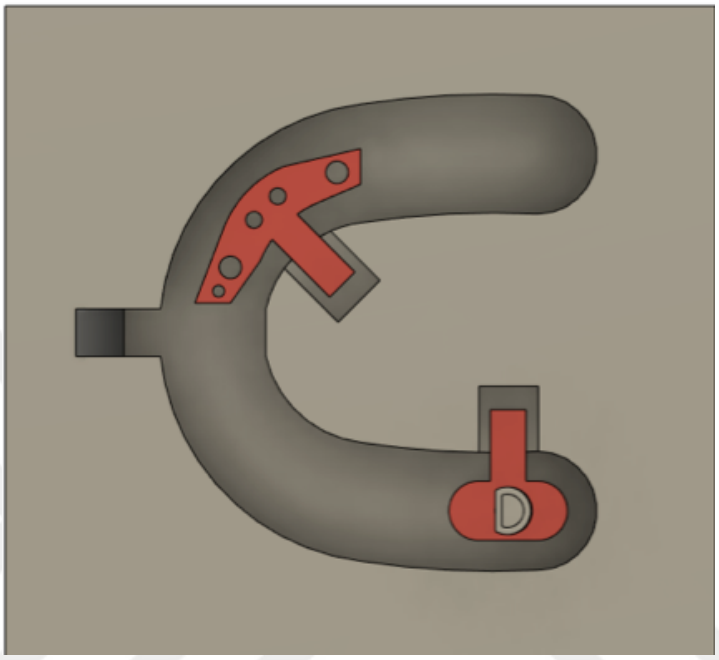

Figure 2.43: The mold design of the C-shaped leg for cSQuad

During the design of the mold in Fig. 2.43, initially the connection points for the 2 ends of the spring was selected. It was observed that choosing the first point at the bottom right corner and the second point at a 45 degree angle to the first point delivered optimum results. The red connection parts in Fig. 2.43 are embedded inside the leg during the molding process and they have holes in them to attach to the leg better. PDMS fills these holes and fixes the position of these 3D printed parts for better durability. These parts can be seen in more detail in Fig. 2.44.

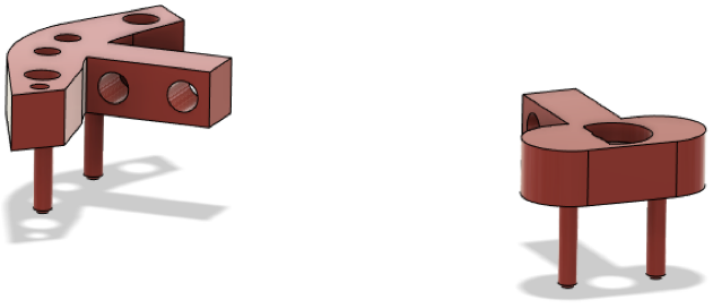

Figure 2.44: 3D printed connection parts for SMA springs

The thin pillars that is seen in Fig. 2.44 was put there to make the parts stand in the right position and align them in the mold and they break as intended during the de-molding process. These red parts do not touch any surface of the mold and they were placed in the mold so that they are at least 2 mm away from any wall of the mold which increases the surface area with the PDMS. In return, they become stronger and durable especially when the SMA's are applying force to them and they can transmit this force evenly to the leg.

An analysis was done using the Autodesk Fusion 360 CAD software to visualize how the leg would compress kinematically and the resulting shape is presented in Fig. 2.45. This kinematic analysis was done to have an idea about the approximate shape of the leg after the compression sequence is started. Hence, the simulation variables were not chosen as the real world values.

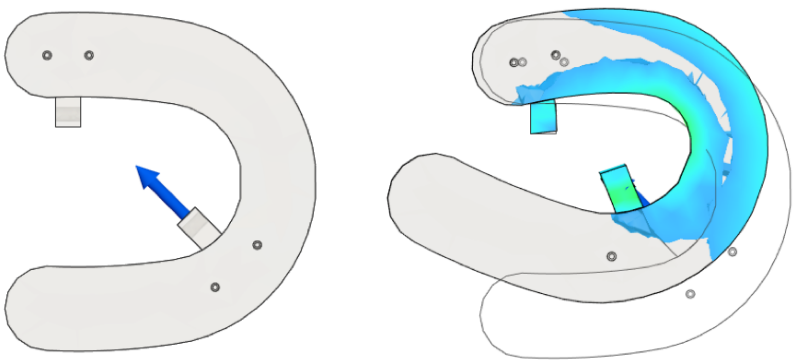

Figure 2.45: Kinematic analysis of the compression of the C shaped leg

The initial tests showed that the actual PDMS leg shows a compression characteristic that highly resembles the shape obtained in the simulation. The compressed and the relaxed leg can be seen in Fig. 2.45.

Fig. 2.45 presents the successful compression of the C shaped leg. However, it also shows that the power is transmitted to the SMA spring with a pair of crocodile cables. However in the actual robots, these legs will rotate continuously and therefore the electrical cables cannot be directly soldered to the 2 ends of the spring. An interface between the legs and the body is necessary to obtain a continuous electrical connection. Hence, a search for a device that transmits

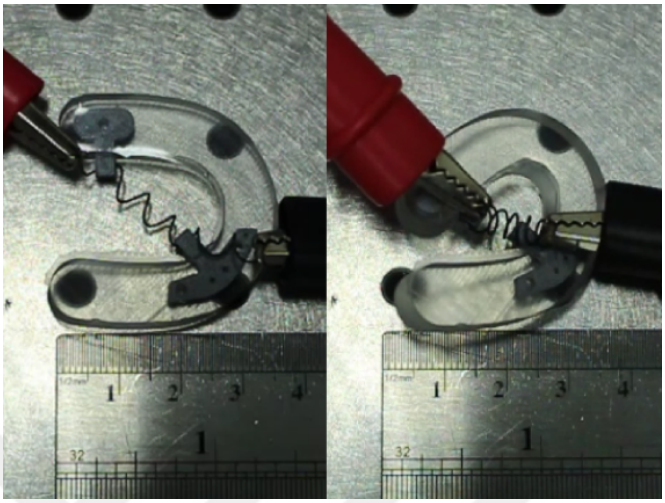

Figure 2.46: The first prototype of the C shaped compressible leg, relaxed(left) and compressed(right)

electricity on rotating bodies was carried out. Initial investigations revealed that there are readily available products in the market for this purpose however they are usually used in macro sized projects hence their size and weight were not suitable for our miniature robot. Therefore, special slip rings that are suitable for cSQuad were designed and fabricated in our lab and they are explained in the next section.

2.3.3.3 Slip-Ring Initial Design and Fabrication

Slip-rings are widely used in the industry especially in the gun turrets of military vehicles. Even though there are smaller versions of them, they are still too large to use in our robot. Hence the design that is presented in Fig. 2.47 was made initially. In this design, the red circles represent the copper traces and the black surface represents the portions where the copper will be removed. This type of slip-rings are called pancake slip-rings because of their resemblances to pancakes. One part is planned to be fixed on the robot body and the second identical part is going to be placed on the leg. There will be springy conductors between them which will ensure continuous power transfer.

The initial slip-ring design was fabricated on an FR4 copper plate using a

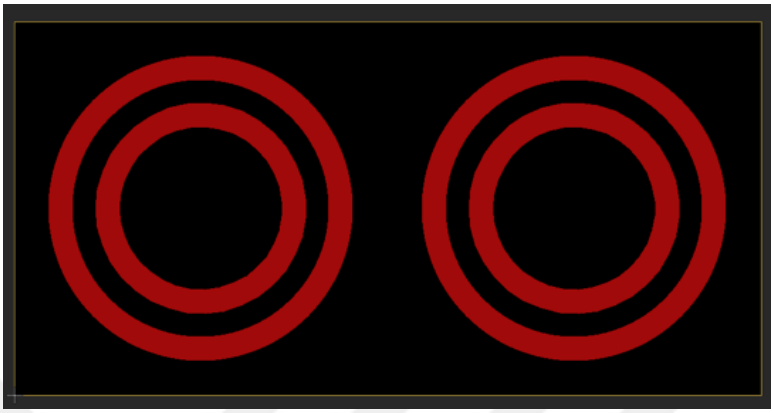

Figure 2.47: The initial electrical design for a slip-ring

CNC router as shown in Fig. 2.48. This method was used because it is one of the easiest and cheapest ways to fabricate a PCB. However, since the copper does not have uniform thickness, short circuits were observed in the final product and it was decided to try out different processes to fabricate the slip-ring.

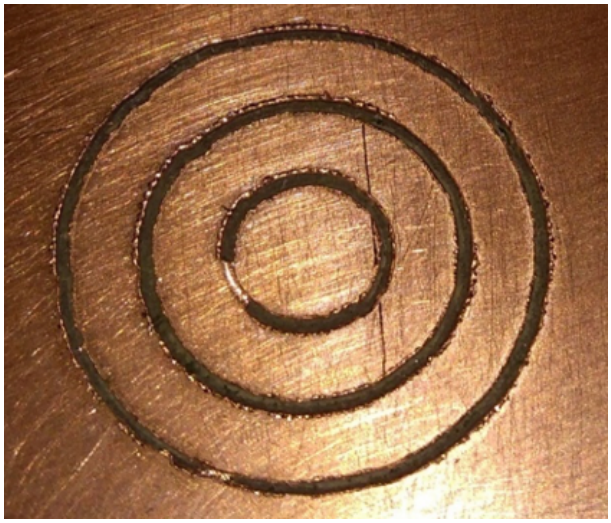

Figure 2.48: The slip-ring fabricated with a CNC router

As a second method, a CNC router was used again but with a difference. This time a masking pen was connected to the CNC instead of a cutting bit. By this way, the copper traces were plotted with the pen and they were protected during the chemical etching process. Chemical etching will be explained in detail after the explanation of the third method. The third method is basically the same with the second method, however a carbon dioxide laser was used instead of a

CNC router to mask the traces. The resulting PCB's are presented in Fig. 2.49.

Figure 2.49: CNC masked (top) and laser masked (bottom) slip-rings

The results for the laser etched PCB in Fig. 2.49 were not promising initially. However, it was found out that the problem was caused by the wrong focusing of the laser and it was fixed. Later on, it was decided to continue with the carbon dioxide laser and the full process of obtaining the slip-ring with the laser is explained below.

The laser method starts with cleaning the copper specimen using acetone, ethanol and pure water. Later, an even layer of black nail polish is applied on the copper surface. Next, the copper is placed on the carbon dioxide laser and the physical etching process is done using a vector file. The laser beam removes the nail polish and exposes the copper. This copper plate is placed inside a container with a mixture of 2 parts of 50% concentration hydrogen peroxide and 1 part of 3% concentration hydrochloric acid. This mixture completely removes the exposed copper in 1 minute and the resulting plate is presented in Fig. 2.50.

Fig. 2.50 shows that the areas that were covered with black nail polish were protected against the acid bath. In order to reveal the copper traces, the nail polish needs to be cleaned. Fig. 2.51 shows the plate after it was wiped with acetone.

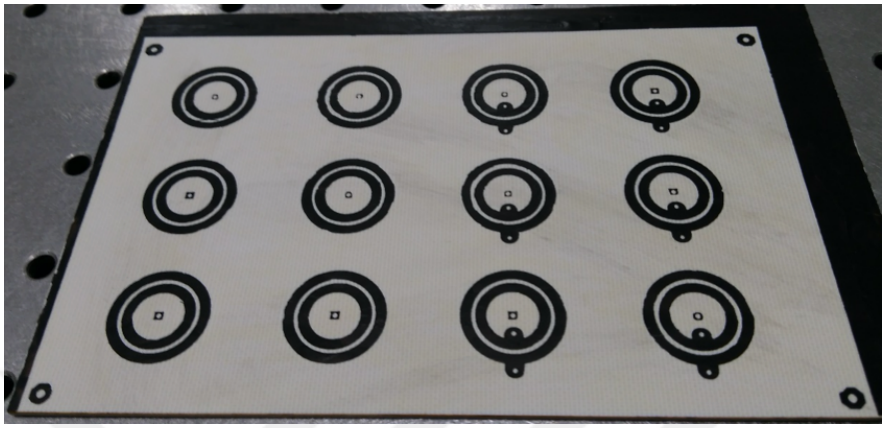

Figure 2.50: The FR2 copper plate for slip-rings after chemical etching

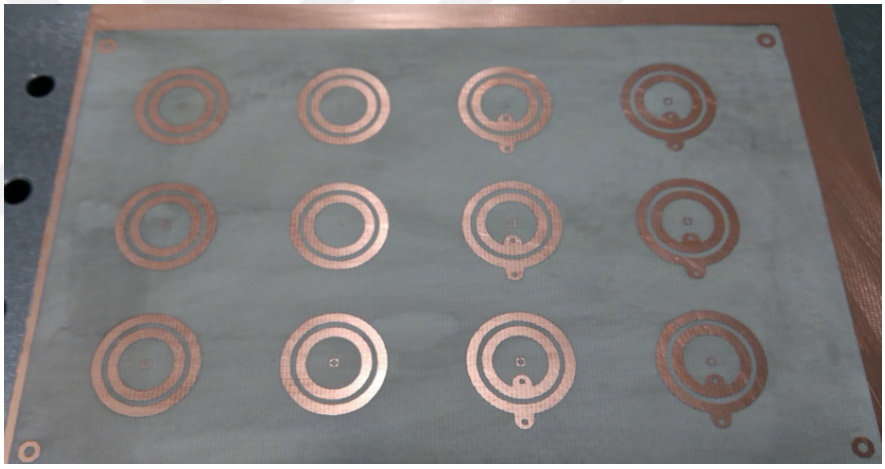

Figure 2.51: The FR2 copper plate for slip-rings after the nail polish is removed

The resulting traces offer almost perfect features but they need to go through one final step before they can be used. The slip-rings should be removed from the plate and to do that, they were placed in the laser again and they were cut from their outer diameters. It was observed that the FR4 material was both hard to cut and its fumes were also not healthy because of the glass fibers that they contain. Hence, FR2 plates were used in this process and the laser was able to cut them perfectly. After the cutting process 0.3 mm thick pure copper pieces were soldered on to the slip-rings that will be fixed on the body. And 90 degree male headers were soldered on to the slip-rings that will be attached to the legs. The resulting slip-ring is presented in Fig. 2.52.

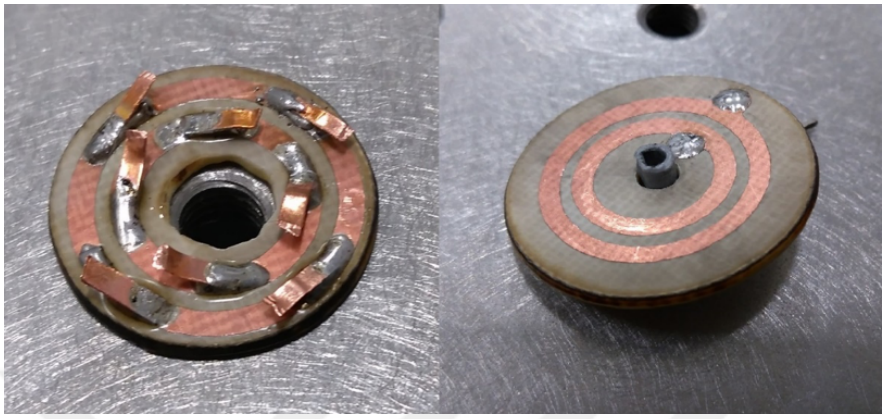

Figure 2.52: The first fabricated slip-ring prototype

This initial design of the slip-ring was attached to the C shaped leg and tested thoroughly. The test results are presented in the next chapter and even though the results are acceptable it was seen that there were room for improvement in this design and the improvements are applied to the final design of the slip-ring which is presented in the next section.

2.3.3.4 Slip-Ring Final Design and Fabrication

The initial design for the slip-ring was a prototype to prove that the concept works. Later on, a new approach was tried and tested mainly because of the following reasons:

- The initial slip-ring had issues regarding alignment,
- It was too labor intensive to solder copper strips for every slip-ring and therefore it was prone to human error,
- Its size could be made smaller,
- The copper strips lost their springy features after a couple of uses,
- The connections were not continuous due to the undulations of the soft robot,

- The pancake approach seemed redundant after discovering new methods.

Basically there were a lot of room for improvement and in the new design the first thing that was changed was the pancake concept. In that concept there are two circular PCB's for both the leg and the body and they need to be aligned perfectly. It was realized that only a single circular PCB would also work by utilizing additional components such as pogo pins. The pogo pins that we use is presented in Fig. 2.53.

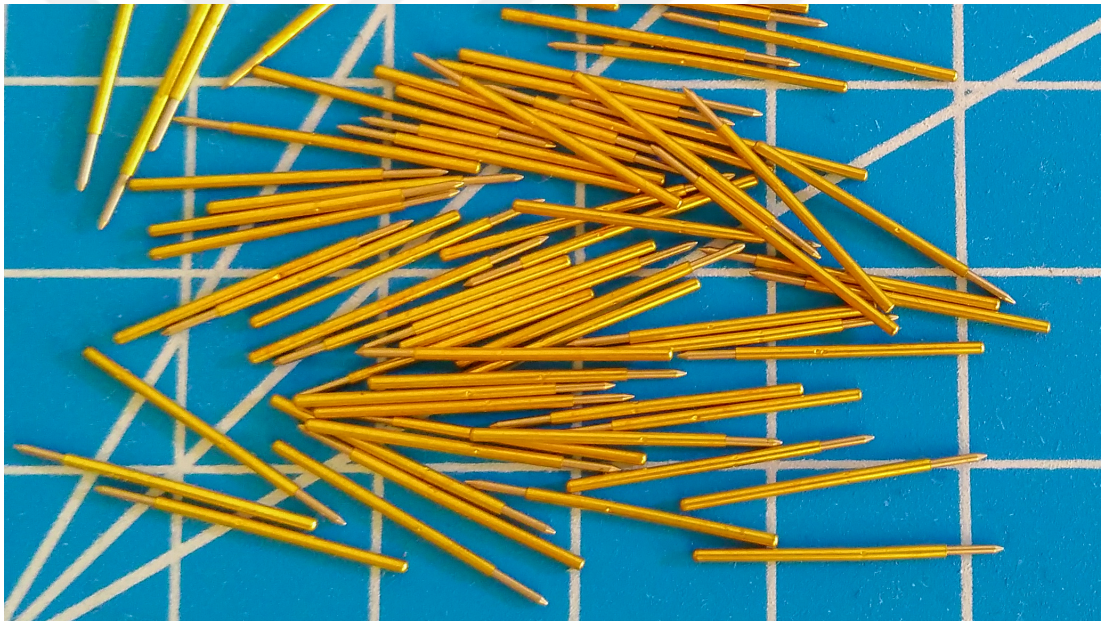

Figure 2.53: The pogo pins that are used for the final slip-ring design

Pogo pins are generally used in testing new PCB's to ensure they work as intended. They have a pin that is attached to a spring inside a conductive capsule. The spring pushes the pin onto the surface. It makes it easier to test new PCB's without actually soldering the components to the pads. However for our case, we used them to work with our slip-ring design and it will be explained in more detail towards the end of the section.

Initially, the slip-ring that connects to the body is redesigned. In Fig. 2.54 it can be seen that the soldering points for the slip-ring are moved inside the slip-ring so that the outer diameter is not increased unnecessarily as the old design.

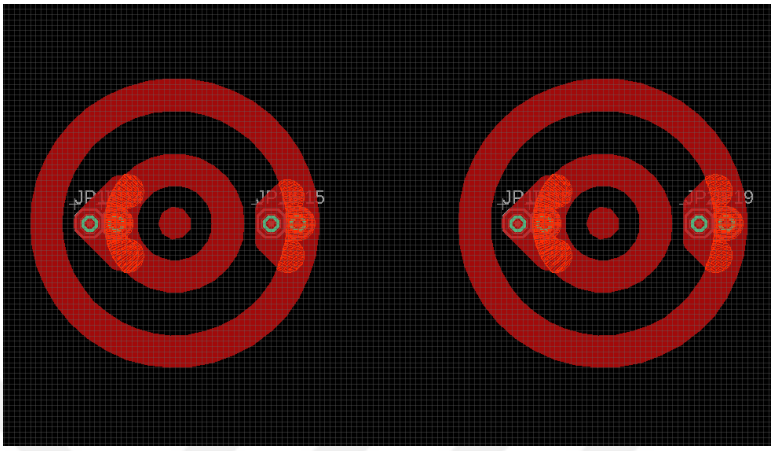

Figure 2.54: The final electrical design for the slip-ring

The design presented in Fig. 2.54 was fabricated as seen in Fig. 2.55.

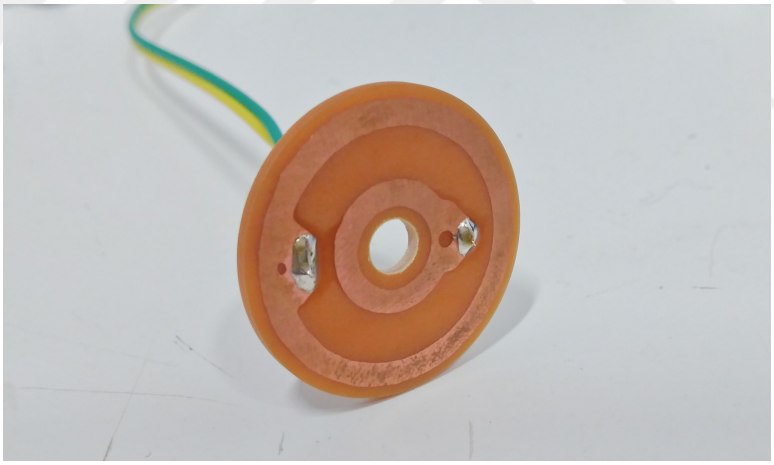

Figure 2.55: The final slip-ring design fabricated with FR4

As mentioned before, the FR4 copper is harder to work on compared to FR2 especially on a laser. However, due to the alignment issues we faced with the last design, it was decided to use a lathe to cut the slip-rings from the copper plates. Since the process induces high cutting forces, the FR2 plates were not strong enough and FR4 plates were used instead. Initially, the exact center of the slip-rings are drilled with a vertical drill with high precision. The pad holes for the connections were also drilled with a 1 mm drill bit at this stage. Then, each slip-ring is roughly cut out from the FR4 plate using a regular saw. Every plate is designed to have 8 slip-rings so at this stage, we obtain 8 roughly cut slip-rings

with an alignment hole in the center. Using this hole in the center, they are inserted on a bolt and tightened with its corresponding nut. This way, all of the slip-rings are aligned before the final step. At the final step, the bolt is connected to the lathe and the outer rough sections of the slip-rings are removed. As a result, we have obtained 8 slip-rings with perfect circular features and perfect alignment. In Fig. 2.56 the back of a slip-ring with the cables soldered can be seen.

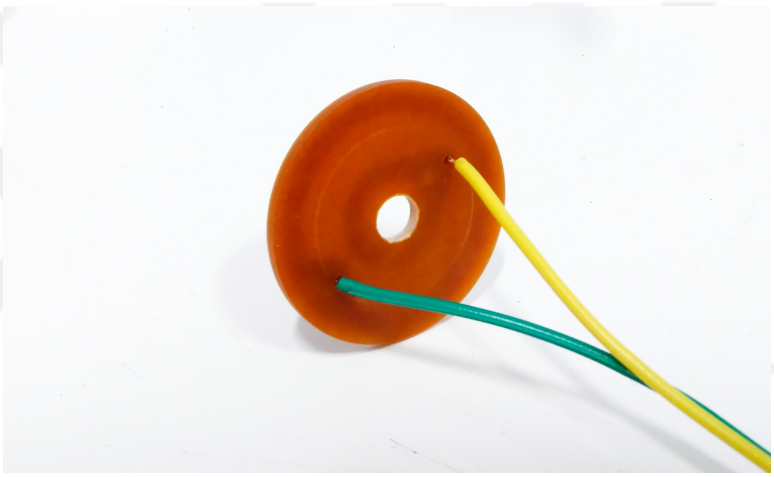

Figure 2.56: The back of the final slip-ring design with cables soldered

As mentioned before, the slip-rings produced for this design are fixed on the body. For the legs, the pogo pins are used and an image of a fabricated leg with pogo pins is presented in Fig. 2.57. The detailed process of how the leg is fabricated and how the pogo pins are placed in the leg will be discussed in the "C-Shaped Leg Final Design and Fabrication" section.

Even though this slip-ring design is used in our final robot, and it works perfectly, we continued to improve it. For the cSQuad, the slip-ring is only necessary for transmitting power. However, in our lab there is also an ongoing work in the field of soft sensors and we wanted to embed these sensors into the leg and obtain data while the leg was rotating. Since the pogo pins are continuously scratching the copper surface, the signal required through these channels were extremely noisy and we came up with a design specifically focused on reducing the noise levels and it is explained in the next section.

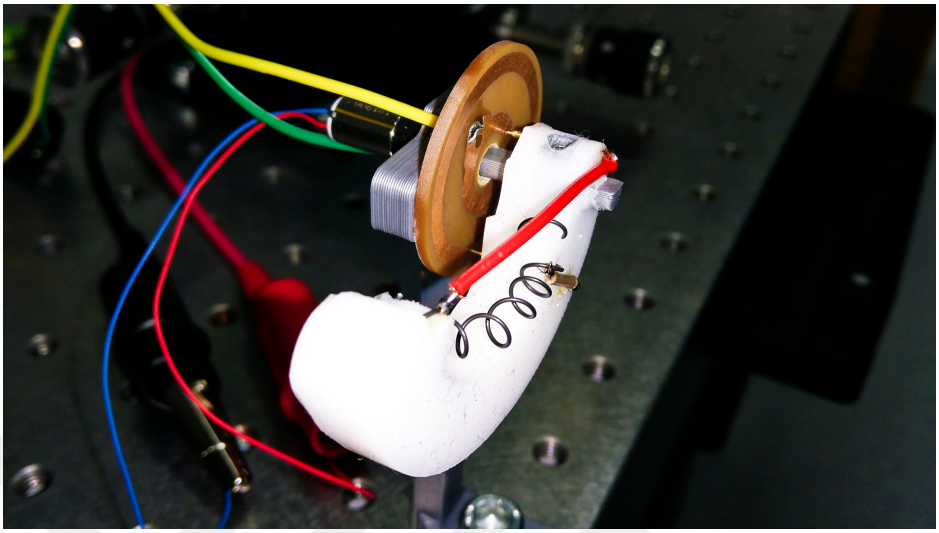

Figure 2.57: The final slip-ring with the pogo pins attached to the C shaped leg

2.3.3.5 Tube-Ring Design and Fabrication

The tube-ring design is an improvement on the slip-ring design to obtain a clear signal for data transfer. It is not used in cSQuad but it was included here to give an idea about how this system could be used for data transfer in the future. It is called a tube-ring because the data is transmitted through copper tubes and miniature bearings. The initial design can be seen in Fig. 2.58.

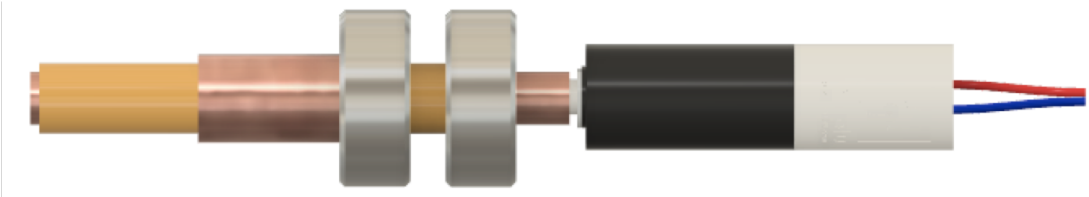

Figure 2.58: The initial design for a tube-ring attached to the DC motor

The CAD design presented in Fig. 2.58 contains two miniature bearings with 3 mm and 5 mm inner diameters and two copper tubes with 3 mm and 5 mm outer diameters. The copper tubes are fitted inside their corresponding bearings initially. Later, they are fitted inside each other with an insulating material in between. In order to visualize it better, the fabricated tube-ring is presented before and after assembly in Fig. 2.59.

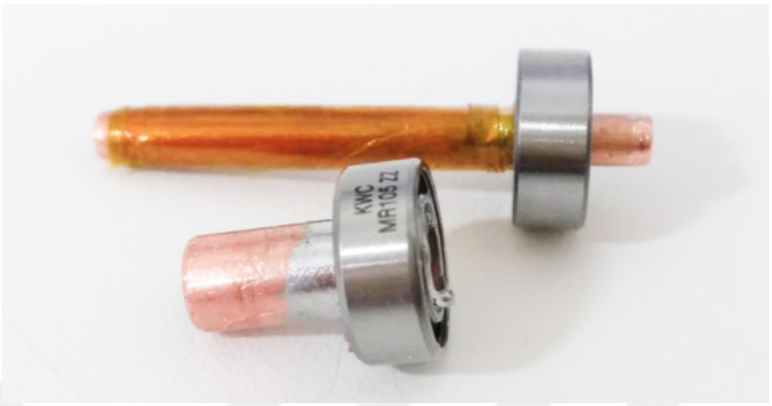

(a)

(b)

Figure 2.59: Partly (a) and fully (b) assembled tube-ring prototype

The tube-ring allows a 2 channel connection using the 2 tube and bearing couples. The outer shells of the bearings are planned to be fixed inside the body and the inner sections of the bearings will rotate with the copper tubes that are attached inside the leg. Since these miniature bearings have miniature balls inside, they ensure a touching connection from multiple points between the inner and outer sections of the bearings and the noise levels are reduced significantly.

To connect the system into the leg, the tip of the 3 mm copper tube is given the shape of D using a CNC milled forming die that can be seen in Fig. 2.60a. In the final version, the dimensions were readjusted and the system was made smaller. The final version of the tube-ring with a D shaped shaft can also be seen in Fig. 2.60b.

Our initial tests showed that this system is suitable to be used for accurate

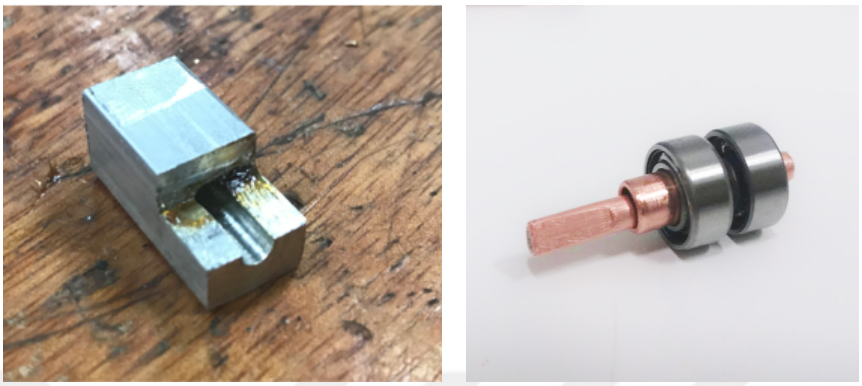

(a) (b)

Figure 2.60: (a) CNC milled die for obtaining a D shaft. (b) Final version of the tube-ring

data transfer. However for cSQuad, the slip-ring design is sufficient since it does not require data transfer to work.

2.3.3.6 C-Shaped Leg Final Design and Fabrication

In the final design of the C shaped leg, the shape of the leg was changed to a half circle to make it easier to model in the future and the CAD design of the mold can be seen in Fig. 2.61.

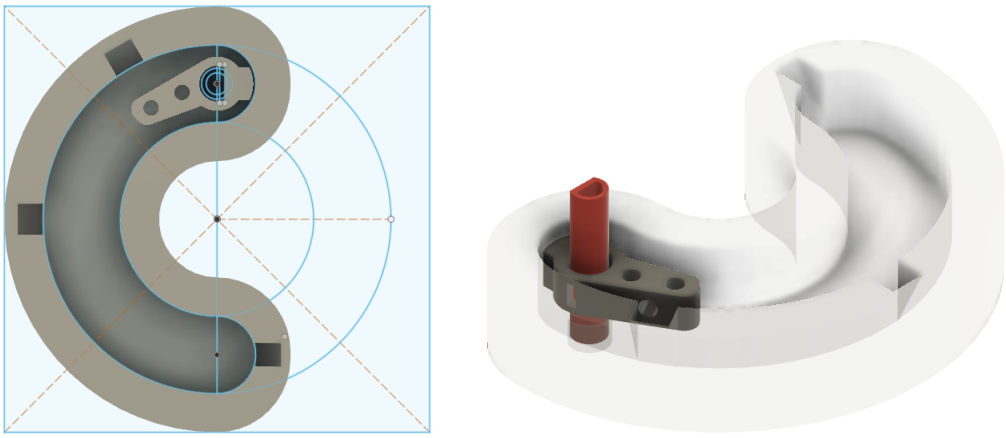

(a) (b)

Figure 2.61: (a) Top view of the final C shaped half circle leg design. (b) The design of the mold for the final version of the leg.

For the initial C shaped leg design for cSQuad, 3D printed parts were embedded inside the PDMS leg as presented before in Fig. 2.46. However, the initial tests showed that the 3D printed parts melt when the SMA spring is operating. Hence, a new method had to be determined to connect the SMA springs into the C shaped legs. At this stage a heat resistant silicone material was tested to see whether the SMA springs could be connected directly into the legs without any additional parts. RTV2 (two component room temperature vulcanizing) silicone is known for its high flexibility and heat endurance. This silicone is usually used for molding and because of that it is designed to withstand high temperatures and it does not rip apart as easily as PDMS does. Therefore the mold in Fig. 2.62 was designed. In this mold it can be seen that the pogo pins are also added inside the 3D printed motor connector parts. The location of the pogo pins were determined so that they align perfectly with the slip-rings once the leg is attached to the motor. A close up image of the pogo pin assembly is presented in Fig. 2.63.

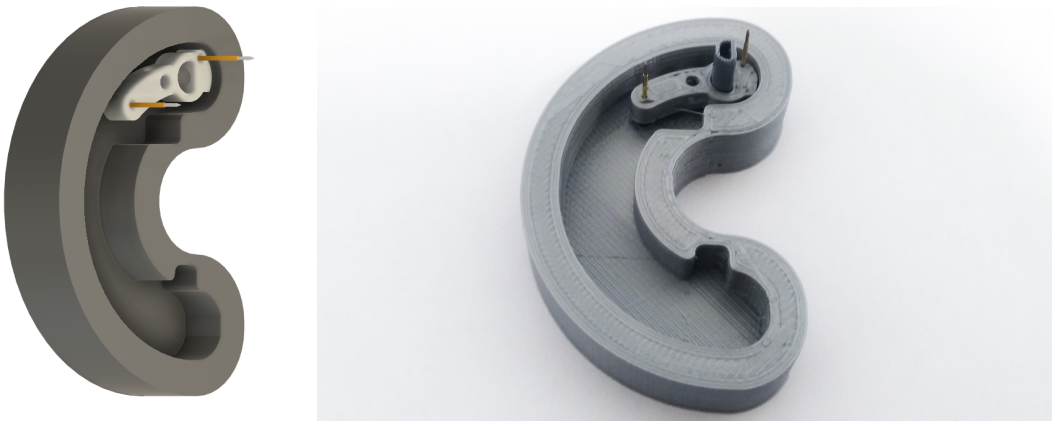

(a) (b)

Figure 2.62: (a) The CAD design of the final C shaped leg mold. (b) The 3D printed mold for the final C shaped leg.

The pogo pins were placed into the grooves in the 3D printed motor connector part and they were glued there. After the molds were ready, the RTV2 silicone was prepared and poured into the molds. The preparation process of RTV2 silicon is exactly the same as PDMS. It also has 2 parts and they are mixed at a specific ratio. However, for the RTV2 silicon, the mixture ratio affects the curing time rather than the stiffness of the material. With the recommended mixture

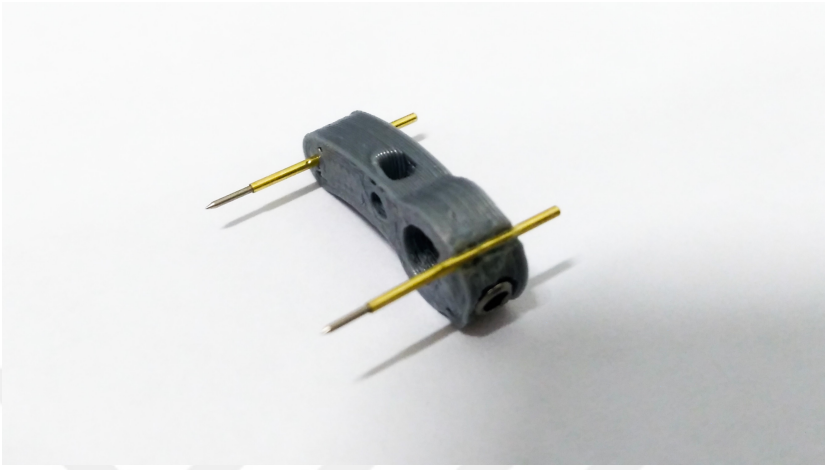

Figure 2.63: The pogo pins connected to the 3D printed motor connector

ratio, the RTV2 silicone cures at room temperature in 24 hours as the name RTV (room temperature vulcanizing) suggests. Increasing the amount of curing agent decreases the curing time. The molds with RTV2 silicone is presented in Fig. 2.64.

Figure 2.64: The molds for final C leg design filled with RTV2 silicone

Once the legs are removed from the mold, they are cleaned by cutting the excess parts and the resulting final legs can be seen in Fig. 2.65.

In the final version of the leg, the SMA springs were attached to the RTV2 silicone directly by piercing. The further end of the SMA spring is connected to one of the pogo pins by using a flexible jumper cable (the red cables in Fig. 2.65)

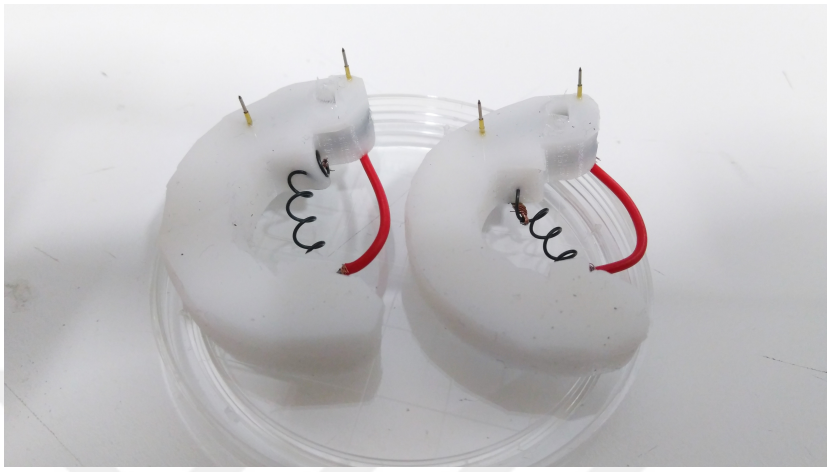

Figure 2.65: The final C shaped legs made with RTV2 silicone

and the nearest end of the SMA spring is connected directly to the pogo pin right next to it. The tests for this leg and the previous legs are presented in the next chapter.

2.3.4 Body Design and Fabrication

The body of the cSQuad is required to be compressible in order to utilize the compressibility of the soft materials to the maximum extend.

The initial design focuses on using the same body that was designed for the SQuad and converting it into a compressible body utilizing the accordion concept that was used in the compressible four bar leg design.

The final design is a completely new body optimized for maximum amount of compression.

2.3.4.1 Initial Body Design and Fabrication

For the initial body design, the accordion design that was first introduced for the four-bar typed compressible legs were used. The compressible accordion parts

were made out of Ecoflex and the rest of the body was made from PDMS. The mold design and the fabricated body is presented in Fig. 2.66.

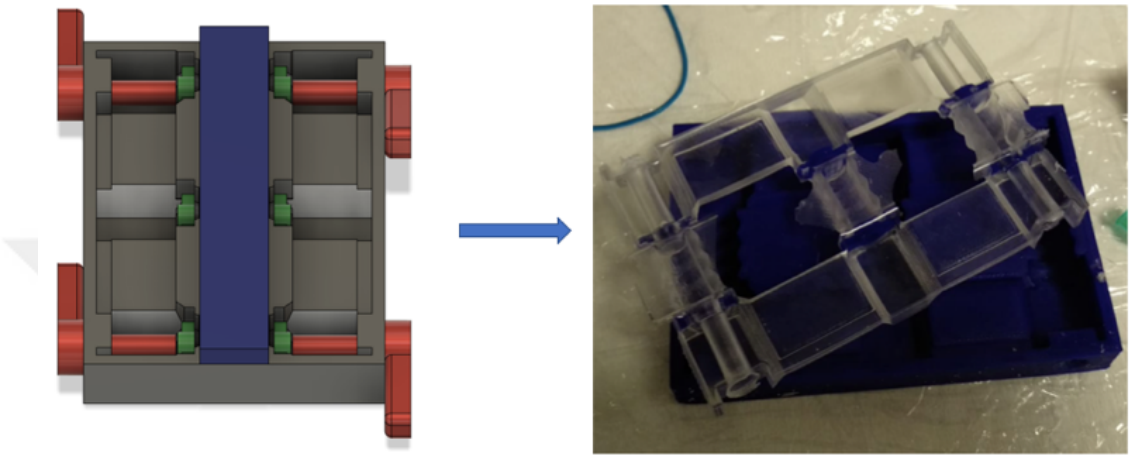

Figure 2.66: The mold design (left) and the fabricated compressible body (right).

In the mold design in Fig. 2.66, the green parts act as connectors for the SMA springs since the springs cannot be connected directly to the PDMS. However, after the body was fabricated, it was observed that these parts do not have enough surface area to hold on to the Ecoflex. It was also observed that since these connector parts are located at the interface between the Ecoflex and PDMS, it makes them even weaker and they tend to rip apart after a few uses as seen in Fig. 2.67.

To improve this initial design, it was decided to use only PDMS as the main material of the body and the number of SMA springs was reduced from 3 to 2. By doing this, the spring locations were moved closer to the center of the robot as opposed to the initial design. This is important because in the initial design, the motor cables had no way of exiting the body because they interfered with the SMA springs. In the new design, the connection parts for the SMA springs were also improved and their surface area was increased. The mold for the improved design is presented in Fig. 2.68.

The mold presented in Fig. 2.68 has one additional feature as well. The white PTFE tubes in the design is put there to make sure that the left part of the robot and the right part are aligned during locomotion. These tubes were first used for

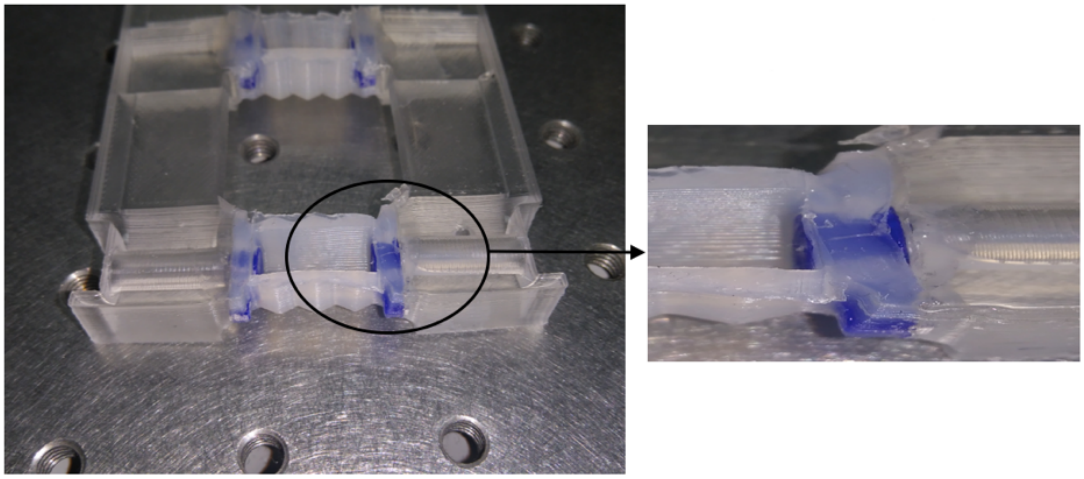

Figure 2.67: The separation problem between the Ecoflex and PDMS for the compressible body.

the piston-cylinder leg design and here they are embedded inside the body and they are supported by the 3D printed blue parts in Fig. 2.68. They can also be seen in the fabricated mold in Fig. 2.69. After the body is fabricated, a steel piston is placed between the opposite tubes and this design makes sure that the compression will take place in only one axis and the robot will locomote straight during and after the compression.

Even though the improved body has the same dimensions as the initial body, the compression amount is theoretically larger. In the first prototype, the distance between the 2 connection parts for the SMA springs were 18.5 mm whereas it is 27.2 mm for the second prototype. If it is assumed that the springs would reduce their length down to 7 mm during operation (maximum compression) then the first and second prototype will compress 11.5 mm and 20.2 mm respectively. It means that the compression performance is enhanced by 75% theoretically for the improved design. The fabricated body for this design is presented in Fig. 2.70.

The fabricated body in Fig. 2.70 offers several advantages over the old bodies in terms of ease of assembly. But the fact that the accordion sections are made from PDMS causes unexpected problems. It was observed that for the C shaped legs, the PDMS has an acceptable compression performance and it does not rip

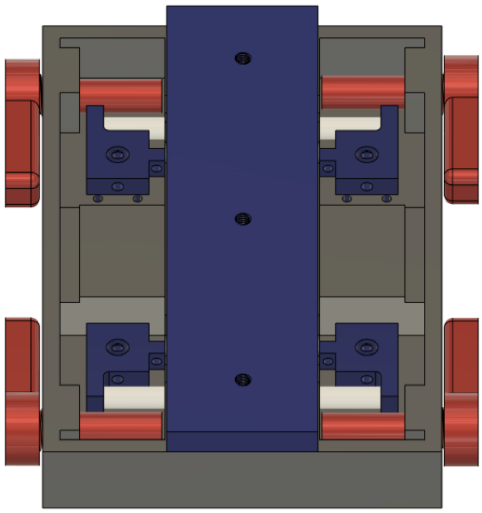

Figure 2.68: The mold design for the improved compressible body.

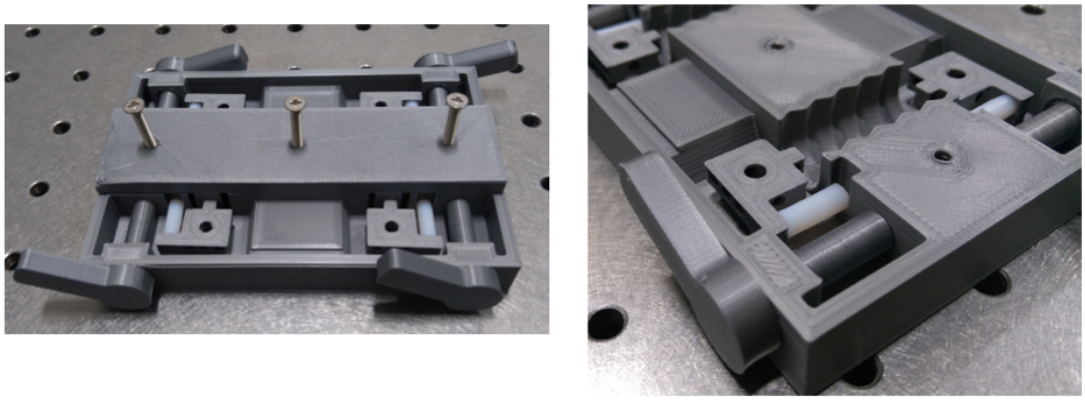

Figure 2.69: The fabricated mold for the improved compressible body.

apart. But as the PDMS gets thinner (as in the case for accordion in the body it is 1.5 mm) it gets brittle and it fails.

At this stage, the utilization of the accordion design for the body was questioned as well. One of the reasons for the accordion design is to utilize it as a spring. It was aimed that after the compression is done and after the SMA cools down the body would go back to its original position thanks to the force applied by these accordion springs. However, due to the fact that PDMS gets brittle when it is thin, a more conventional spring design was considered.

In the final design of the body,linear beams were used to both act like a spring

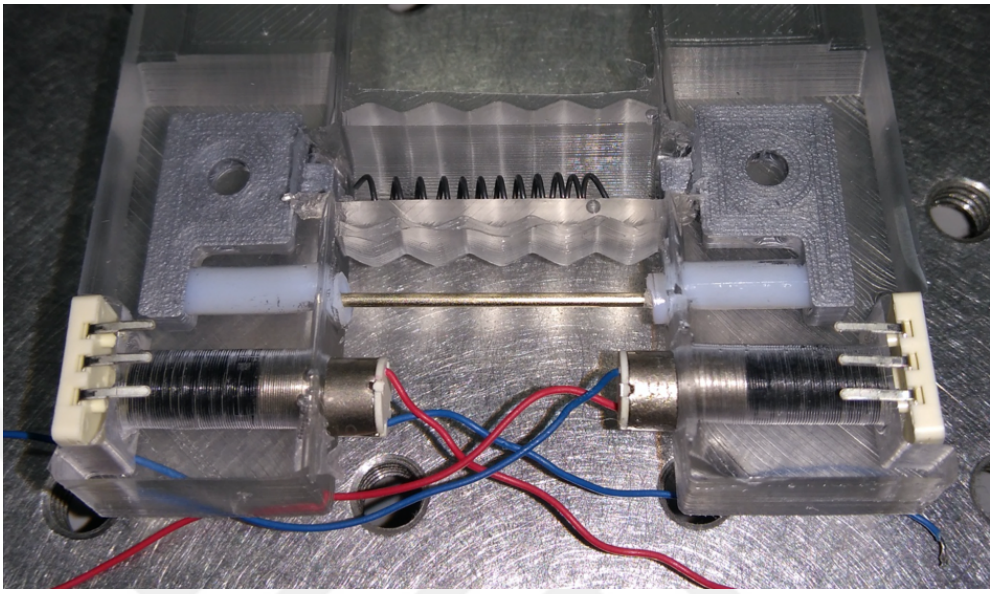

Figure 2.70: The fabricated compressible body with additional components such as motors, encoders and PTFE tubes.

and to connect the left and right sides of the body.

2.3.4.2 Final Body Design and Fabrication

As mentioned in the last section, the final design of the compressible body incorporates beams rather than accordions. These beams are designed in a way that they form an X shape in the center of the body. The initial mold for the final design is presented in Fig. 2.71.

In this first prototype design, it can be seen that the PTFE tubes are removed for simpler fabrication and overall the amount of parts required to obtain the body is reduced compared to older designs. This reduces the possible problems in alignment and it makes it easier to assemble the body. The fabricated body is presented in Fig. 2.72.

The first prototype for the final body with the X shaped beams is presented in Fig. 2.72. The fully assembled robot with this body is presented in Fig. 2.73.

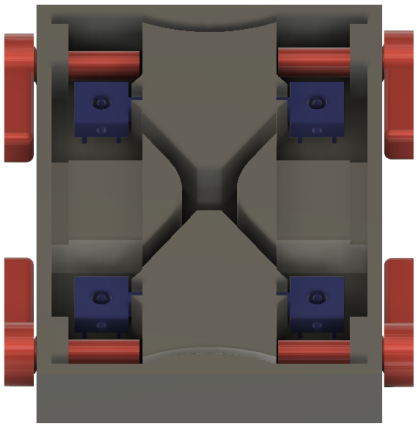

Figure 2.71: The mold design for the compressible body with X shaped center.

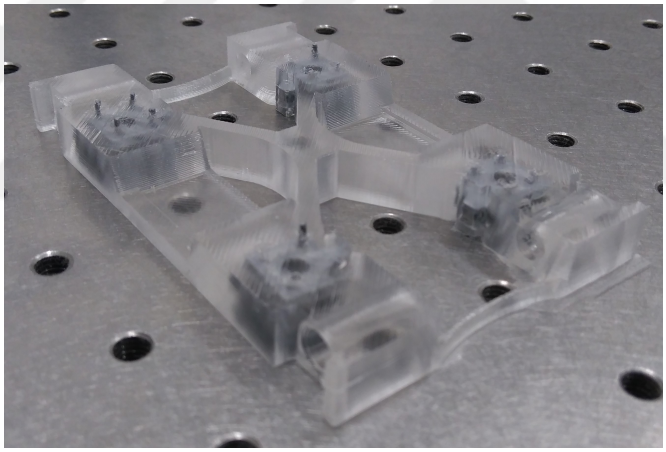

Figure 2.72: The fabricated body with X shaped center.

The robot in Fig. 2.73 gives several clues about the problems that this body design has. First of all, the weight of the PCB makes the robot buckle and gives the legs a negative camber angle . This is not an intended or desired feature because even though negative camber may increase the directional stability during straight locomotion, it makes it harder to steer the robot.

Another problem is the direction of the thin strips located in the front and rear tips of the robot. These PDMS strips are intended to limit the maximum distance between the left side of the robot and the right side of the robot as seen in Fig. 2.74. In this figure the right side of the robot was compressed and the left side was not touched. Even though the PDMS strip on the left side worked

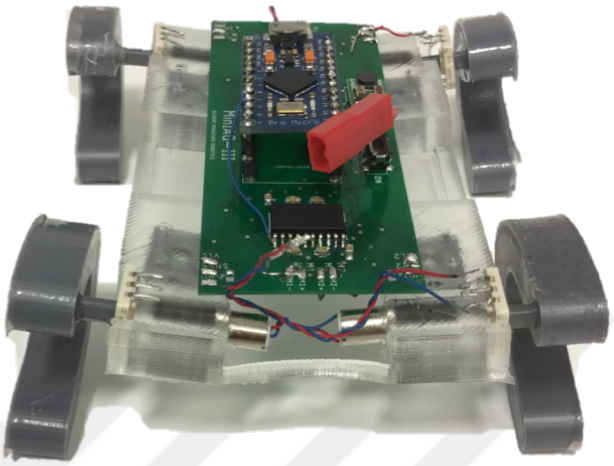

Figure 2.73: The front view of the fully assembled robot with X shaped center.

as intended, the strip in the right side of the figure buckles inwards and this is a problem because the strip will interfere with the motor cables once they are attached. This was observed as seen in Fig. 2.75.

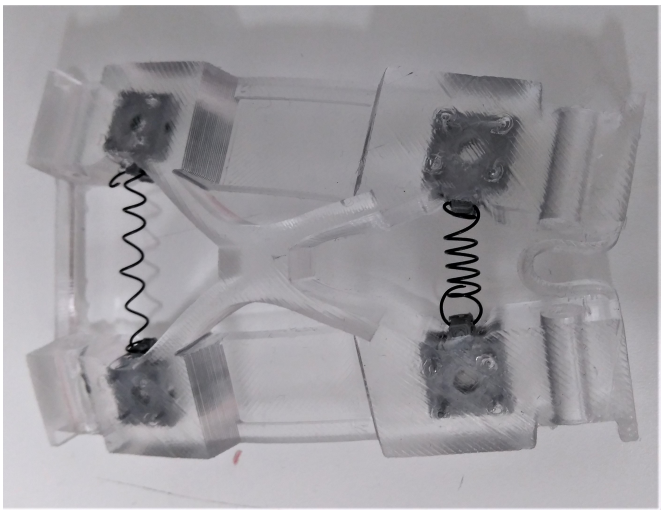

Figure 2.74: The buckling problem for the X shaped compressible body.

In Fig. 2.75 another major issue about the motor size can be seen as well. When the body is fully compressed, the motors are touching each other and they reduce the compression performance. It is also potentially harmful for the motors since the motor cables come out from the back of the motors and they are

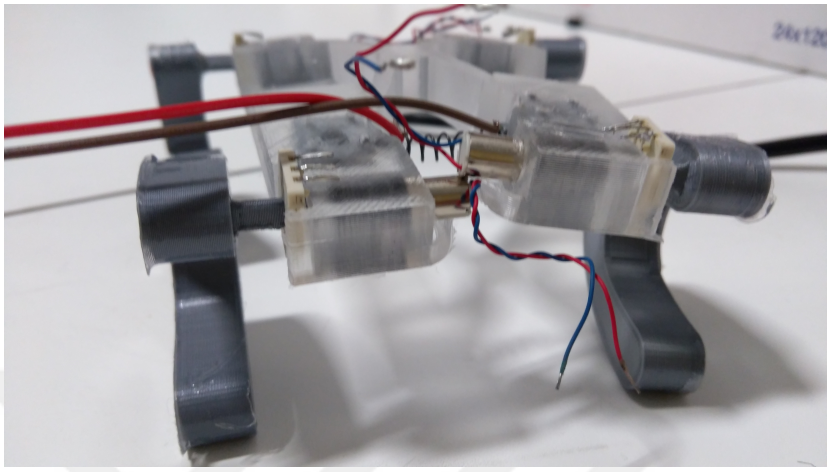

Figure 2.75: The motor interference problem during body compression.

in danger of rupturing because of this unwanted contact. Since the motor size is a hard constraint, the only way to solve this issue is to enlarge the motor opening inside the body so that the body would encapsulate the whole length of the motors. To do this, the length of the motor openings in the body was increased from 10 mm to 15 mm. A new mold was designed to solve the problems explained above and it is presented in Fig. 2.76.

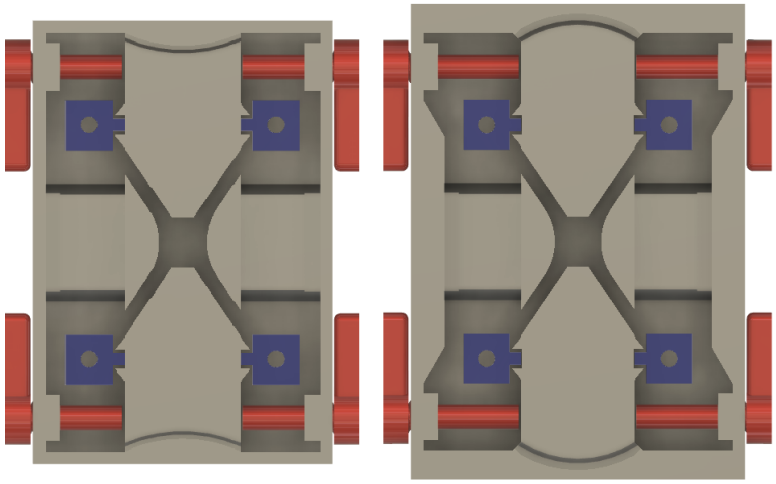

Figure 2.76: The first (left) and the second (right) iteration for the mold of the final body design.

Even though the new mold solves the apparent technical issues, upon close

inspection some additional fundamental problems can be spotted. For this prototype, unlike the SQuad, the body elongates as it compresses. Hence the side beams are subject to tensile stress and they make it harder for the body to compress. To compensate for the additional stress, the side beams of the body tend to buckle. This was first observed during the initial tests and it can be seen in Fig. 2.74. In this test, the left side of the robot is released and the right side is compressed. It can be seen here, that the left side is pulled toward the right side because of the beams connecting the front and rear of the body. It was observed that if both of the SMA springs are compressed the side beams buckle as seen in an FEM analysis conducted using Autodesk Fusion 360 software in Fig. 2.77.

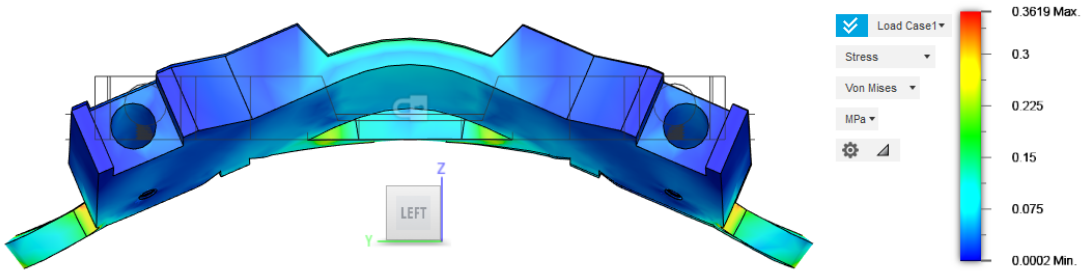

Figure 2.77: The FEM analysis of the X shaped compressible body (side view).

The top view of this analysis can be seen in Fig. 2.78 where the blue arrows represent the forces applied to the body by the SMA springs and the body is fixed to the square hole in the center.

The analysis presented in Fig. 2.78 also shows the stress on the side beams which is unnecessarily making the compression process requiring more energy. To get rid of this problem, the side beams are completely removed from the body and a new design was made as seen in Fig. 2.79 which is the third and final iteration of the final design of the compressible body. The final design of the body is 20 mm longer and 9 mm narrower than the second iteration.

The final design for the compressible body does not use any embedded 3D printed parts to connect the SMA springs because there is practically no space

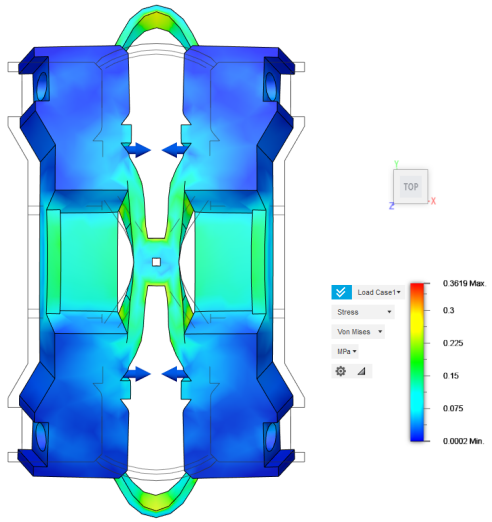

Figure 2.78: The FEM analysis of the X shaped compressible body (top view).

since the side beams are removed. Hence another approach was tested where steel wires were poked from the four holes that can be seen in the right side of Fig. 2.79. These steel wires were then knotted and they created an anchoring point for the SMA springs to be connected. Even though this solution is not ideal it was observed that it worked and it was used in the final design.

Another improvement in the final body design is the ability to attach and detach the leg assembly. As explained before, the C shaped legs require slip-rings to be able to be compressed.Each leg also requires a motor and an encoder as well. When these components are attached to the body one by one, it makes it complicated and more time consuming to assemble a whole robot. To solve this issue, a 3D printed flexible part is designed. This part is called the motor package and it is printed out of TPU. The DC motor is tight fitted inside this part along with the encoder. The slip-ring also attaches to this part and all of the cables are routed through channels inside this part which makes it more organized when soldering the cables. All of the components are pre-assembled on motor package as seen in Fig. 2.80. The assembly of this part and the whole robot will be explained in the following sections and the compression performance of the final body design will be discussed in the next chapter.

Figure 2.79: The second iteration (left) and the last (right) iteration of the final compressible body design.

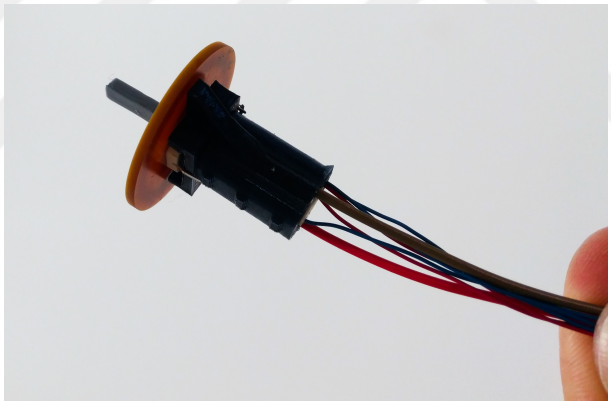

Figure 2.80: The motor package with the slip-ring, the DC motor and the encoder assembled..

2.3.5 Electronics Design

The electronics design for the cSQuad is similar to SQuad. Since cSQuad is also a quadruped, the components used for motor controlling is exactly the same with SQuad. For this robot however, the shape memory alloys should also be considered since they rely on electricity to work.

The shape memory alloys require heat to operate and the easiest way to obtain heat without combustion for our robot is to transmit electrical current through the SMA springs. The resistance of the SMA wires will result in dissipation in terms of heat. The initial tests with the tethered versions of cSQuad made use

of lab bench power supplies where the voltage and the current can be controlled. Current control is crucial for the SMA springs since they are metal and therefore have low resistance.

Even though the current can be controlled and limited with an adjustable power supply, when the robot becomes untethered, a new approach should be found. Initially, the DRV8835 stepper motor driver was selected as a candidate to control the SMA springs. These drivers have 2 channels each and these channels have safety features such as current limiting or temperature protection. These features were tested on a test setup on a breadboard and it was observed that DRV8835 motor drivers successfully work with the SMA springs. Hence, a PCB was made as presented in Fig. 2.81.

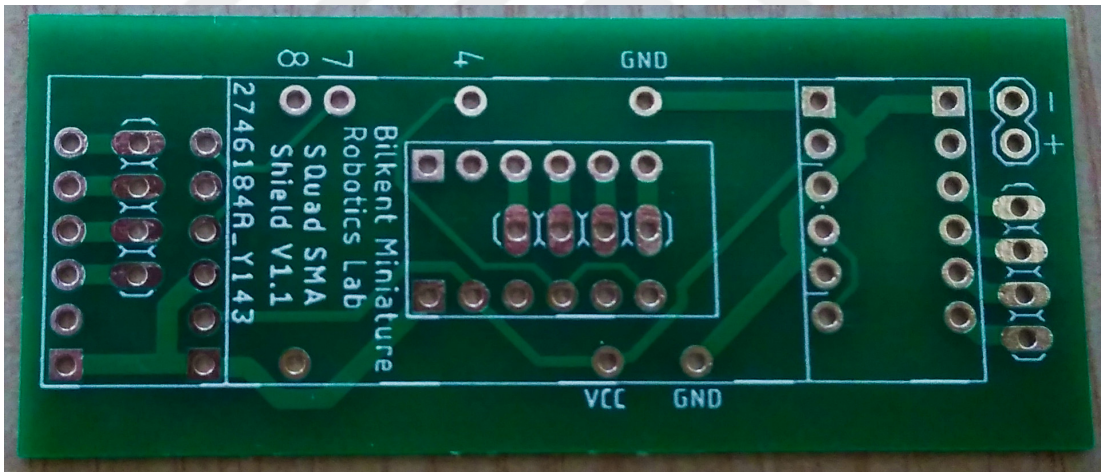

Figure 2.81: The PCB made for DRV8835 motor drivers.

The board in Fig. 2.81 is designed to have 3 DRV8835 motor drivers for controlling 3 pairs of SMA springs. The digital pins 4, 7 and 8 of the Arduino are used to activate the DRV8835 drivers and the whole board is powered with an external battery. The board is designed to be assembled on top of the main controller board as a shield. Even though this design worked with the SMA springs on the body, it failed for the legs.Later, it was discovered that the DRV8835 has a feature called undervoltage lockout. This caused the DRV8835 to reset itself and go into protection mode when it was connected to the SMA springs on the C-shaped legs. Upon closer inspection, it was discovered that this behavior was due to the friction between the pogo pins and the slip-ring. This friction caused

high frequency noise and it triggered the protection systems of the DRV8835 driver. Since there was no other way to transmit current to the legs other than the slip-rings, the DRV8835 driver had to be scrapped for something more simple such as relays. The relay used for the cSQuad is Huike HK23F-DC5V-SHG and it is presented in Fig. 2.82.

Figure 2.82: Huike HK23F-DC5V-SHG 5V relay.

The only problem with the relays is that they are simple on-off switches without any sort of current control. To limit the current, external methods was used such as connecting the SMA spring pairs in series. This way, the resistance theoretically increased two times. The SMA springs on the body, the SMA springs on the front legs and the SMA springs on the rear legs are connected in series respectively. Additionally, the voltage of the external battery is reduced from 7.4 V to 3.7 V. Initially, 7.4 V batteries were used to obtain a more powerful and fast compression. However, as the voltage decreased, it was observed that the current also decreased. The drop in voltage made the compression process slower but it didn't result in loss of compression amount. Three relays were soldered to the control board of the cSQuad to control 6 SMA springs.

Due to convenience and also time and budget constraints, it was decided to use the same PCB that was already ordered for the original SQuad. This flexible PCB that was presented in Fig. 2.25 was modified for the cSQuad. Initially, the 3 relays were prepared by soldering the cables to the necessary ports as seen in Fig. 2.83. Then the cables coming from the relays were soldered to the main

PCB for signal control and also to an external 3.7 V battery for the power. The final version of the electronic board can be seen in the next section.

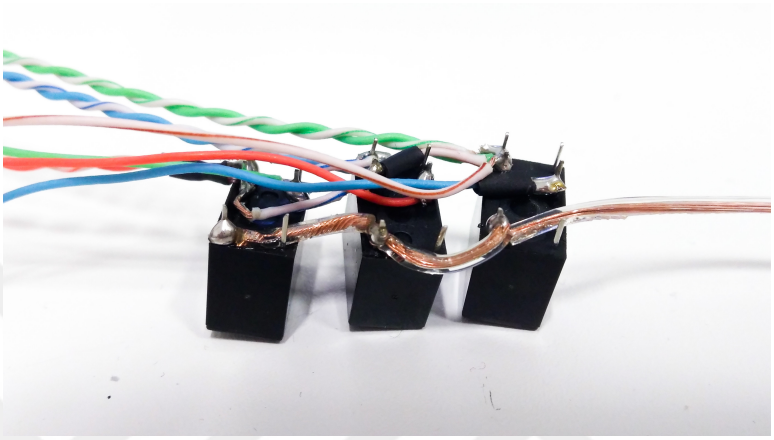

Figure 2.83: Three relays with cables ready to be soldered into the flexible PCB for cSQuad.

2.3.6 Assembly of cSQuad

The assembly of compressible SQuad is much more complicated than the original SQuad due to additional components added for the compression systems for the body and the four legs. In order to make sure that every part would fit without interference, the assembly was first done in CAD software as presented in Fig. 2.84.

Even though they are not visible in Fig. 2.84, there are 4 SMA springs assembled to each leg and 2 SMA springs assembled on the body which will be visible in the fabricated robot in the following figures.

The leg assembly is the most labor intensive and complicated part during the assembly process of the robot. Each leg assembly requires a C shaped leg, 2 pogo pins, 1 SMA spring, 1 slip-ring, 1 DC motor, 1 D shaft for the DC motor, 1 encoder, 1 motor package part and various cables. The components required to assemble a set of C shaped legs is shown in Fig. 2.85.

Once the assembly of the four legs are completed, the motor packages are

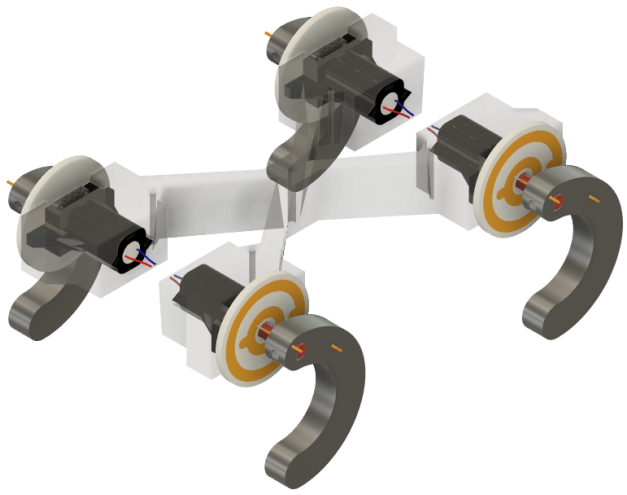

Figure 2.84: The CAD assembly of the final design of the compressible SQuad (cSQuad).

plugged in directly to the compressible body. After this stage, the soldering of the cables to the control board are done and the assembly is completed.

For the intermediate steps during the design phase, solid FR4 boards were used for convenience since they are cheaper than soft PCB's. However for the final robot, in order to use as much as soft components, the exact same soft PCB that was used in the original SQuad was used. The fact that the body gets compressed during operation, enforces a stress on the soft PCB and it makes it buckle uncontrollably, damaging the solders especially at the center of the PCB where the L293DD motor drivers are positioned. In order to prevent this, the soft PCB was given a curved shape beforehand and the surface mount type L293DD's were soldered via cables to the board. The curvature also provided room for the additional components required to control the shape memory alloys such as the relays. The relays are hidden under the PCB as seen in Fig. 2.86.

The robot in Fig. 2.86 does not have compressible legs and the figure shows the front SMA spring and the electronic components. The fully compressible robot with the four compressible legs and the compressible body is presented in Fig. 2.87.

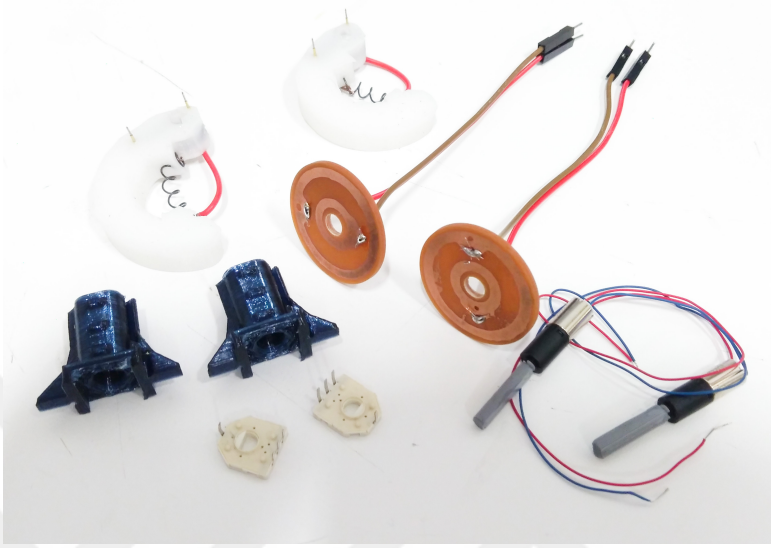

Figure 2.85: The parts required to assemble a pair of C-shaped legs for cSQuad.

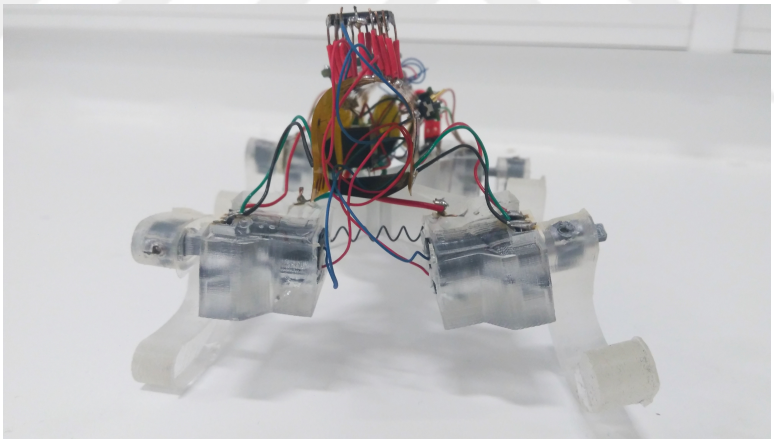

Figure 2.86: The front view of the cSQuad without leg compression.

2.4 Control of SQuad and cSQuad

The controller is based on a classical model of a DC motor which includes a voltage source, a resistance and back emf induced by the DC motor[31]. The inductance is not taken into account for convenience since we do not measure or control the current input to the system and the value of inductance is small enough to neglect for the specific motors that are used. The states of the system consists of the rotation angle of the motor(θ) and the rotational rate of the motor($\dot{\theta}$). The control system is a full state feedback control system which is

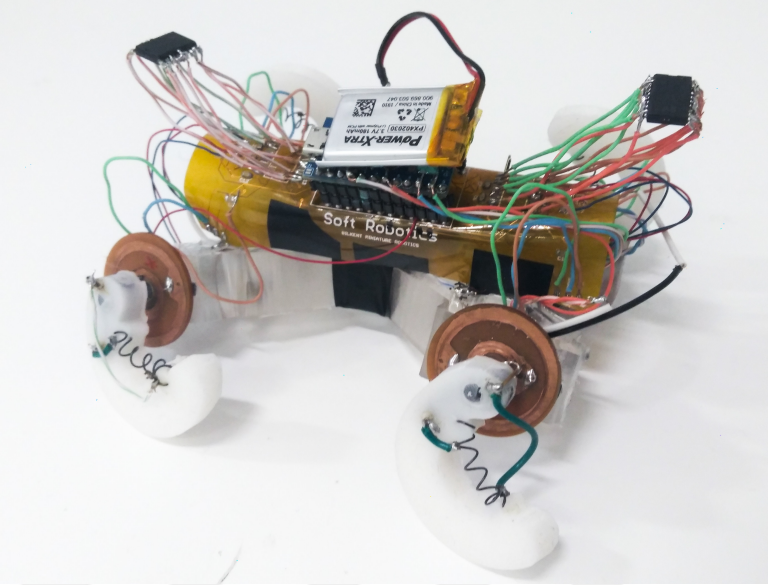

Figure 2.87: The fully compressible cSQuad.

based on a Linear Quadratic Regulator(LQR). In order to have a full state feedback control, all of the states should be measured, whereas our system is only able to read the position information of the motor using the rotary position encoders. The rotational rate($\dot{\theta}$) could not be measured directly using the rotary position encoders hence it needs to be estimated using an observer, ideally a Kalman filter. Hence, a Linear Quadratic Estimator(LQE) was used as an observer to obtain a full state feedback controller. By using LQR along with the LQE, we have obtained a Linear Quadratic Gaussian Controller(LQG) to control the gait of the robot.Using the LQG, the gait of the robot is set to a trot gait, where the two diagonal leg pairs are half a period apart in phase from each other, but running at the same frequency.

Chapter 3

Experiments and Results

This chapter presents the experimental results that were obtained for both SQuad and cSQuad.

First, the results for SQuad are presented. The locomotion performance of SQuad was tested in terms of speed and body undulation characteristics. To do this, measurements for pitch and roll angle and centroid position were recorded using an infrared motion tracking system and the results were discussed. Obstacle climbing performance of SQuad and the maximum angle that it can climb was tested and an implementation of a microphone was also discussed. The experiments and results for SQuad were published in [1].

For the cSQuad compression tests were done for both the legs and the body separately. Then, the fully untethered cSQuad equipped with compressible legs and body was tested during locomotion.

3.1 Experiments and Results for SQuad

In order to test and compare the capabilities of SQuad, its hard twin and several other configurations such as robots with hard body, soft legs and soft body, hard legs; a set of experiments were conducted. Ideally it would have been more fair if the weights of the robots were exactly the same. The soft body is only about 2.1 grams heavier than its hard twin body which is negligible considering the total weight of SQuad (69 grams). However, a single soft leg is about 2.8 grams heavier than its 3D printed twin. This makes SQuad about 13 grams heavier than its fully hard twin robot and due to this fact and also the undulations of the PDMS body; a stronger motor with a higher gear ratio was used in the soft body. Even though the high gear ratio motor (700:1 ratio) is slightly longer than the standard motor (136:1 ratio), the outer dimensions of the robots are kept exactly the same by adjusting the positions of the legs on the motor connector. The speeds of the motors are also kept the same at 0.5 Hz for all experiments. The hard PLA legs were coated with a thin layer of PDMS to eliminate the differences that would be caused by the material friction properties.

The walking speed, pitch and roll angle and the body centroid height was measured using the OptiTrack Motion Capture System which makes use of 6 IR cameras. Finally, obstacle climbing performance of SQuad, and the maximum slope that it can climb was measured and the onboard microphone was tested.

3.1.1 Speed Analysis

The walking characteristics of the robots are studied first, and trot gait is selected for the experiments. The first data presented is the speed data for all the robots at 0.5 Hz motor frequency. A screen shot of 4 different configurations of the robots from the walking experiments that was also presented in the last chapter is re-presented in Fig. 3.1.

The speed data is given in Table 3.1 and it reveals the advantage that the soft

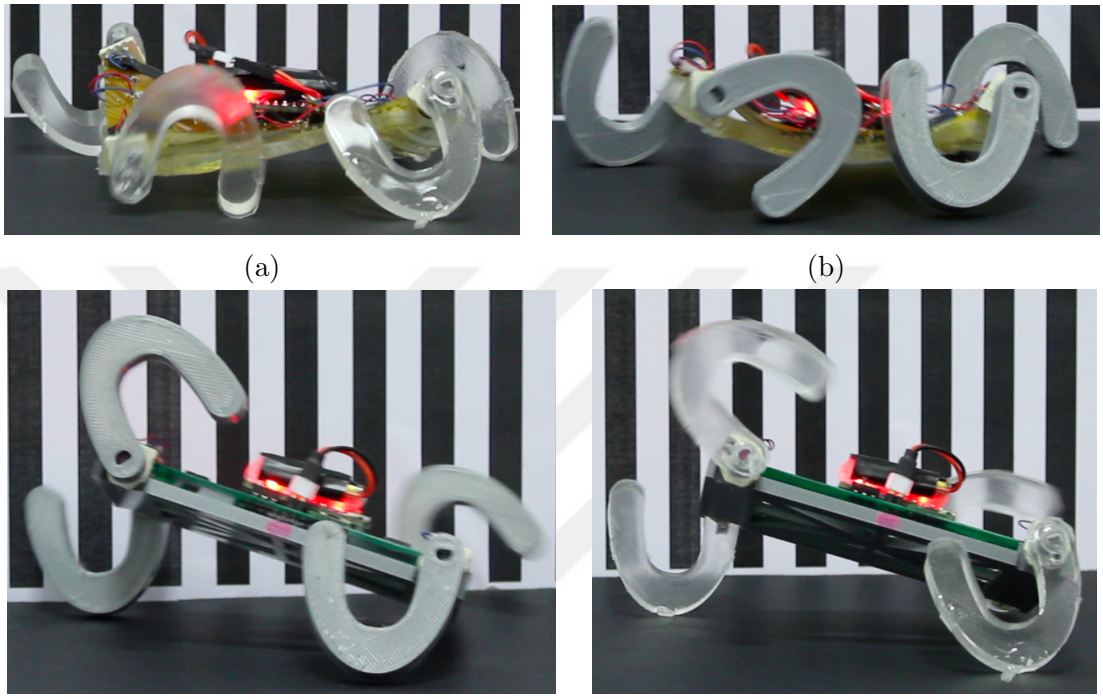

(a) (b)

(c) (d)

Figure 3.1: Walking pictures of 4 different robot configurations. (a) SQuad, (b) soft body - hard leg, (c) hard body - hard leg, (d) hard body - soft leg.

Table 3.1: Translational Speeds in terms of Body Lengths per Second for Different Configurations

Robot Type	**Robot Speed (Body Lengths / s)**
SQuad	**0.5406**
Soft Body - Hard Leg Hybrid	**0.5192**
Hard Body - Hard Leg	**0.7006**
Hard Body - Soft Leg Hybrid	**0.8323**

legs provide when it comes to traction. For both soft body and hard body, the soft legs are slightly faster than the hard legs. This is mainly due to the fact that soft legs conform better with the ground, increasing the surface area that is in contact with the ground hence decreasing the chance of slipping. Regardless of the leg type, soft body performs slower walking motion than the hard body. This is rather expected since some of the input energy is used on robot's undulation rather than its locomotion.

3.1.2 Pitch and Roll Angle Analysis

Pitch and roll angle analysis is crucial to determine the smoothness of the walking. 3 markers were placed on both the soft and the hard bodies to track the motion of the robots. For the hard body, the motion tracking was straightforward since the relative positions of the markers did not change and the software could easily output the roll-pitch-yaw and position data. However for the soft body, post processing was required. The position data from the markers on the soft body was obtained individually and later, the pitch and roll angles were calculated by creating vectors between the markers and using rotation matrices.

It is hard to define the pitch angle for a soft robot since it has a different value on every individual position on the body. However for convenience, we have defined the pitch angle of our soft robot as the angle between the front tip and the rear tip of the soft body. Similarly for the roll data, the front and rear tip was used.

According to the data presented in Fig. 3.2 the pitch angle for the soft bodied robots remain between $\pm 10^{\circ}$ making the translational motion smoother than the hard bodied robots. The soft leg results in higher pitch angle in the positive range and lower in the negative range for the soft bodied robots however the difference is not considerable. The impact forces at the moment where a leg touches the ground are more visible for the hard legged soft bodied robot.

For the hard bodied robot the pitch is mainly between 0° and 20°. The pitch

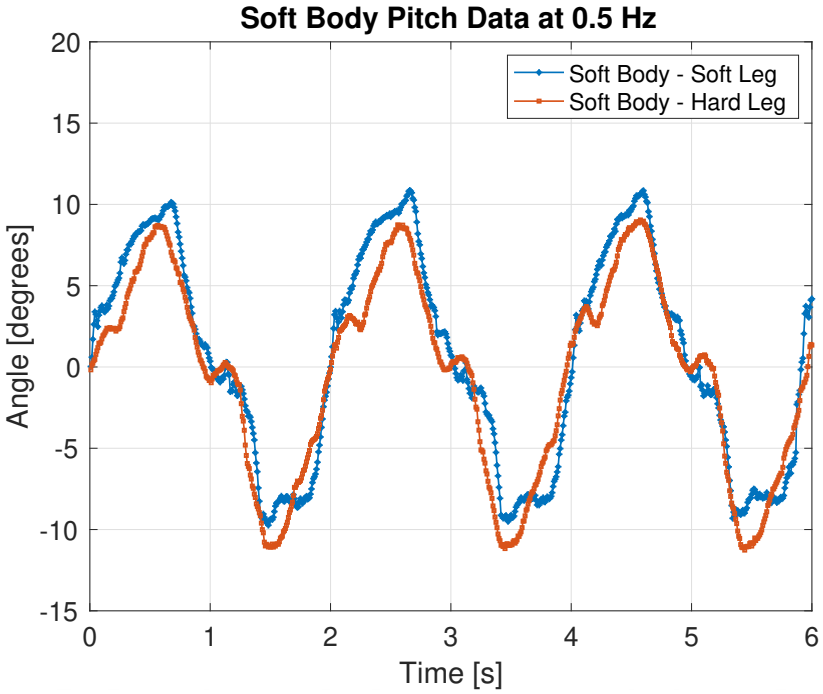

(a) Soft Body Configurations

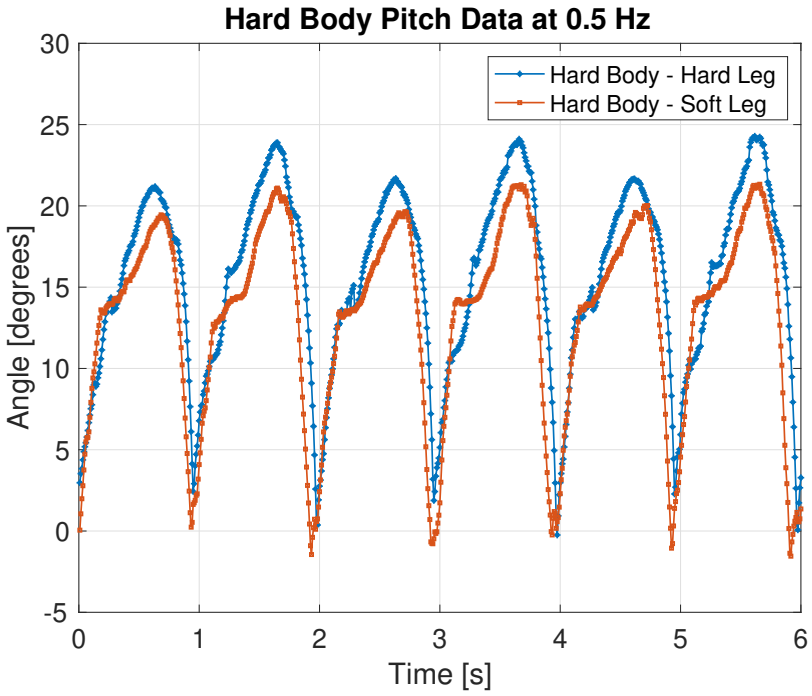

(b) Hard Body Configurations

Figure 3.2: Pitch Angle Data of Soft and Hard Bodies

up behaviour is caused by the moment balance of the robot during forward locomotion and for the hard leg the pitch tends to go higher. It was observed that the reason for this is that the rear legs slip during the pitch up phase causing the front of the robot to rise more.

The pitch data also contains information about the energy loss due to body undulations of the soft robot. A single cycle of pitch up and pitch down phase takes about 1 second for the hard bodied robots whereas it takes about 1.5 seconds for the soft bodied robots which correlate with the speed data found in Table 3.1.

The pitch angle depends heavily on the stiffness of the body whereas the roll angle depends more on the stiffness of the legs. From Fig. 3.3 we see only small difference between 4 different robot configurations for the roll angle mainly due to the fact that the soft legs are much stiffer than the soft body. Even though the hard legs are also much stiffer than the soft legs, the small amount of force applied to them makes this difference not as significant as in the case of the soft body.

The roll data also includes information about how the soft body is better at dampening the impact forces during locomotion. When the roll angle switches from positive to negative and vice versa in Fig. 3.3b, the data clearly shows small peaks which indicate the impacts of the legs with the ground. For the soft body however this situation either does not exist or it is minimal.

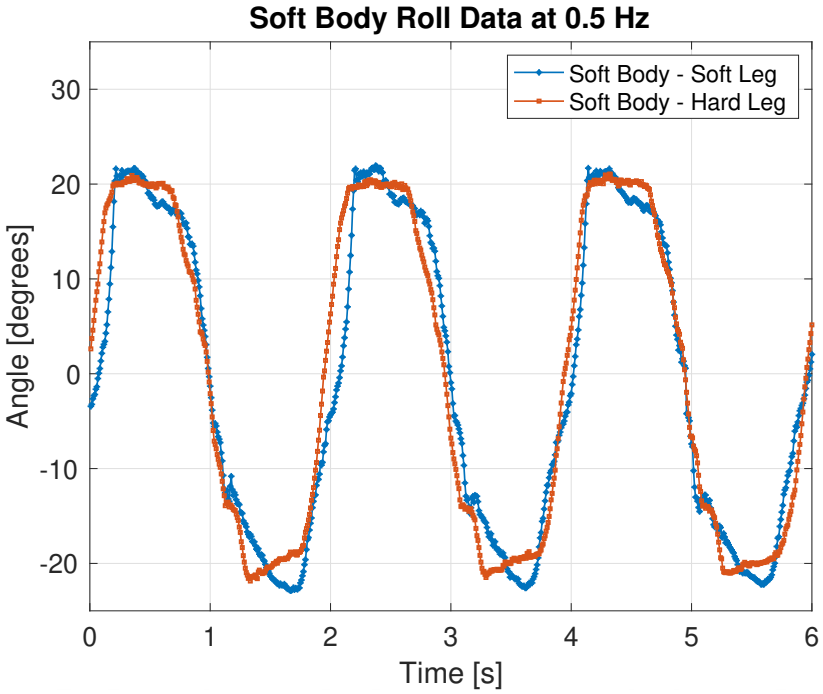

(a) Soft Body Configurations

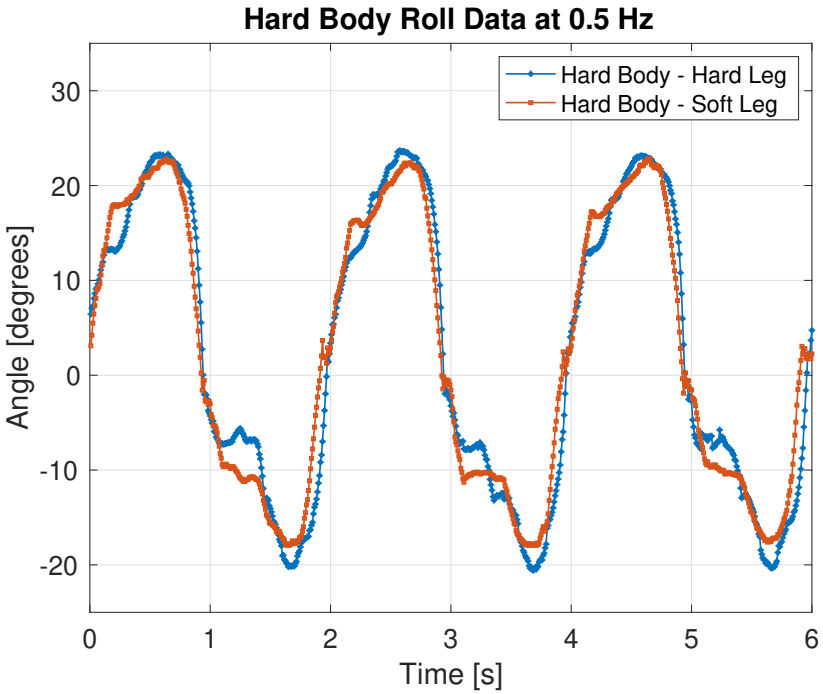

(b) Hard Body Configurations

Figure 3.3: Roll Angle Data of Soft and Hard Bodies

3.1.3 Body Centroid Position Analysis

The center of gravity of the soft robot constantly changes due to body undulations and leg rotations. The center of gravity of hard robot also is not constant due to the leg rotations. Therefore it is extremely difficult to track the center of gravity of the robots precisely. However, in order to get a sense of how smooth the locomotion is; a position analysis was done for the center of geometry, or centroid of the bodies.

It is straightforward to calculate the centroid position of the hard body using the position data obtained by the motion capture system. For the soft body it was tried to place a marker right at the centroid but the motion capture system could not track it accurately especially when the body buckled inwards. Therefore the centroid position was assumed as the center between the front tip and rear tip of the body for convenience. Even though it is not the ideal way to determine the centroid for the soft body, it was observed that this is a fair assumption after comparing the data with the experiment videos.

When the hard robot is sitting with its body parallel to the ground and when the legs are adjusted to result in maximum height; centroid height is approximately 36mm. For the soft robot, this value drops a couple of milimeters since it tends to bend downwards under the load of its own weight.

From the data presented in Fig. 3.4 it can be seen that the centroid of the soft body generally tends to be below 36mm and it drops down to 20mm at its minimum.

For the hard body; the soft legged hybrid has the same high peaks as the hard legged robot. However the lowest peaks of soft legged hybrid are considerably higher than the hard legged robot. This behaviour is observed visually as well and the reason is that when the hard body drops from maximum pitch to minimum pitch, hard leg slips during initial impact; whereas the soft leg grips to the point of first contact, causing the centroid to remain higher.

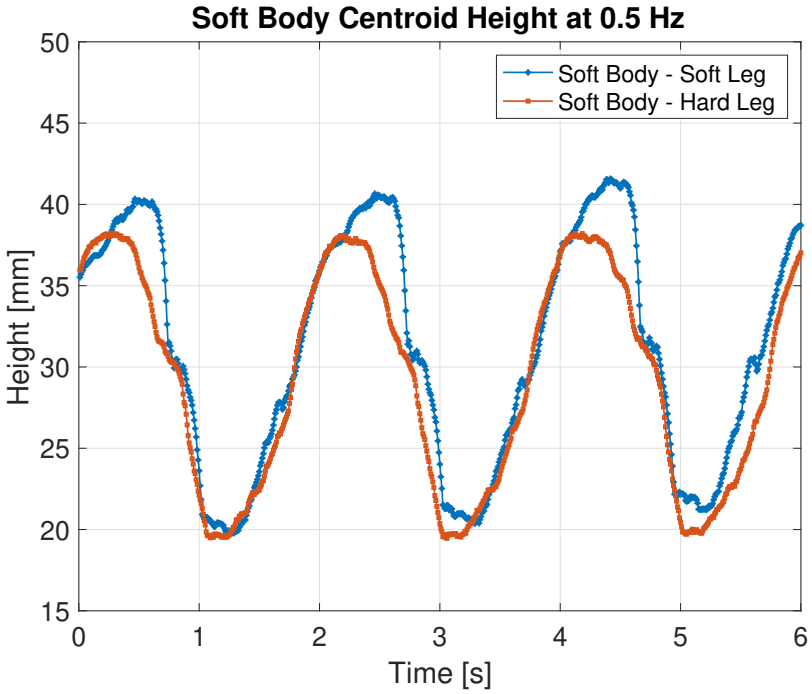

(a) Soft Body Configurations

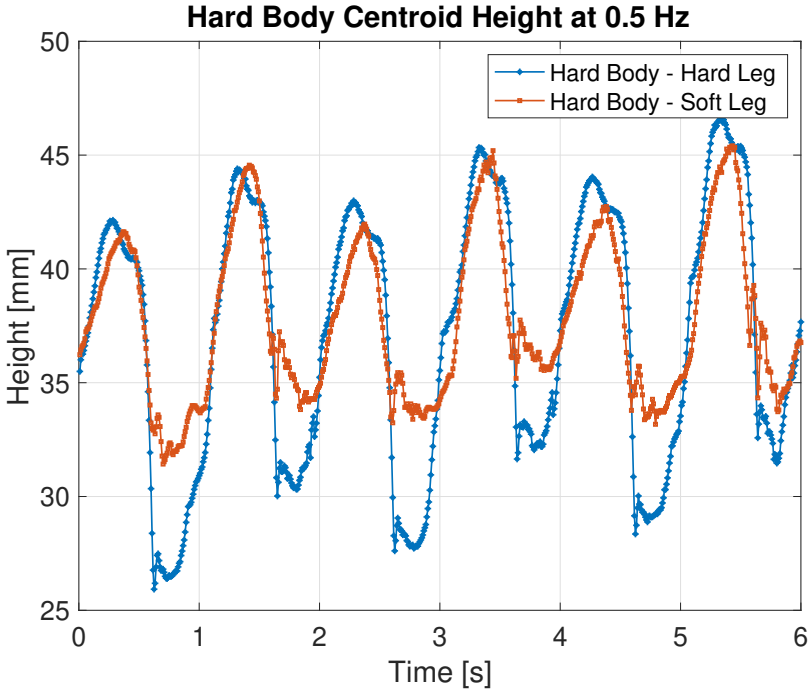

(b) Hard Body Configurations

Figure 3.4: Centroid Height Data of Soft and Hard Bodies

Generally a low centroid position is preferred for better obstacle climbing performance since it reduces the chance of rolling during climbing. Hence, the soft body should have an advantage since the centroid drops to lower heights than the hard body and this was observed in the experiments which are discussed in the next section.

3.1.4 Obstacle Climbing Analysis

Evaluating and comparing the performance of the robots by testing their ability to climb obstacles is a common method. For the obstacle climbing tests, the speed of the motors were set to 0.5 Hz and the gait type was chosen as trot gait. During the tests, the obstacle height was gradually increased and the maximum heights that the robots can scale was recorded.

Table 3.2: Maximum Obstacles Scaled in terms of Body Height

Robot Type	**Obstacle (Body Height)**
SQuad	**1.44 x Body Heights**
Soft Body - Hard Leg Hybrid	**1.13 x Body Heights**
Hard Body - Hard Leg	**0.88 x Body Heights**
Hard Body - Soft Leg Hybrid	**1.08 x Body Heights**

The maximum obstacle height that the robots could climb were presented in terms of body heights in Table. 3.2. The body height is chosen as the neutral height when the roll and pitch angle is zero and the legs are positioned so that the robots are at their maximum heights which is 36mm.

As expected, the soft bodied and soft legged robot (SQuad) performed the best with an impressive obstacle height of 51.8mm (1.44 Body Heights) whereas the fully hard test robot performed the worst at 31.7mm (0.88 Body Heights).

The effect of the body type is significant for the obstacle climbing tests. Regardless of the leg type, the soft bodied robots were able to climb higher obstacles than the hard bodied robots could. Similarly, regardless of the body type, both

the soft body and hard body performs better with a soft leg rather than a hard leg.

A screen shot of SQuad climbing the obstacle 1.44 times its body height is shown in Fig. 3.5.

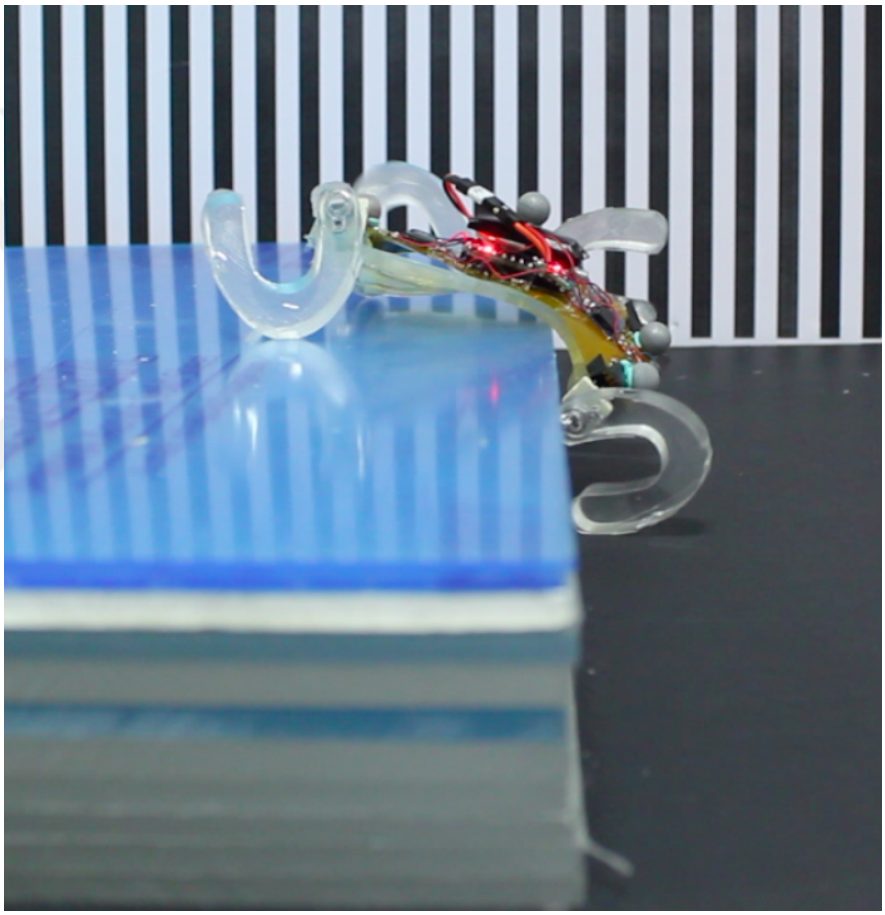

Figure 3.5: SQuad climbing the obstacle 1.44 times its body height.

3.1.5 Testing Maximum Climbing Angle on an Inclined Surface

During the first design stages of SQuad, a goal was made to make SQuad able to climb a slope of 60°. In order to achieve this, a soft tail structure was added to the main body of SQuad as presented before in Fig. 2.20. During the initial

tests, all of the attention was directed toward the design of the tail and the importance of the surface was neglected. In the first trials, a surface with cotton and velvet fabrics was used and it caused a poor performance. The friction coefficient between these surfaces and the PDMS legs were too low to obtain a result that is close to the initial goal of 60°. Therefore, the experiment setup was redesigned and the surface was changed with an acrylic sheet and it was observed that the climbing performance was increased considerably. Additionally, the PDMS legs were coated with thin layers of double sided tape to increase the traction. Thanks to these modifications, SQuad was able to climb 52° before it started rolling down the slope. A screenshot from the experiment where SQuad is climbing 52° is presented in Fig. 3.6.

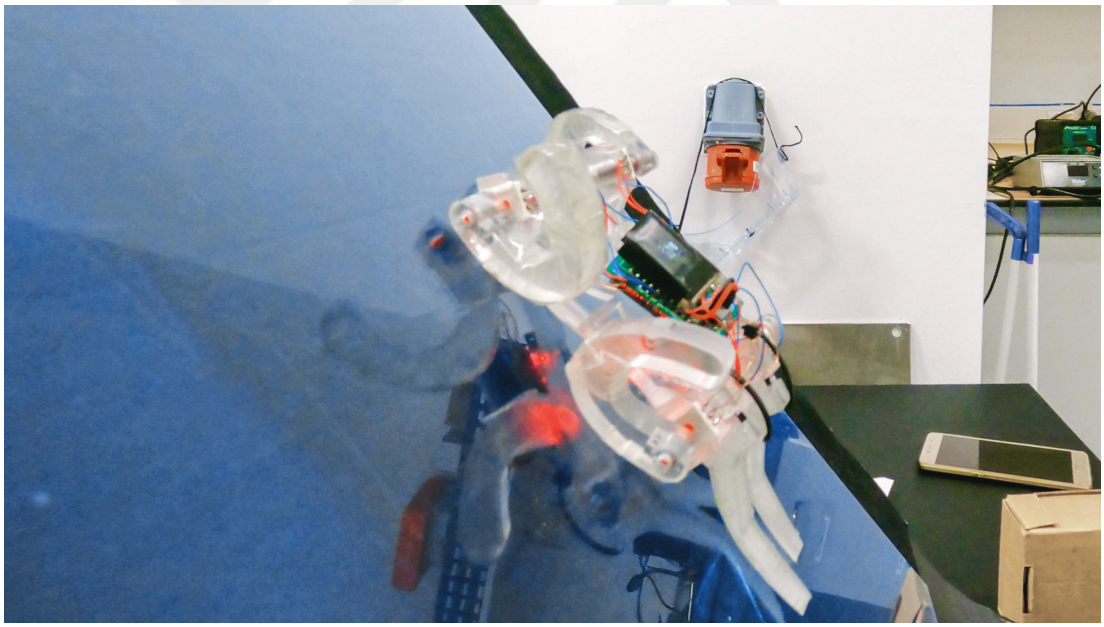

Figure 3.6: SQuad climbing a slope of 52°.

Even though these ideal conditions may not be present in real case scenarios, this result is still valuable to show how the capabilities of a soft robot may be improved by small modifications such as adding a soft tail structure to the main body of the robot.

3.1.6 Testing the Onboard Microphone

The final feature that the SQuad has is its capability to detect sound levels around it. In order to be effectively used in search and rescue operations, we wanted to add additional features that may be useful in scenarios such as finding people under a rubble after an earthquake.

Adding this microphone also shows how modular SQuad can be. The microphone module of Adafruit MAX 4466 was used and the existing PCB was not even modified to add this microphone. Only three pins were directly soldered onto the board and the microphone was ready for operation.

The only downside of adding the microphone directly was the added noise levels that were caused by the motors. Hence, in order to isolate the microphone output from this noise, either a filtering system was going to be designed, or the power source of the microphone was going to be separated from the rest of the system. The filtering attempts using only software was not sufficient to obtain usable data. Additional circuitry and physical components were needed to obtain a perfect filtering. Instead of this, we tried to connect the power inlet of the microphone directly into the 3.7 V lithium ion battery rather than the power coming from the Arduino. After connecting the microphone into the noise-free power lines, we obtained data that we could use. Our aim with adding a microphone was to prove that the SQuad is able to detect sound levels in terms of amplitude.. It requires a lot more computation power than the Arduino could offer to detect specific words and act accordingly. Hence, we only coded Arduino to stop its motors and light an LED once the signal amplitude is above a specific value. An experiment was done where the SQuad stops its movement and lights up an LED when it detects a sound with an irregularly high amplitude. The screenshots of this experiment is presented in Fig. 3.7.

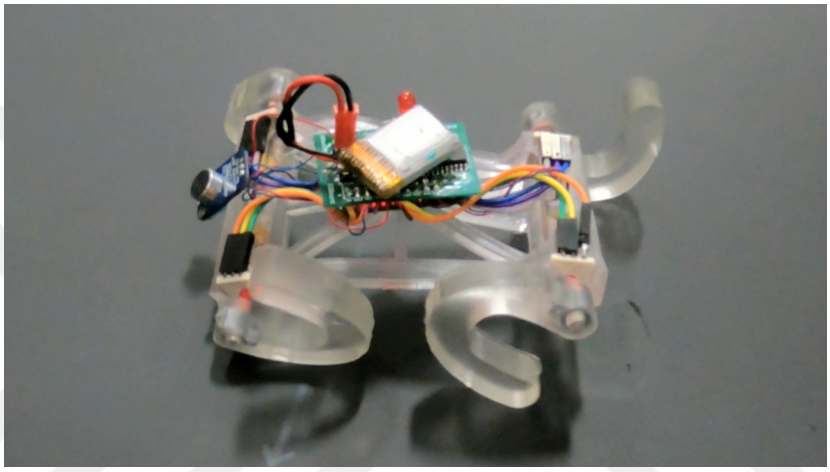

(a)

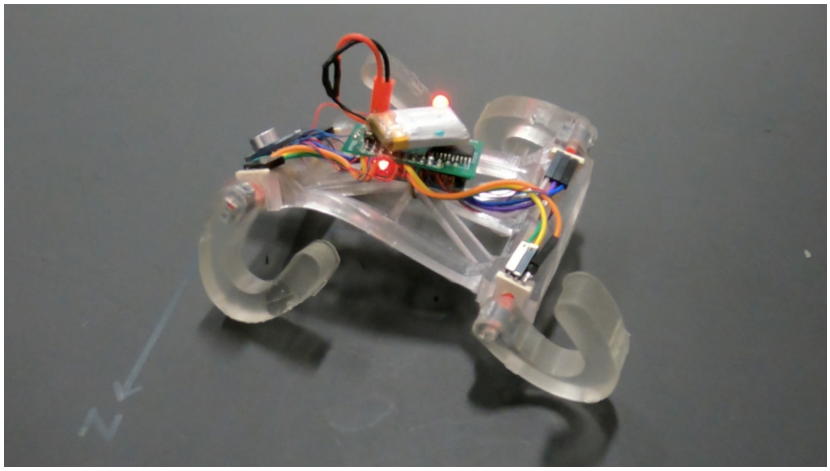

(b)

Figure 3.7: (a)SQuad is moving with the LED turned of. (b) SQuad detects sound, it stops and lights the LED.

3.2 Compression Performance of cSQuad

In this section, the designs made for the C shaped leg and the compressible body for the cSQuad will be tested individually. Later, the final tests will include the fully operational untethered cSQuad locomoting through an obstacle with a narrowing path to demonstrate the compression capabilities of the robot.

3.2.1 C Shaped Leg Compression Tests

In the last chapter, the design and fabrication steps of the initial C leg prototypes and the final versions were discussed. It was explained that in order to transfer electricity from the body to the legs, a slip-ring system was necessary. In this section, all iterations of the C shaped leg designs will be tested along with the slip-ring designs.

First, a test setup was designed and fabricated using a 3D printer to test the initial design of the slip-ring. In this design, the slip-ring that is designed to be connected to the body was fixed on the test setup as seen in Fig. 3.8.

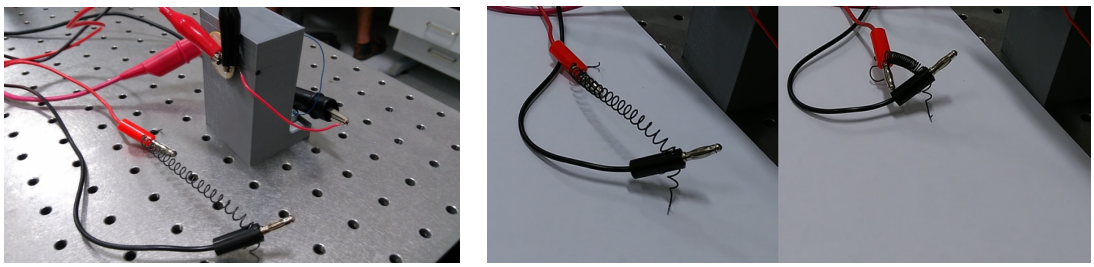

(a) (b)

Figure 3.8: (a) Test setup for the slip-ring. (b) An SMA spring before (left) and after (right) a current is applied.

In the test setup presented in Fig. 3.8a, the SMA spring is connected via jumper cables to the slip-ring that was designed to be mounted on the C leg. Even though this test was static and the 2 slip-rings did not move relative to each other, it initially showed that the slip-ring circuits are capable of transmitting currents

as high as 2 amperes continuously and later they were also given 6 amperes and they continued operating successfully.

As a next step, the slip-ring was connected to the PDMS leg and the connections between the slip-ring and the SMA spring was made. In the first trials, it was observed that the SMA does not hold solder and therefore the cables were tightly knot together to the SMA spring. Then a solder was applied to the knotted copper so that the knot does not get untied. The resulting PDMS C shaped leg with a slip-ring is presented in Fig. 3.9.

Figure 3.9: Uncompressed (left) and compressed (right) C shaped PDMS leg with the slip-ring

After it was confirmed that the slip-ring works in a static setup, a dynamic test setup was designed and fabricated. In this next test setup, the C leg is connected to the motor and the sensor just like it would be in the actual body of the robot as seen in Fig. 3.10.

The first tests using the rotational test setup in Fig. 3.10 is presented in Fig. 3.11. Initially, the C leg was rotated for 3 seconds and then it was stopped. After it stopped the current was applied to the system and the compression is observed as in Fig. 3.11a. Later, the capability of the slip-ring while the leg still rotates was put to test. In Fig. 3.11b, the leg was rotated for 8 seconds and during this time, current was given to the system. After the leg stopped, the compression was observed. Hence, this test proves that the slip-ring works both during rotation and when the leg comes to a stop. However, it is also observed visually that the

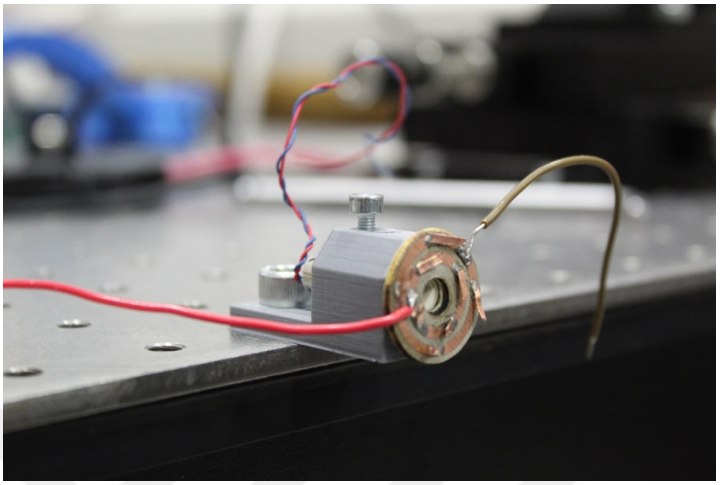

Figure 3.10: The rotational test setup for the initial slip-ring desing

compression performance is better when the leg is not rotating. This might be caused by two reasons. The first is that the inertial effects are exerting a force on the spring which makes it harder to compress. And the second is that the spring cools down because of air flow and it reduces the performance of the SMA.

Even though the initial test were successful, there were some issues regarding the durability of the 3D printed parts inside the PDMS legs. These 3D printed parts are basically connection docks for the SMA springs and as the SMA springs heat up, these parts tend to melt. Fig. 3.12 shows a case where a current of 6 Amperes were conducted through the SMA springs and it shows how the 3D printed part melts and burns. Eventually the 3D printed part fails and the spring detaches from the leg. Even though we typically apply 2 Amperes instead of 6 Amperes, this result hints that every time the SMA spring heats up (even at 2 Amperes), it weakens the 3D printed part and it would result in low durability of the parts in the long run. Considering that the leg becomes scrapped after a failure, it would have been costly to ignore this problem in terms of time, labor and money. Therefore, as explained in the last chapter, the PDMS leg was replaced with the RTV2 silicone leg which does not require any 3D printed parts inside. The RTV2 silicone is extremely heat resistant compared to PDMS and it can withstand the forces that the SMA spring applies.

As explained in the last chapter, the slip-ring design was modified and finalized

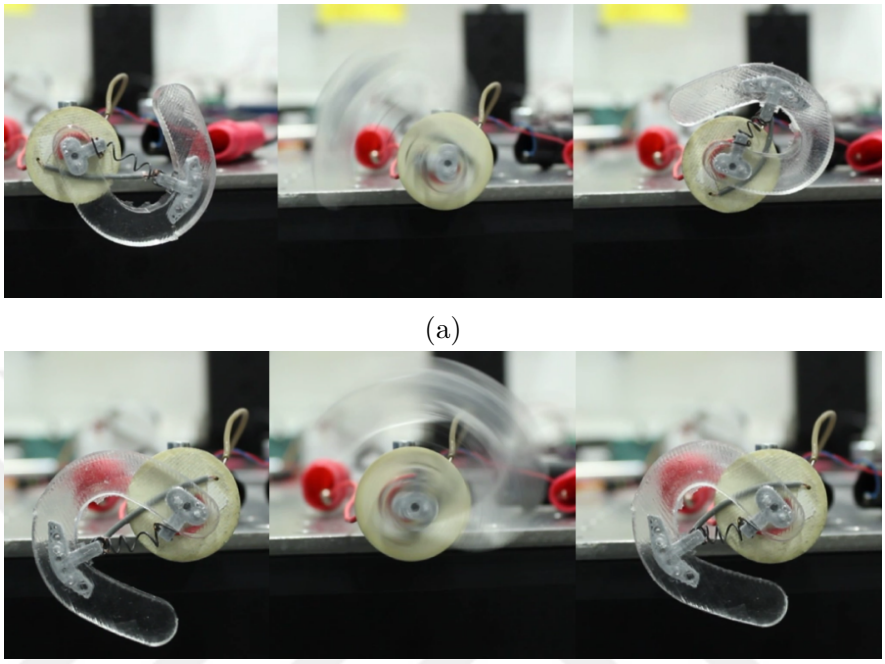

(a)

(b)

Figure 3.11: (a) The compression of PDMS C leg after 3 seconds of rotation. (b) The compression of PDMS C leg during 8 seconds of rotation.

by incorporating pogo pins inside the C shaped legs. The legs made with RTV2 silicone was used in the final design of the slip-ring and the figure for the test setup is re-presented in Fig. 3.13.

The final design in Fig. 3.14 is an important improvement because it makes it less complicated to fabricate the C shaped legs and also it reduces the number of parts in the leg assembly of the robot considerably. The tests for this leg is presented in Fig. 3.15.

The final tests for the C shaped leg is done to make sure that all of the 4 legs can be compressed during operation. Therefore, 4 slip-ring systems were installed to a dummy robot body as seen in Fig. 3.15.

The electronics and the C legs made from RTV2 silicone is assembled to the body in Fig. 3.15 and the final tests for the leg compression have been conducted. The SMA springs for front leg pair and the rear leg pair have been connected in series. This way, if one of the legs don't compress, the the corresponding pair will

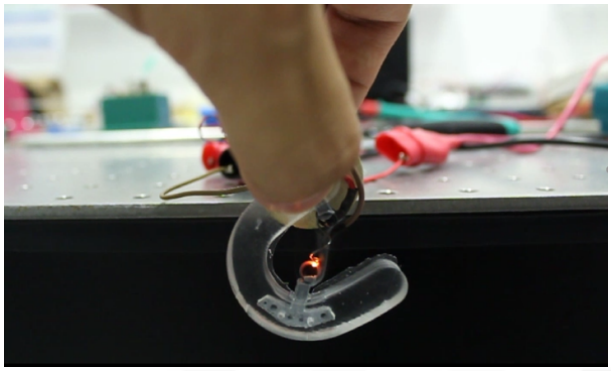

Figure 3.12: The failure of the PDMS C shaped leg during compression

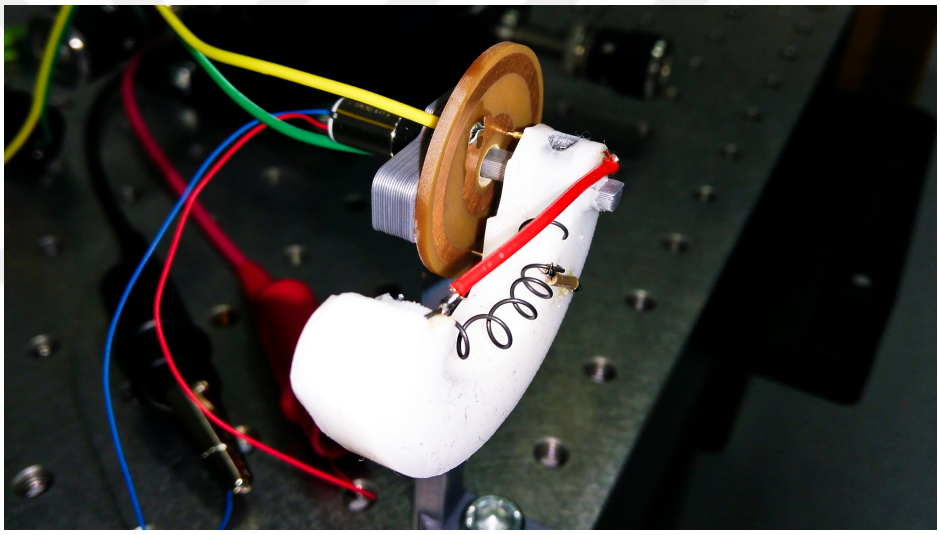

Figure 3.13: The final slip-ring with the pogo pins attached to the C shaped leg

also not compress. This makes sure that the robot is balanced in case of a single leg failure and it does not try to rotate towards the side opposite to the failure. Also, connecting 2 SMA springs in series increases the total resistance which helps limiting the maximum amount of current drawn from the battery. In return, the legs compress slower but it was observed that the difference in compression time was not noteworthy. The screenshots from the final leg compression tests are presented in Fig. 3.16.

In order to not overload the battery, the front legs are compressed first for 5 seconds. Then the rear legs are compressed for 5 second. During the whole process, all of the legs rotate with 1 Hz motor frequency using trot gait. All of

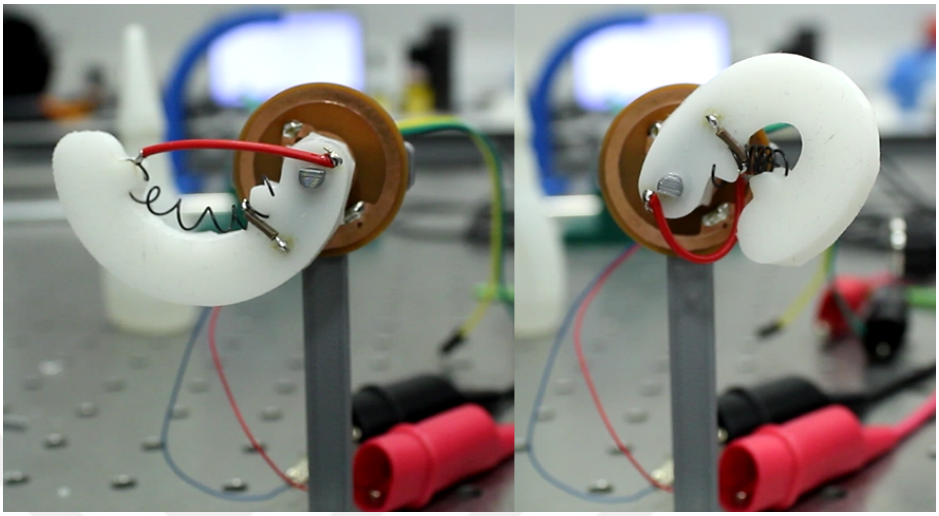

Figure 3.14: The test for final design of the slip-ring with the RTV2 silicone C shaped leg

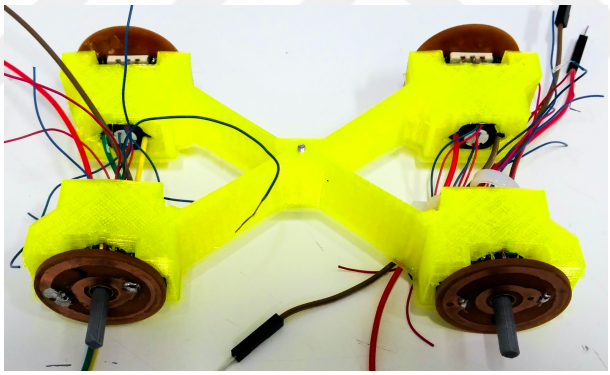

Figure 3.15: The robot body equipped with 4 slip-ring systems for the final leg compression test

the tests in this section conclude that the leg compression works for the cSQuad.

3.2.2 Body Compression Tests

Compression tests for the body is more straightforward compared to the tests for the C shaped leg. Here, the tests don't require additional means for electrical connections such as the slip-rings. The initial compression tests were done on the body that was presented in Fig. 2.74. The front view of this test is presented in Fig. 3.17.

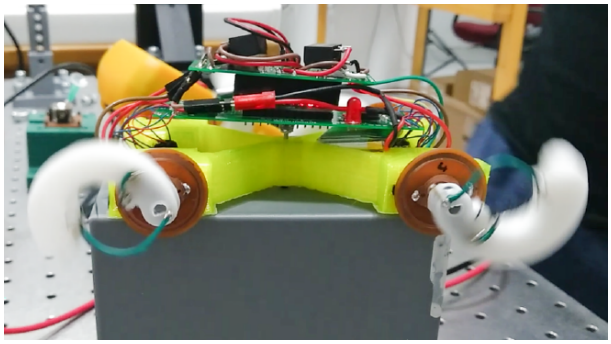

(a)

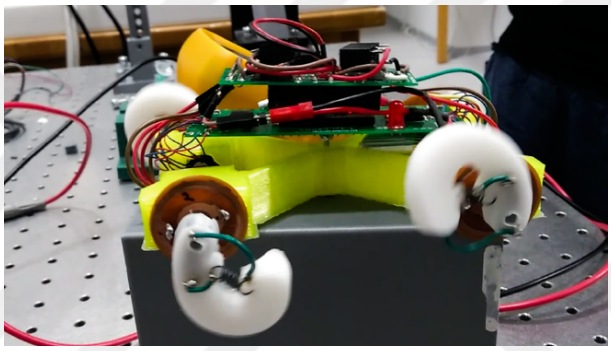

(b)

Figure 3.16: (a) Final compression test for 4 C legs (uncompressed). (b) Final compression test for 4 C legs (compressed).

The test in Fig. 3.17 shows that the initial width of the body is 62 mm and the width of the body after compression is approximately 41 mm. This means that the compression amount is 21 mm which is 33.9% of the initial width of the body. However, as explained in the design chapter, this body had to be scrapped due to the negative camber angle it provides and due to the unwanted stress created on the side beams of the robot as shown in Fig. 2.78.

The compression test for the final version of the body is presented in Fig. 3.18. Here it can be seen that the end of the motors are touching after compression which indicates that the compression amount is 21 mm which is the maximum distance between the motors. The original width of the body is 65 mm hence the compressed width of the body becomes 44 mm. Therefore the compression amount is approximately 32.3% of the original width of the body.

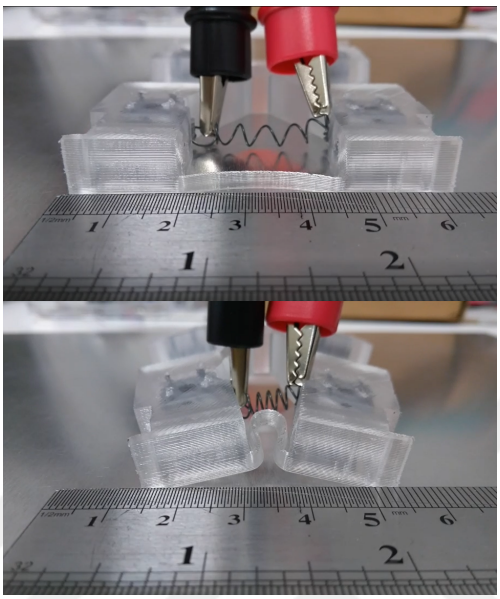

Figure 3.17: The uncompressed (top) and compressed (bottom) body with X shaped center.

3.2.3 Final Compression Tests of the Untethered Robot

In order to obtain the overall compression performance of the robot, the leg compression and the body compression should take place together. In order to achieve this, a robot with a flexible PCB, with 4 compressible legs and a compressible body is fabricated and assembled.

As explained before, this robot makes use of relays to control the activation of the shape memory alloy springs. It incorporates two 3.7 V batteries, one for the logical boards and motors and the other for solely powering the SMA's. When powered on, the robot starts to locomote with trot gait for 5 seconds with 0.5 Hz motor speed. In the next 5 seconds the relay for the rear legs is activated and they consequently get compressed. The front legs get compressed with the same method and finally during the last 5 seconds, the SMA springs on the body get compressed. All the while, the legs continue to rotate with their assigned phase.

During the locomotion it is difficult to measure the exact cross sectional area of the robot since the legs continuously rotate and the soft body of the robot undulates. In order to calculate the exact change in cross sectional area at any

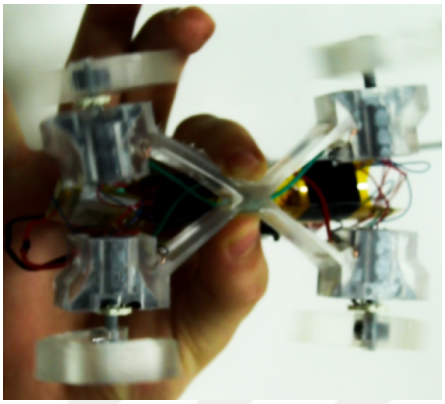

(a)

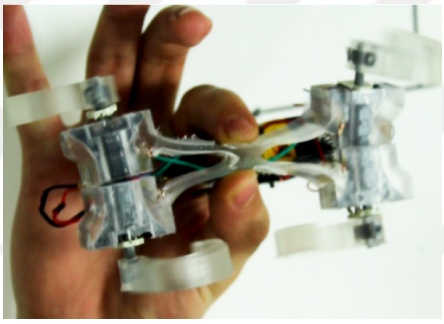

(b)

Figure 3.18: (a) Final compression test for the body (uncompressed). (b) Final compression test for the body (compressed).

time, a model for the body and the legs is required. However, with the test setup presented in Fig. 3.19 we can prove that the cSQuad can go through an opening that is smaller than its original cross section and we can also measure the compression amount experimentally.

The final robot has a width of approximately 115 mm when all the legs are connected. The test in Fig. 3.19 shows that the robot can locomote inside a path that is 90 mm in width. Which means that the cSQuad can locomote through paths that are 21.7% narrower its original size. In addition, it is measured that once the cSQuad activates all of the SMA springs, its width reduces down to 85 mm which means technically the minimum width that the cSQuad can fit into is approximately 26.1% less than its original width.

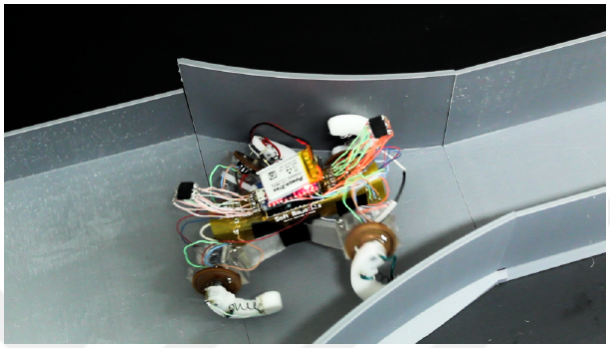

(a)

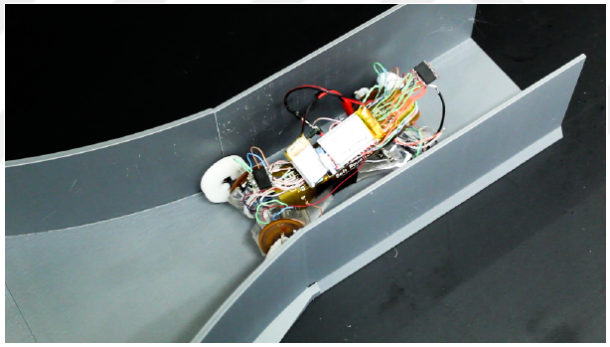

(b)

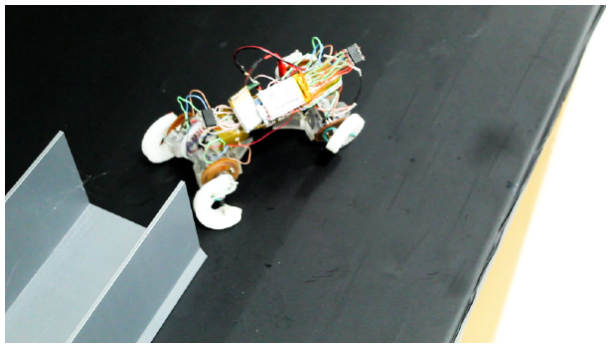

(c)

Figure 3.19: (a) The uncompressed cSQuad unable to go through the narrowing path. (b) Compressed cSQuad locomoting through the narrowing path. (c) Compressed cSQuad exiting the test setup.

Chapter 4

Conclusion and Future Directions

4.1 Summary and Conclusion

This thesis presents a soft quadruped (cSQuad) that has the ability to compress its legs and body with the purpose of passing through openings that are smaller than its cross-section. cSQuad is the third generation of a C-legged quadruped series that have been designed and fabricated in Bilkent Miniature Robotics Lab and it carries similar characteristics with the first generation CQuad and the second generation SQuad. Therefore, the thesis starts with explaining the CQuad which is an origami style foldable C-legged quadruped. Then the design and fabrication steps of SQuad is explained briefly. Since SQuad is the first soft robot fabricated in our lab, the information about how to fabricate parts using PDMS or other soft polymers is explained in this section. SQuad also shares mostly the same electronic components and the same control code with cSQuad. Hence, a detailed explanation on the logic of the board and the physical design of the board are also given in the section dedicated to SQuad.

Next, the thesis presents the design and fabrication steps of the cSQuad. Initially, the method for compression is chosen and the rest of the design is based around the fact that SMA springs were going to be deployed in the robot. The

four-bar type leg design was created initially but the first fabricated parts suggested that the four-bar design was not suitable for cSQuad mainly because it couldn't support the weight of the robot and also it was decided that using a kinematic chain in a soft robot limited the potential advantages of having a soft robot. Therefore a switch in design was made towards C-shaped legs which brought additional problems especially regarding electricity. Unlike SQuad, the C-shaped legs of the cSQuad are equipped with SMAs and they need to be actuated. Since the legs rotate continuously, it is impossible to solder cables to the legs directly because the cables would get tangled with every rotation. Hence a slip-ring system was designed and fabricated which solved the problem of transmitting electricity to a rotating system. After the leg design was finished, the body design was explained. The initial compressible body design was based on SQuad but it used Ecoflex and PDMS together which resulted in mechanical failures at the interface between these materials. An X shaped body was later designed and several analyses were made to improve this design. In the end, this X shaped body was used and some improvements were made for better assembly of the robot. The biggest improvement for the ease of assembly was the design of a part called motor package. The motor package was printed using soft TPU polymer and it is designed to carry the motor, the sensor and the slip-ring and the cables had guides so that there were no cable mess. This motor package is assembled outside and it is slided into the body externally. Then the assembly is done when the cables are soldered into the main board. This makes it easier to assemble a robot and it also makes it easier to repair or change a part.

A set of experiments were done for both SQuad and cSQuad. For the SQuad, the tests regarding pitch and roll angle and centroid position analysis showed that SQuad was better in providing a smoother and overall better locomotion compared to the rigid and hybrid twins. It also proved that being soft provided to be advantageous for obstacle scaling performance compared to being rigid. For the cSQuad, once the design and fabrication stage was completed, it was put to test. Initially, it was aimed that the cSQuad would be able to reduce its cross-section area by 25%. This value was chosen as a design exercise and it does not. The tests showed that it can reduce its cross-section area by 26.1% when

its not moving and it can go through openings that are 21.7% narrower than its cross-section.

The experiments for SQuad showed the drastic differences between using hard and soft materials. Even though similar locomotion analysis for cSQuad has not been done, we expect and observe that as the body of the cSQuad compresses, the robot will have larger rolling angles which may eventually result in tipping over of the robot. This would happen mainly because the distance between the legs would decrease. And also the center of gravity of the robot would move further up from the ground because of the stiffened body. Hence, just like in SQuad experiments, we see a change in stiffness for the cSQuad as the compression happens. Therefore, in this study, with each experiment we consequently achieve a change in robot stiffness by changing the material or changing the geometry of the robot. However, this change happens in discrete steps. For example for the SQuad we can either have a robot body made out of soft PDMS or rigid 3D printed material. Or for the cSQuad the robot is either in fully compressed mode or it's in released mode. These discrete steps also require a lot of effort such as using high power SMA springs or changing the parts of the robot. We could achieve same or similar results by embedding the ability of stiffness change into the material itself. For example, a smart material that changes its stiffness with changing temperature may be embedded inside the SQuad and by controlling this temperature actively, the SQuad could both be made stiffer or softer depending on the environment that it's on. For faster speeds, we would want the robot body to be stiffer and for better obstacle climbing we would want the body to be softer. Having a single robot to achieve multiple tasks would be cost effective but as another advantage, since the stiffness can be set continuously rather than discretely, the optimum settings for every task can be studied precisely and this information can be used to optimize the robot design even further. SQuad and cSQuad can be convenient to be used as a test bed for trying new smart materials.

4.2 Contributions

The major contribution of this work is that it presents an untethered soft quadruped that can compress both its legs and body using SMAs. Even though there are similar works in literature [26, 27], to our knowledge cSQuad is a unique work that combines features such as being a soft bodied and soft C-shaped legged quadruped, having both the legs and body to be compressible, utilizing and controlling SMAs, using a soft PCB and being mobile. Having all these features together, makes cSQuad a novel work that potentially add value to the literature.

In addition to its novelty, cSQuad uses slip-rings with pogo pins to transmit power to rotating shape memory alloys in miniature scale. Even though SMAs are used frequently in industrial applications, to our knowledge there is not another example of a slip-ring system that use pogo-pins together with shape memory alloys in a miniature soft quadruped robot. Therefore it is another contribution which can be used for the robots to be designed in the future.

4.3 Future Directions

One of the main controversies in soft robotics is the definition of soft robots. As explained in the literature review in the first chapter, the definition that is generally accepted is that a robot does not have to be fully soft to be considered a soft robot. It is sufficient for the robot to comply with its surrounding environment to be considered soft. However, as the technology advances, there are more opportunities to convert some rigid components of a soft robot into soft components in an effort to reach the highest potential that the robot has to offer. It is uncertain whether this approach would be successful for every robot but there should still be examples that would study the benefits and disadvantages of such parts that are converted from being rigid to soft for future reference. In an attempt to make the cSQuad even softer, the rotary encoder sensor can be made soft in the future.

To do this, several soft sensors made out of electrically conductive soft polymers can be embedded inside specific parts of the body. As the robot undulates, the readings coming from these sensors can be used as inputs to decide the attitude of the robot. Eventually, this data can be used to control the gait and other aspects of locomotion such as steering. In fact we have already started to experiment with the soft sensors that we fabricate from conductive TPU filaments and a prototype of a soft body that has 4 embedded soft sensors can be seen in Fig. 4.1.

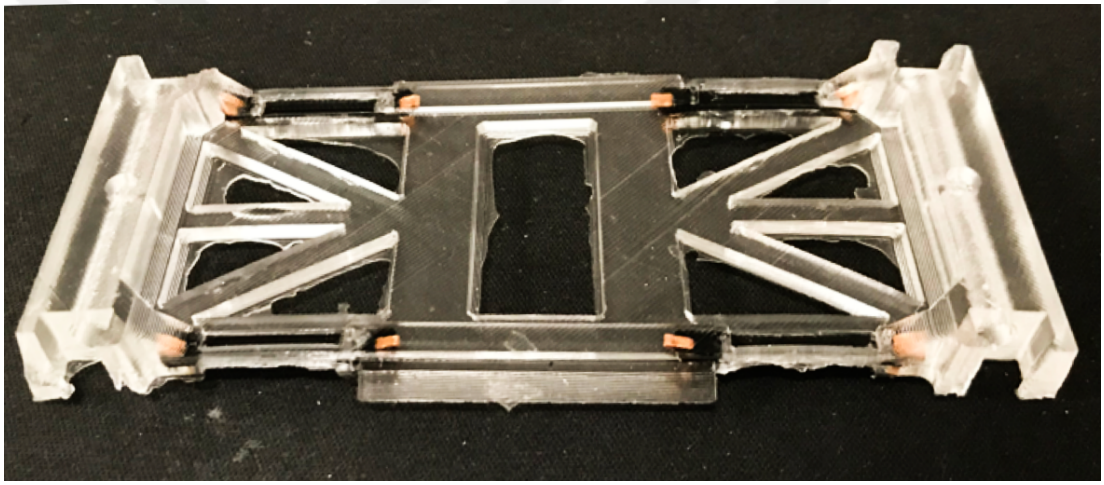

Figure 4.1: The first prototype body equipped with 4 soft sensors.

Another component that has the potential to be made softer is the PCB of the cSQuad. Even though cSQuad has already a flexible board, this board is not integrated perfectly onto the robot. First of all, the board includes premade rigid boards such as the Arduino micro controller or the voltage regulator. Having rigid boards on top of a soft board decreases the flexibility. Hence, a solution which integrates every component into a single flexible board can be found in the future. Even though the integrated circuits (ICs) would still be rigid, their sizes are usually small enough to neglect. Another problem with the PCB of cSQuad is that it is not protected from the working environment of the robot. Because of this, it is easier for the solders to come out as they come in contact with external objects. A solution that solves both the durability problem and the flexibility problem can be achieved with using a 3D printed PCB that uses silver inks. These inks can be printed on many surfaces. Therefore in the

future they can be printed right on top of the body of the robot. And after the soldering of the IC chips are done, an additional protective layer of PDMS can be poured on top of the board to seal and protect it.

Bibliography

[1] M. A. I. Kalin, C. Aygul, A. Turkmen, J. Kwiczak-Yigitbasi, B. Baytekin, and O. Ozcan, "Design, fabrication, and locomotion analysis of an untethered miniature soft quadruped, squad," *IEEE Robotics and Automation Letters*, vol. 5, no. 3, pp. 3854–3860, 2020.

[2] C. Laschi, B. Mazzolai, and M. Cianchetti, "Soft robotics: Technologies and systems pushing the boundaries of robot abilities," *Science Robotics*, vol. 1, no. 1, 2016.

[3] M. Wehner, R. L. Truby, D. J. Fitzgerald, B. Mosadegh, G. M. Whitesides, J. A. Lewis, and R. J. Wood, "An integrated design and fabrication strategy for entirely soft, autonomous robots," *Nature*, vol. 536, pp. 451–455, Aug 2016.

[4] S. Hirose and Y. Umetani, "The development of soft gripper for the versatile robot hand," *Mechanism and Machine Theory*, vol. 13, no. 3, pp. 351–359, 1978.

[5] K. Suzumori, S. Iikura, and H. Tanaka, "Flexible microactuator for miniature robots," in *[1991] Proceedings. IEEE Micro Electro Mechanical Systems*, pp. 204–209, 1991.

[6] K. Suzumori, S. Iikura, and H. Tanaka, "Applying a flexible microactuator to robotic mechanisms," *IEEE Control Systems Magazine*, vol. 12, no. 1, pp. 21–27, 1992.

[7] M. D. Grissom, V. Chitrakaran, D. Dienno, M. Csencits, M. Pritts, B. Jones, W. McMahan, D. Dawson, C. Rahn, and I. Walker, "Design and experimental testing of the OctArm soft robot manipulator," in *Unmanned Systems Technology VIII* (G. R. Gerhart, C. M. Shoemaker, and D. W. Gage, eds.), vol. 6230, pp. 491 – 500, International Society for Optics and Photonics, SPIE, 2006.

[8] E. Brown, N. Rodenberg, J. Amend, A. Mozeika, E. Steltz, M. R. Zakin, H. Lipson, and H. M. Jaeger, "Universal robotic gripper based on the jamming of granular material," *Proceedings of the National Academy of Sciences*, vol. 107, no. 44, pp. 18809–18814, 2010.

[9] J. Amend, N. Cheng, S. Fakhouri, and B. Culley, "Soft robotics commercialization: Jamming grippers from research to product," *Soft Robotics*, vol. 3, pp. 213–222, Dec. 2016.

[10] A. Koivikko, D.-M. Drotlef, C. B. Dayan, V. Sariola, and M. Sitti, "3d-printed pneumatically controlled soft suction cups for gripping fragile, small, and rough objects," *Advanced Intelligent Systems*, vol. n/a, no. n/a, p. 2100034.

[11] G. D. Howard, J. Brett, J. O'Connor, J. Letchford, and G. W. Delaney, "One-shot 3d-printed multimaterial soft robotic jamming grippers," *Soft Robotics*, June 2021.

[12] A. Koivikko, D.-M. Drotlef, M. Sitti, and V. Sariola, "Magnetically switchable soft suction grippers," *Extreme Mechanics Letters*, vol. 44, p. 101263, 2021.

[13] F. Ongaro, S. Scheggi, C. Yoon, F. v. den Brink, S. H. Oh, D. H. Gracias, and S. Misra, "Autonomous planning and control of soft untethered grippers in unstructured environments," *Journal of Micro-Bio Robotics*, vol. 12, pp. 45–52, Jun 2017.

[14] N. W. Bartlett, M. T. Tolley, J. T. B. Overvelde, J. C. Weaver, B. Mosadegh, K. Bertoldi, G. M. Whitesides, and R. J. Wood, "A 3d-printed, functionally

graded soft robot powered by combustion," *Science*, vol. 349, pp. 161–165, July 2015.

[15] X. Huang, K. Kumar, M. Khalid Jawed, Z. Ye, and C. Majidi, "Soft electrically actuated quadruped (seaq)—integrating a flex circuit board and elastomeric limbs for versatile mobility," *IEEE Robotics and Automation Letters*, vol. 4, no. 3, pp. 2415–2422, 2019.

[16] H. Jin, E. Dong, M. Xu, C. Liu, G. Alici, and Y. Jie, "Soft and smart modular structures actuated by shape memory alloy (SMA) wires as tentacles of soft robots," *Smart Materials and Structures*, vol. 25, p. 085026, July 2016.

[17] T. Umedachi, V. Vikas, and B. A. Trimmer, "Softworms : the design and control of non-pneumatic, 3d-printed, deformable robots," *Bioinspiration & Biomimetics*, vol. 11, p. 025001, Mar. 2016.

[18] M. Cianchetti, M. Calisti, L. Margheri, M. Kuba, and C. Laschi, "Bioinspired locomotion and grasping in water: the soft eight-arm OCTOPUS robot," *Bioinspiration & Biomimetics*, vol. 10, p. 035003, may 2015.

[19] C. Laschi, M. Cianchetti, B. Mazzolai, L. Margheri, M. Follador, and P. Dario, "Soft robot arm inspired by the octopus," *Advanced Robotics*, vol. 26, no. 7, pp. 709–727, 2012.

[20] M. T. Tolley, R. F. Shepherd, B. Mosadegh, K. C. Galloway, M. Wehner, M. Karpelson, R. J. Wood, and G. M. Whitesides, "A resilient, untethered soft robot," *Soft Robotics*, vol. 1, pp. 213–223, Sept. 2014.

[21] F. Jiang, Z. Zhang, X. Wang, G. Cheng, Z. Zhang, and J. Ding, "Pneumatically actuated self-healing bionic crawling soft robot," *Journal of Intelligent & Robotic Systems*, vol. 100, pp. 445–454, Mar. 2020.

[22] W. Huang, J. Xiao, and Z. Xu, "A variable structure pneumatic soft robot," *Scientific Reports*, vol. 10, Nov. 2020.

[23] D. Drotman, S. Jadhav, M. Karimi, P. de Zonia, and M. T. Tolley, "3d printed soft actuators for a legged robot capable of navigating unstructured

terrain," in *2017 IEEE International Conference on Robotics and Automation (ICRA)*, pp. 5532–5538, 2017.

[24] J. Wirekoh and Y.-L. Park, "Design of flat pneumatic artificial muscles," *Smart Materials and Structures*, vol. 26, p. 035009, Feb. 2017.

[25] M. Baumgartner, F. Hartmann, M. Drack, D. Preninger, D. Wirthl, R. Gerstmayr, L. Lehner, G. Mao, R. Pruckner, S. Demchyshyn, L. Reiter, M. Strobel, T. Stockinger, D. Schiller, S. Kimeswenger, F. Greibich, G. Buchberger, E. Bradt, S. Hild, S. Bauer, and M. Kaltenbrunner, "Resilient yet entirely degradable gelatin-based biogels for soft robots and electronics," *Nature Materials*, vol. 19, pp. 1102–1109, Oct 2020.

[26] D.-Y. Lee, J.-S. Koh, J.-S. Kim, S.-W. Kim, and K.-J. Cho, "Deformable-wheel robot based on soft material," *International Journal of Precision Engineering and Manufacturing*, vol. 14, pp. 1439–1445, Aug. 2013.

[27] D.-Y. Lee, S.-R. Kim, J.-S. Kim, J.-J. Park, and K.-J. Cho, "Origami wheel transformer: A variable-diameter wheel drive robot using an origami structure," *Soft Robotics*, vol. 4, no. 2, pp. 163–180, 2017. PMID: 29182094.

[28] A. F. Guc, M. A. I. Kalin, C. Karakadioglu, and O. Ozcan, "C-quad: A miniature, foldable quadruped with c-shaped compliant legs," in *2017 IEEE International Conference on Robotics and Biomimetics (ROBIO)*, pp. 26–31, 2017.

[29] U. Saranli, M. Buehler, and D. E. Koditschek, "Rhex: A simple and highly mobile hexapod robot," *The International Journal of Robotics Research*, vol. 20, no. 7, pp. 616–631, 2001.

[30] R. S. Pierre and S. Bergbreiter, "Gait exploration of sub-2 g robots using magnetic actuation," *IEEE Robotics and Automation Letters*, vol. 2, no. 1, pp. 34–40, 2017.

[31] G. F. Franklin, J. D. Powell, and A. Emami-Naeini, *Feedback Control of Dynamic Systems*. Reading, MA: Addison-Wesley, 1994.